N67 12964

(ACCESSION NUMBER)

(THRU)

1

90

(PAGES)

(CODE)

30

CR 80344

(NASA CR OR TMX OR AD NUMBER)

(CATEGORY)

FACILITY FORM 602

GPO PRICE $ _____

CFSTI PRICE(S) $ _____

Hard copy (HC) 3.00

Microfiche (MF) .75

ff 653 July 65

LMSC M-27-66-1

FINAL REPORT, CONTRACT NASw-917

FEASIBILITY STUDY

OF SEVERAL X-RAY EXPERIMENTS FOR AN

ORBITING ASTRONOMICAL OBSERVATORY

August 17, 1966

Philip C. Fisher

Lockheed Palo Alto Research Laboratory
Palo Alto, California

PREFACE

The success of the investigation described in this report can be attributed to the continued (and occassionally inspired) efforts of a number of individuals. A. J. Meyerott and D. T. Roethig were responsible respectively for a major share of the laboratory and computational aspects of the investigation. P. Kirkpatrick deserves special recognition for his contributions and advice on a variety of matters, including x-ray optics. In addition to Kirkpatrick two other individuals have consistently pioneered the understanding of relevant x-ray phenomena, and their influence is also acknowledged here. The latter two gentlemen are H. Friedman and A. P. Lukirskii; their combined publications in the years prior to 1963 provided the basis of many of the concepts discussed in the report.

Finally, it must be noted that the Lockheed Independent Research Program shared financial responsibility for this investigation along with contracts NASw-909 and 917 of the National Aeronautics and Space Administration.

TABLE OF CONTENTS

PREFACE ii

1. INTRODUCTION 1

2. NATURE OF PROBLEMS STUDIED 1

3. HIGH SENSITIVITY COLLECTOR 6

A. Theoretical Behavior 6

B. Rocket Prototype 11

C. Satellite Applications 14

4. HIGH SENSITIVITY DETECTORS 14

A. Arrays of Gas Proportional Counters 14

B. Bare Photocathode Devices 14

(1) An X-ray Conversion Stage 14

(2) A Rocket Test Unit 19

(3) An Image Amplifier 19

5. MEDIUM RESOLUTION (~ 1%) SPECTROGRAPH 25

A. Spectrograph Components 25

B. Resolution of an Idealized Grating Mosaic 27

C. Resolution of a Practical Grating Mosaic 32

D. A Practical Grating Mosaic 33

E. Estimated Efficiency of a Practical Grating Mosaic 38

F. Laboratory Verification of Spectrograph's Behavior 42

(1) X-ray Optics 42

(2) Electron Optics 48

G. Anticipated Performance of a Satellite Spectrograph 49

6. SUMMARY OF STUDY RESULTS 52

A. Problems Solved 52

TABLE OF CONTENTS (cont'd)

B. Problems to be Solved 52

7. RECOMMENDATIONS AND CONCLUSIONS 53

REFERENCES 54

APPENDICIES

A. High Sensitivity X-ray Detectors, reprinted from IEEE Trans. on Nuclear Science, NS-13, 580 (1966) A 1

B. Measurement of Stellar X-ray Spectra, Astronomical J., (1966) in press B 1

C. Listing of Fortran Program for Idealized-Grating Calculations C 1

D. Listing of Fortran Program for Practical-Grating Calculations D 1

1. INTRODUCTION

The work to be described by this report was directed toward evaluation of several x-ray measurement techniques believed to be particularly well-suited to investigations of celestial x-ray sources from an Orbiting Astronomical Observatory. The major effort under the contract (NASw-917) amounted to the design of necessary components for a fast spectrograph which would permit detailed measurements of x-ray spectra. Such measurements were stated as a long range objective of our second proposal to the NASA for investigation of stellar x-ray phenomena, the hope at that time (December 1960) being that element abundance determinations might eventually be made. The same proposal noted an interest in crossed mirror x-ray collection devices which developed over several years into a concern for x-ray reflection systems of the highest possible efficiency. By the spring of 1963, experimental knowledge of the flux of night sky x-ray sources was sufficient to warrant more detailed pursuit of instrumentation to accomplish these two general goals.

The scope of contract NASw-917 specifically called for preliminary design studies to determine the feasibility of several experiments for satellite use. Several requisite tasks of these studies were to be performed under contract NASw-909, which provided for flight of x-ray detection systems aboard a pair of Aerobee rockets. In particular, large area gas proportional counters, a Venetian blind mirror array (for x-ray collection), and a bare photocathode system (for x-ray detection) were to be tested and flown. This report contains the satellite-experiment design information gleaned from both the laboratory study under contract NASw-917, and the flight experiment under contract NASw-909.

2. NATURE OF PROBLEMS STUDIED

Three main problem areas were singled out for investigation. The first of these areas involved an x-ray optical collection device, called a Venetian blind, in which the highest possible collection efficiency was to be combined with a modest angular resolution. Parts (a) and (b) of Figure 1 indicate

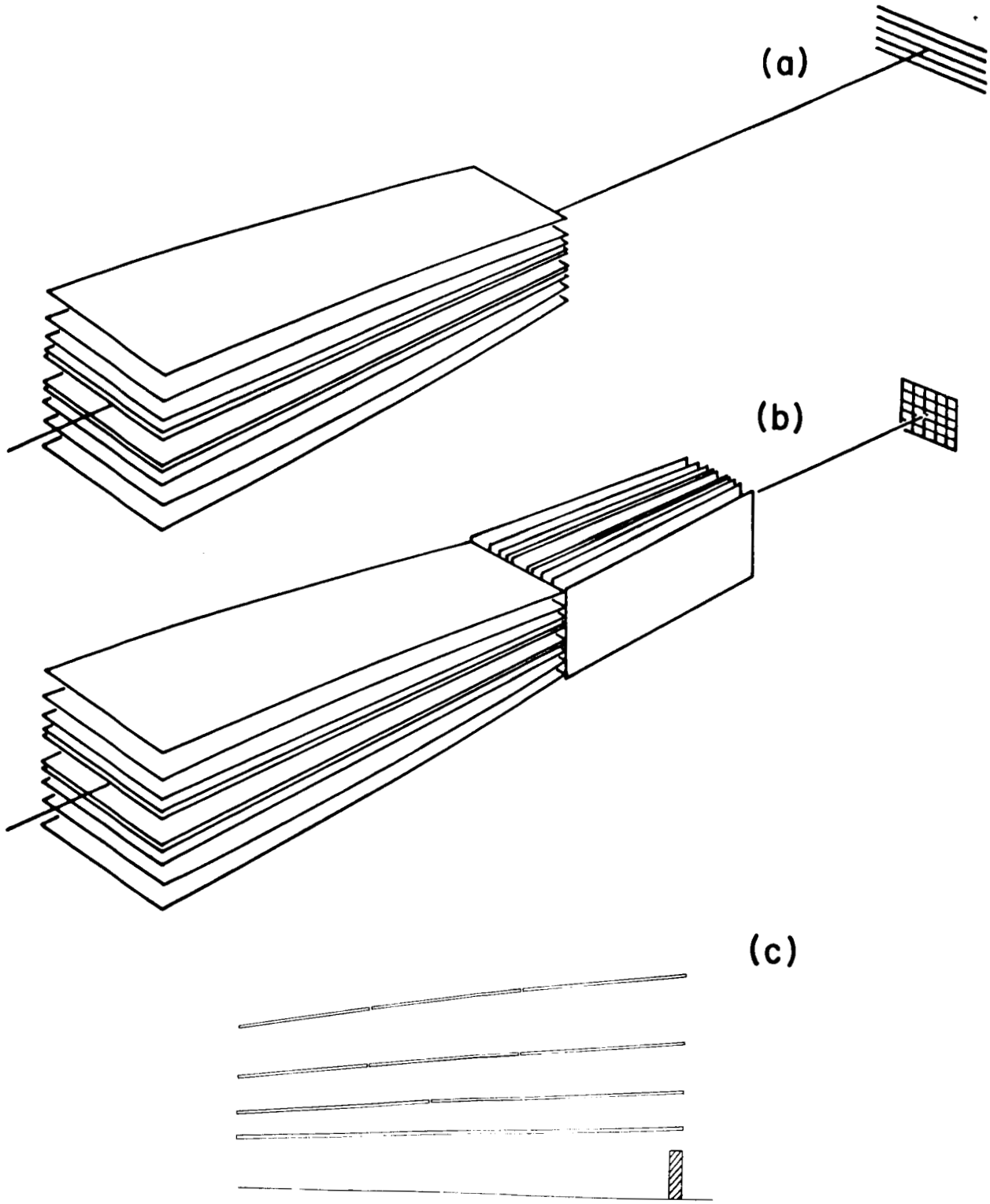

Fig. 1. Two types of Venetian blind optical collection system, and one manner of fabricating their reflection surfaces from a number of individual elements, are indicated.

simple and crossed Venetian blind systems respectively, while part (c) of the figure shows how the collectors might be fabricated. A comparison of the sensitivity of a simple Venetian blind system to the sensitivity of both a double-focusing (actually an imaging) optical reflector and a simple large area gas counter is contained in Appendix A, arguments presented there being deliberately contrived to give the most pessimistic appraisal of the value of the simple Venetian blind.

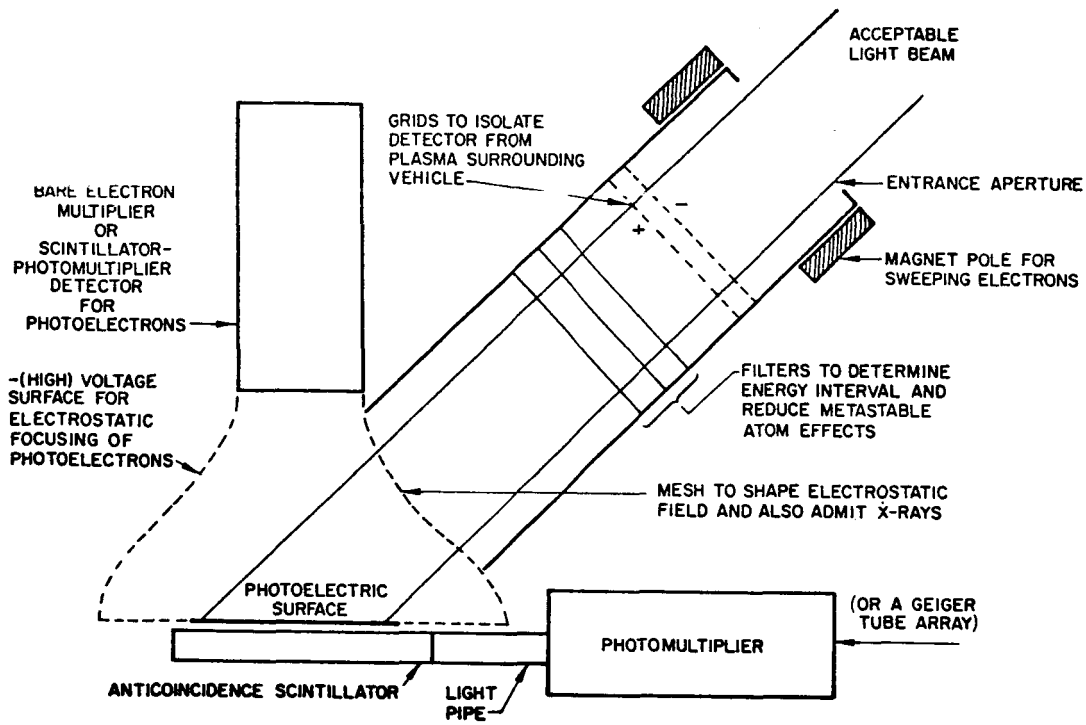

Fig. 2. January 1963 schematic of a bare photocathode detector.

The second major area for investigation was concerned with the simultaneous high-efficiency, low-noise detection and amplification of the information contained by a large quantity of soft x-rays. Two quite different approaches were considered. The first approach was based on an array of individual, mechanically-collimated large-area gas proportional counters. As Appendix A contains the description of just such a counter array, constructed under contract NASw-1073 for OAO-A1, further discussion of gas counter systems has been virtually eliminated from the text of this report. The second approach was based on bare photocathode detection of the softest ($\lesssim$ 3 keV) x rays. Individual x rays were to be detected by observation of the photoelectrons ejected from an appropriate material, the actual components being arranged somewhat like those shown schematically in Figure 2. In that figure, although

a variety of electromagnetic radiations might be accepted by the entrance aperture, visible and ultraviolet light were to be removed by suitable filters at the same time that soft particles were removed by either the repelling electrostic fields or the filters. The remaining radiation (x rays) was to be converted to electrons by the photoelectric surface and these were to be accellerated and focussed onto an electron detector. In order to reject cosmic-ray-produced electrons from the photoelectric surface, an anti-coincidence element was included in the detection system. Related detectors might well be used in conjunction with the Venetian blind collector mentioned above, or in some sort of x-ray image amplifier which may be required to facilitate recording the spectrum of a discrete source, or the intensity distribution of an extended source. Flight of this type of device was suggested in an August 1960 proposal, partly to evaluate the background problems associated with x-ray detection systems employing bare photocathodes. The fourth chapter of this report describes a similar device constructed for rocket use, and then evaluates in some detail the characteristics of a several-stage image amplifier using a bare photocathode for the x-ray conversion stage.

By combining the above two types of apparatus with a novel arrangement for dispersion of different energy x rays, it appeared possible to construct a spectrograph of about one percent energy resolution which would be continuously sensitive to all wavelengths throughout the 0.3 to 3 keV energy range. Determination of the feasibility of fabricating such a spectrograph constituted the third major area to be investigated under this contract. Parts (a) and (b) of Figure 3 show spring 1963 versions of this spectrograph, while part (c) of that figure shows the energy dispersion arrangement as first discussed in a January 1963 proposal. In parts (a) and (b) of Figure 3, the designations B and D refer to the x-ray system used to convert information about the x-ray spectrum into a more useful form, the letter C refers to an anticoincidence system for rejecting cosmic ray events, and the letters E and F refer to an image amplifier and electronic readout system. X rays entered the various spectrographs from the left of the figure, while the dispersed spectra appear at the right of the figure. A more complete description of the spectrograph is given in Chapter 5 of this report which deals with the design characteristics of the energy dispersing components

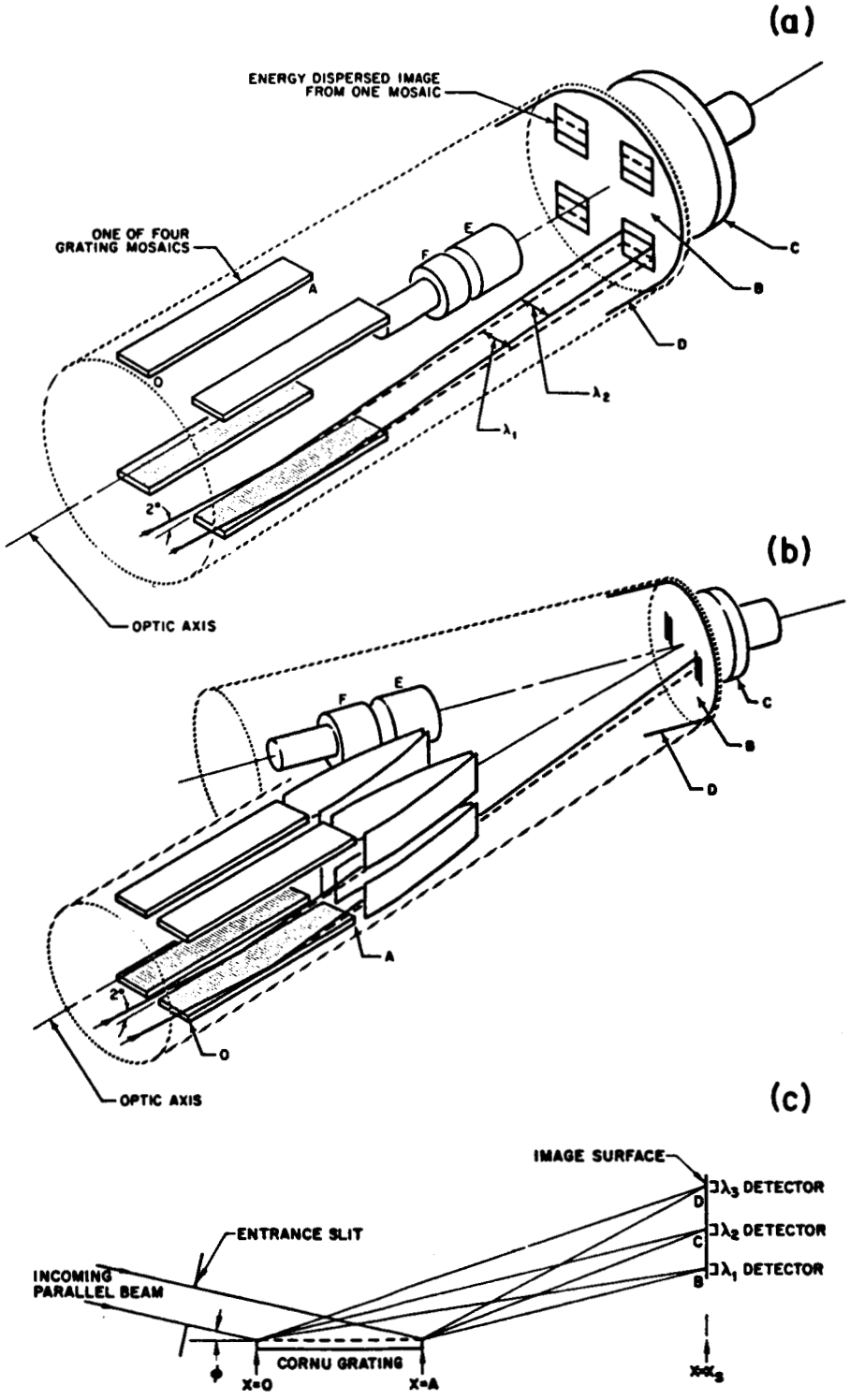

Fig. 3. June 1963 schematics of spectrographs for medium (~ 1%) energy resolution are given as parts (a) and (b) of the figure, while the January 1963 schematic of a related grating is shown in part (c).

and the laboratory demonstration of the validity of the spectrograph's design. Appendix B presents the first public disclosure of the general features of the spectrograph which is discussed at some length in Chapter 5.

The above instruments may all be characterized by the fact that each was optimized to provide one particular type of experimental information. In contrast to many conventional types of astronomical optics, no deliberate attempt was made to provide a basic device which could be utilized for a variety of measurements by addition of special equipment. Emphasis on a set of special-purpose instruments seemed proper in view of the large weight capability anticipated for satellite flights in the 1970's.

3. HIGH SENSITIVITY COLLECTOR

A. Theoretical Behavior

A comparison of the relative sensitivities of several types of soft x-ray detection systems is given in Appendix A. Therefore, most of this section is devoted to defining the geometric form of simple x-ray optical collectors and indicating where such collectors may be of use. Figure 4 presents results from measurements of Rieser[1] and Lukirskii et al.[2] of the reflection efficiency of thick evaporated layers of gold and titanium. While there are some contradictions in the available results, all data clearly show that quite small angles of incidence must be employed if efficient reflection is to occur. This leads to a fundamental conflict if an optical system of the largest possible effective aperture is to be constructed. A compromise must be made between the small angles of incidence which must be employed for high efficiency reflection and the large angles of ray deviation that are required if large aperture is to be obtained.

Figure 5 indicates the nature of this conflict. This particular Venetian blind could have been constructed from a number of individual, identically-sized slats which were arranged in a number of rows of reflecting surfaces, just as shown in the collector of Figure 1. Consider paraxial rays from an infinitely distant point source striking the various reflecting surfaces. Successively larger angles of reflection must be undergone by rays entering the Venetian blind at successively larger angles off-axis. The curves in Figure 5 show a typical variation of effective aperture with photon energy for a blind having six gold surfaces, each of which was assumed to have a reflection efficiency like that measured by Rieser[1].

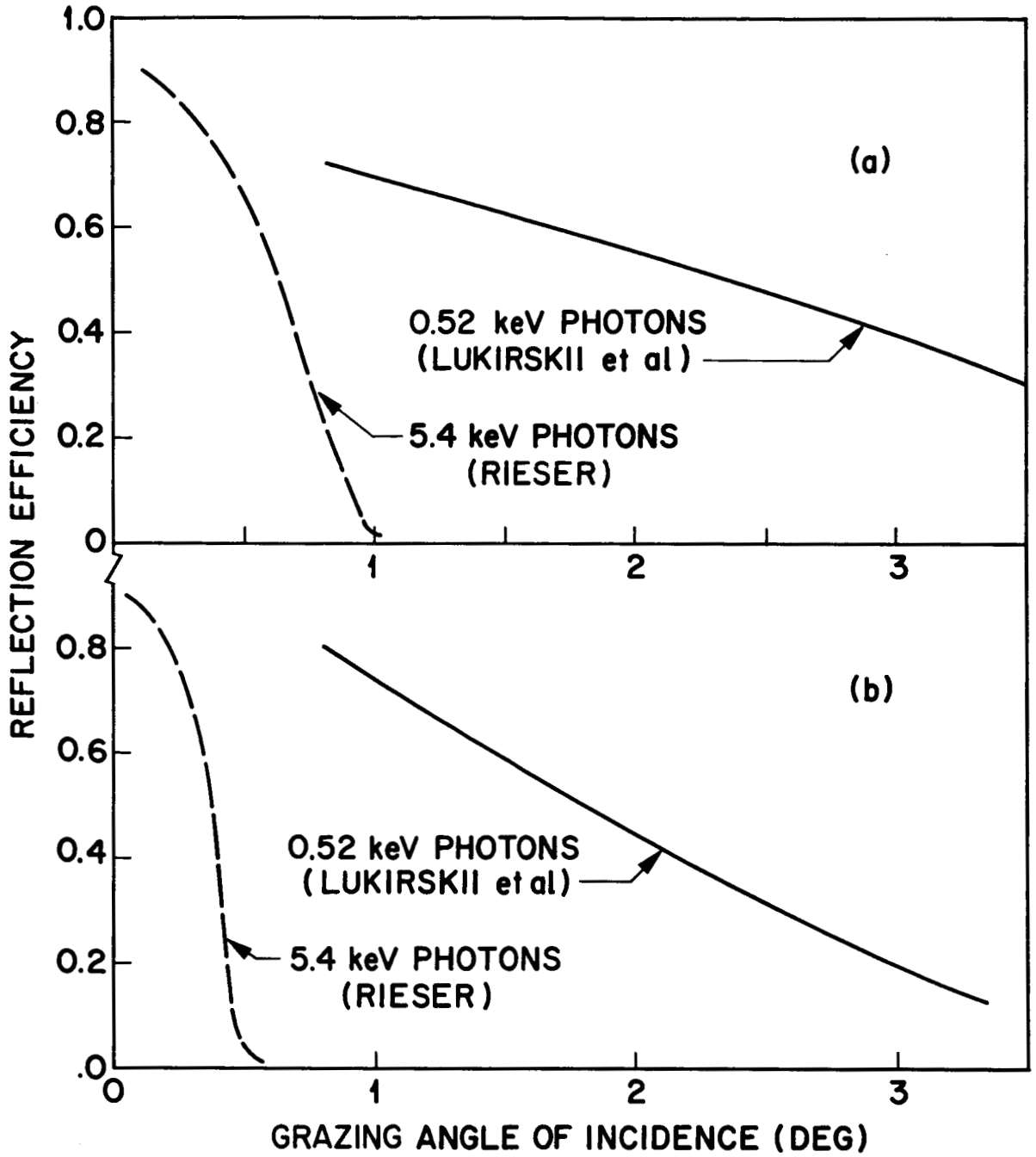

Fig. 4. Efficiency for reflection of x-rays from thick evaporated surfaces of gold and titanium are given in parts (a) and (b) of the figure. The dashed-line curves represent the results of Rieser[1] while the solid-line curves are from Lukirskii et al[2].

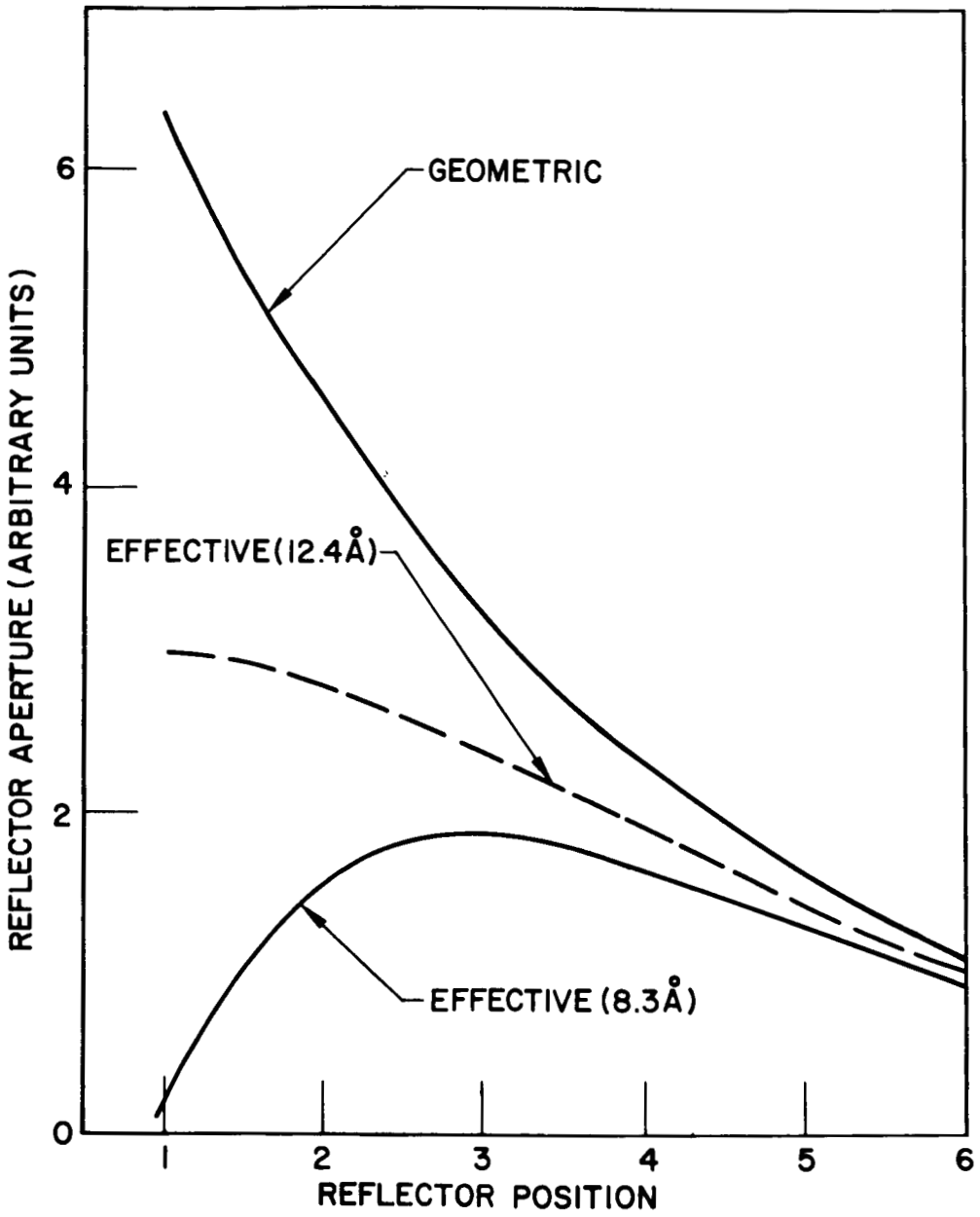

Fig. 5. Typical variation of aperture with photon energy of different reflectors of a Venetian blind optical system like that shown in part (a) of Figure 1. If the actual overall length of the assembly (x-ray collector plus detector) is taken as 2.5 meters, then the scale of the ordinate is in centimeters.

Reflector number one was the furthest off the collector's axis and so possessed the largest geometric aperture, even though the effective aperture was found to be insignificant for 1.5-keV (8.3-A) or harder radiation. Although the aperture of each reflector is a well defined quantity, smooth curves have been drawn through these quantities to facilitate understanding the variation of aperture with reflector position off the collector's plane of symmetry. A convenient design procedure for arriving at a practical collector of few-keV x rays has been to obtain the largest possible aperture at an x-ray energy of one keV and accept whatever lesser aperture is available at higher energies. This procedure seems to yield about the same aperture, at a photon energy of 2 keV, as would have been obtained if 2 keV had been used as the design energy.

There are at least two geometric forms that appear appropriate for collectors of celestial x-rays: axially symmetric surfaces, and nested parabolic cylinders. The choice of geometry depends on what information is most desired and what external constraints most affect the manner of performing a given experiment. An array of nested parabolic cylinder segments seems best suited to rapidly surveying moderately large sky areas with modest angular resolution ($\lesssim$ 15' of arc) and the highest possible sensitivity as such an arrangement can overcome both the limited field of view and the relatively smaller aperture which are characteristic of the finite-length axially-symmetric surface.

If somewhat higher angular resolution is desired, then (a nest of) axially symmetric surfaces is more appropriate. Kirkpatrick[3] has discussed the merits of the simple (parabolic) surfaces and the imaging (parabolic-hyperbolic or parabolic-elliptical) surfaces which might be used. The choice of surface shape can be made on the basis of the actual angular resolution desired, the quantity of data handling equipment available to the experiment, and the difficulty of maintaining the necessary alignment of a number of optical surfaces in the space environment. To permit resolution of a few seconds of arc, an imaging system such as the parabolic-hyperbolic arrangement of Giacconi and Rossi[4] may well be the most practical solution. In contrast to the simple paraboloidal surface, which can only focus a source lying on the optical axis, the imaging system is capable of providing a picture of an extended region. Unfortunately, imaging systems require two reflections and such an instrument's effective aperture falls off more rapidly with increasing

photon energy than does the aperture of the single-reflection optical system.

As noted above, the image of a paraxial source produced by a parabolic reflector will not appear sharply focused. X-rays coming in at an angle $\theta/2$ to the axis of a Venetian blind of overall length L will be reflected to the image plane and in that plane will fall a distance θL off the blind's plane of symmetry if incident at the outer end of the reflectors. X-rays arriving at the same angle and incident at the detector end of the blind's reflectors will be reflected to an image plane position that is a lesser distance off the blind's plane of symmetry. Consequently, the actual extent of an image increases with increasing off-axis source angle as well as with increasing length of the blind's reflectors. Consider, for example, a ten-meter long Venetian blind system composed of reflectors extending for (2.5 meters which is) one quarter the distance from the blind's entrance to the detector. A distant point source off-axis by one half degree would produce an image off the blind's plane of symmetry that spanned some four to five centimeters of the image plane. By outfitting the image plane with a small number of detectors as indicated in Figure 1 (a), it appears possible to simultaneously observe sources lying within $\pm 1/2^{\circ}$ of the blind's axis, while maintaining an angular resolution in any one detector of about one-sixth degree.

No mention has been made of the crossed Venetian blind system (a logical extension of the crossed reflectors of Baez[5]) shown as part (b) of Figure 1. The only obvious advantage of such a system is the different techniques of construction which might be involved, as compared to those required for axially symmetric reflectors. As the latter type of reflector has now been successfully fabricated, both as a simple parabola by Boyd[6] and as an imaging system by Giacconi et al.[7], the different construction techniques are no longer of particular concern. Actually, the crossed Venetian blind has several serious problems. It involves two different reflections of the incident flux and therefore may not be particularly appropriate for a detector system of maximum sensitivity. That is, the inefficiencies of double reflection may outweigh the lower background level associated with the smaller x-ray counter which could be used. Second, and as noted in the preceding paragraph, the Venetian blind provides an extended image of an off-axis source. If the ability to resolve an extended region during a single observation is desired, then the characteristics of either one or a nest of imaging reflectors may

be superior to those available from a crossed Venetian blind system. While no actual tests of a crossed-blind arrangement were made during the course of this contract, it seems likely that such a test would eliminate the crossed-blind system from consideration as a flight instrument.

B. Rocket Prototype

Figure 6 shows a rocket-sized Venetian blind flown on September 30, 1965. As can be seen by inspection of Figure 8 of Appendix A, complete instrument redundancy was obtained as the rocket prototype actually involved two complete and independent units. The slats used for the mirror array were produced by optically polishing nickel-coated 2.0" x 8.0" x 0.080" beryllium plates. A 200 Angstrom layer of gold was evaporated onto each of the polished surfaces. The calculated efficiency of the collector for an infinitely distant axial source as given in Figure 9 of Appendix A, is reproduced here as part of Figure 7. This efficiency was obtained by finding the angle of reflection for the midpoint of each slat, determining the reflection efficiency of the slat by interpolation of (Rieser's[1]) data like that presented in Figure 4, and then simply summing the contributions of all slats. Figure 7 also presents the overall efficiency of several Venetian blind systems where allowance has been made for the transmission of several gas-counter window materials, and also for conversion of the collected x-rays by a CsI photocathode.

Close inspection of Figure 6 shows that the polished surface of each slat was held tangent to the desired parabola by three spring-loaded clamps. An earlier positioning device was based on a vise-like grip along each complete end of each slat. Although care was used in the design of the earlier clamp, the gripping action always caused distortion of the slat and eventually caused that clamp to be discarded in favor of the spring-loaded clamp. For this particular blind, the surface of each <u>flat</u> slat was brought into proper alignment by simple micrometer measurements made with respect to machined parabolic templates. This alignment was checked by placing a line-shaped light source at the parabola's focus and observing the array of lines emanating from the entrance end of the blind. Very precise slat alignment was not required because the flight detector aperture was some four times larger than the reflected image of a distant point source from any single slat.

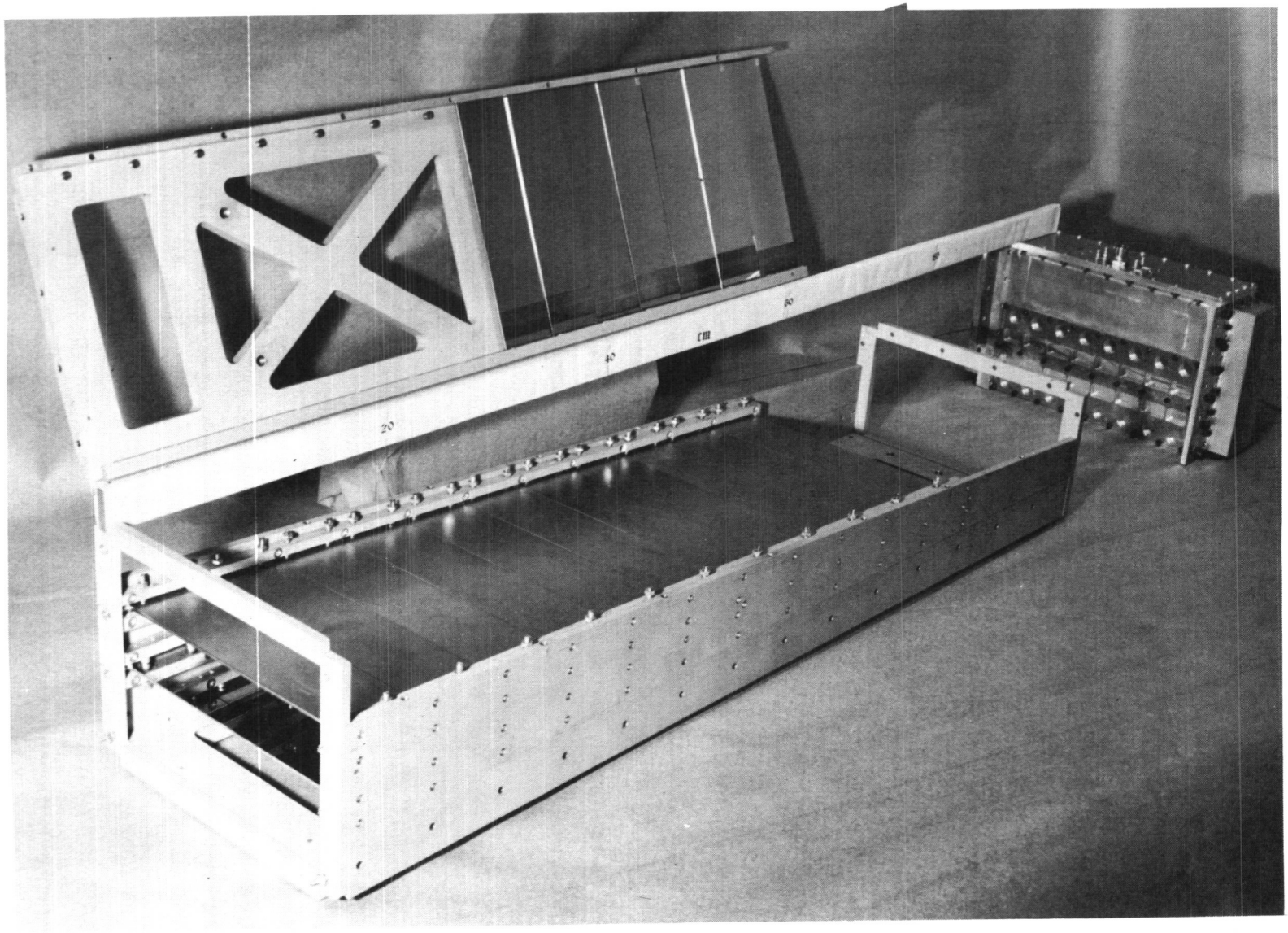

Fig. 6. View of partly assembled dual Venetian blind system flown in September 1965. Two of the four rows of slats are in place, and a third incomplete row appears near the top of the figure. Various reflections help to clearly outline edges of some of the individual slats in the third row. Two mylar-window proportional counters are shown at the instrument's focal plane.

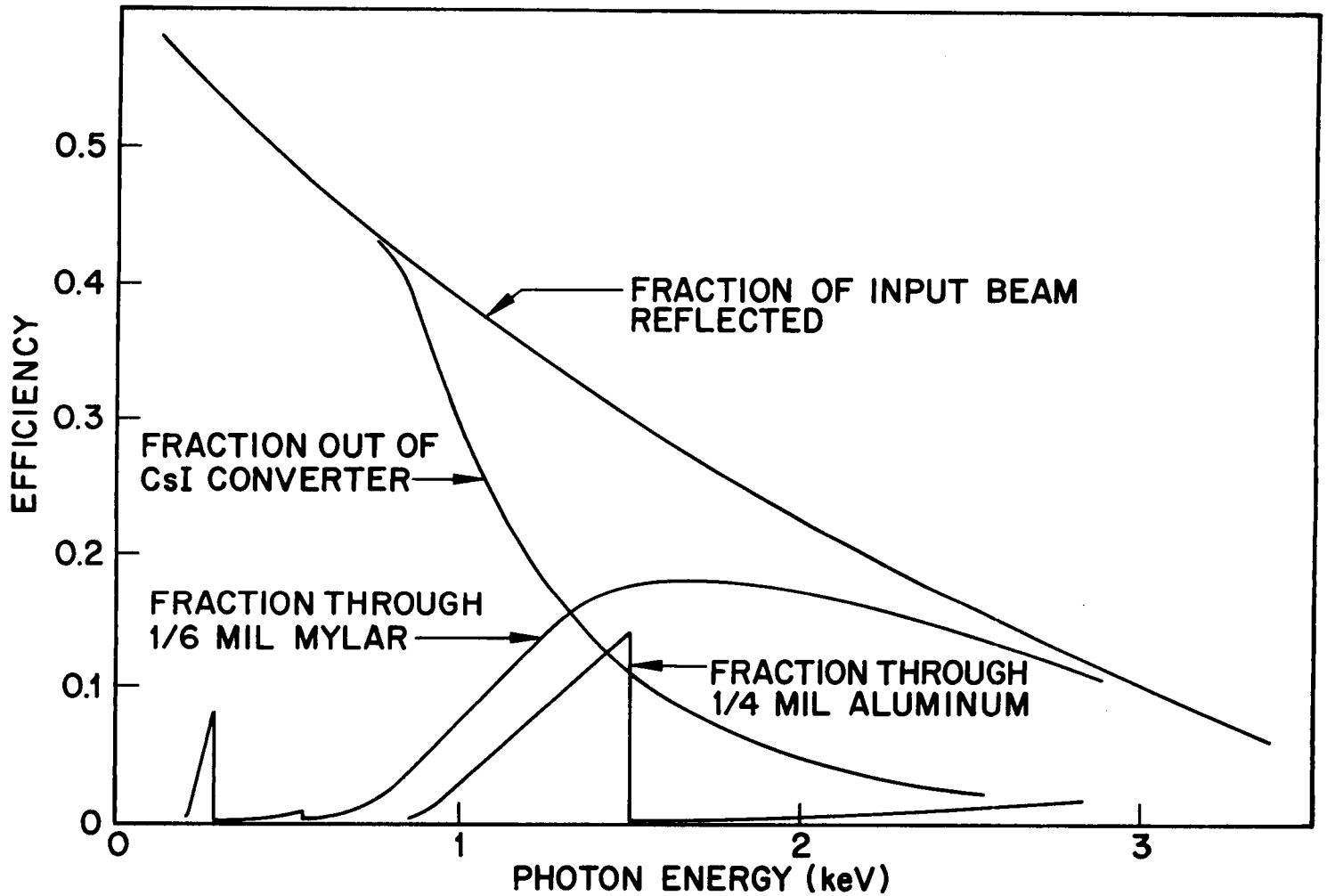

Fig. 7. Calculated efficiency of several Venetian-blind-detector systems like that shown in Figure 6. The curve labelled "fraction of input beam reflected" was taken from Figure 9 of Appendix A.

Although the Venetian blind system did yield data, the rocket was not properly oriented during flight and so no x-ray sources were observed.

C. Satellite Applications

The conceptual application of simple Venetian blind systems is considered at some length in Appendix A. Where observing time is limited, maximum sensitivity is desired, and modest angular resolution is appropriate, the Venetian blind appears to be a useful device.

4. HIGH SENSITIVITY DETECTORS

A. Arrays of Gas Proportional Counters

These systems and their potential size and sensitivity are discussed in Appendix A and so no detailed remarks are made here. However, fragmentary information from a complete year's monitoring of the gain of 18 separate gas counters of the OAO-A1 x-ray experiment indicates that the counter gains decreased at a rate of the order of 3% to 5% per year. Because this change is comparable to the errors of the individual gain measurements, conceivably no change may have occurred. Although the cause of the potential gain shift is not known, any real change was sufficiently small that the feasibility for satellite use of a large aperture array of sealed gas proportional counters seems to have been successfully demonstrated. Indeed, it appears unwise to build a large-area gas-counter experiment based on geiger rather than proportional region operation if sufficient data handling capacity is allowed to permit the available spectral information to be acquired.

B. Bare Photocathode Devices

(1) An X-ray Conversion Stage

The effort to develop bare photocathode detection techniques was made because related detectors were believed to be of use in conjunction with optical collectors of low energy photons, such as the Venetian blind described in the preceding chapter and the x-ray spectrograph to be discussed in the next chapter. The fundamental problem in the latter application is how to efficiently recognize and detect a small quantity of x rays while simultaneously retaining a knowledge of the image plane locations where these x rays were converted into electrical signals, or into a different and more readily measurable form of radiation.

Before deciding on the bare photocathode as a low energy x-ray detector, five quite different forms of x-ray conversion stage were considered. These forms included scintillator-phototube combinations, a solid state detector mosaic, a mosaic of open electron multipliers (either of tubular or mesh construction), a spark chamber, and the x-ray-to-electron-to-photon conversion procedure finally selected. To be acceptable, the x-ray converter was to be able to resolve of the order of 30 lines per millimeter. A tacit assumption was that the highest possible conversion efficiency would be of little use if the noise level was comparable to or exceeded the available signal level. A noise level of at most one-half electron cm^{-2} sec^{-1} seemed necessary for the particular detector application under consideration. Since the cosmic ray background of a satellite experiment is anticipated to be of the order of 1 count cm^{-2} sec^{-1}, reduction of photocathode noise much below this level is only worthwhile if some sort of coincidence arrangement is utilized to eliminate unwanted cosmic ray events.

Considering the scintillator-phototube combination first, a noise level of the order of 10 electrons cm^{-2} sec^{-1} is usually associated with conventional extremely-quiet but visible-light-sensitive photocathodes. By cooling the tube to dry ice temperatures, a tenfold reduction in noise can be obtained. Unpublished Lockheed data obtained in 1961 yielded conversion efficiencies of 5 and 2.5 photoelectrons out of a typical S-11 photocathode per keV of x-ray energy deposited in NaI and CsI scintillators respectively. Therefore, the ultimate signal available from absorption of an individual one-half-keV x-ray in an alkali halide scintillator is comparable to or slightly larger than the signal from a single (noise)electron. For x-rays more energetic than a few keV, the ratio of photoelectrons in a signal event to electrons in a noise event is sufficiently large that the effects of individual x rays may be rather easily recognized. However, where long integration times are required to observe very weak x-ray fluxes, the cumulative effect of noise events could still effectively mask the desired signal events. As the conversion of many x-rays of a given low energy is a statistical process involving Poisson rather than Gaussian statistics, unambiguous elimination of noise events from a small number of signal events is quite difficult. These considerations lead to the current rejection of a scintillator-phototube arrangement for converting x-ray information into recorded signals. If new techniques are developed that would considerably simplify use of

appreciably cooled photocathodes in a satellite environment, then the use of scintillators would be reconsidered, although a rocket test of an x-ray spectrograph might not involve use of such a phototube.

An alternate means of converting the x-ray image would be to employ a mosaic of solid state detectors. By cooling the mosaic to liquid nitrogen temperatures (and applying sufficient voltage to permit multiplication in a manner analogous to that in a gas counter), photons of the order of 0.5 keV have been observed. However, it is not yet clear whether sufficient spatial resolution or simplicity of operation can be obtained to permit use of such a mosaic for the detection of quite small numbers of low energy x-rays on a long-lived satellite. The statistics of the x-ray absorption process and the $\sim$ 3 eV per electron-hole-pair of solid state devices provides an inherent limit of about ten percent (full width at half maximum) to the resolution of x-ray energies near 1 keV. Therefore it is clear that a solid state detector cannot obtain 1% energy resolution for the range of x-ray energies of interest here. While this type of device has obvious uses, it seems poorly suited to the role of the primary detection element in an x-ray spectrograph designed for 0.2 - 3 keV x-rays.

The third conversion device considered was based on an array of bare tubular, or mesh-type, multipliers. Although the desired spatial resolution probably could be attained, the noise problems associated with this type of x-ray conversion appartus are believed to be comparable to (or only slightly less severe than) those of the scintillator-phototube arrangement. In addition, many individual elements must operate properly and the walls of the elements are finite and so reduce the available aperture (and therefore the effective efficiency) of the conversion stage. The presently unavoidable combination of seemingly undesirable features eliminated this type of device from contention for the initial stage of the x-ray image amplification system.

A spark chamber was also considered as a conversion system, because of its obvious simplicity in terms of a digital output and because the output signal amplitude could be virtually independent of the energy of the x-ray detected. As it appeared quite difficult to get very soft ($\sim$ 1/2 keV) x rays into such a chamber, this type of apparatus did not appear convenient for an x-ray conversion stage. However, it may well be that further development of spark chambers, like that of Lansiart et al.[8],

will eventually lead to a suitable device for recording an accelerated-photoelectron image derived from the initial x-ray information.

The remaining conversion procedure to be discussed appears to be the arrangement which best surmounts all of the relevant problems known at this time. In this arrangement, x rays eject photoelectrons from a high-work-function photocathode having a noise level of ≤ 1 electron cm^{-2} sec^{-1}. Conversion efficiencies for SrF_2 and CsI photocathodes have been measured by Lukirskii et al.[9, 10] and are given in Figure 8, as either of these materials might yield a suitable photocathode. The photoelectrons are accelerated in an electrostatic field and produce at the anode a two dimensional image of the photocathode's information. It must be remembered that the distribution in energy of a large number of photoelectrons produced by a monochromatic beam of photons will contain some electrons nearly as energetic as the input photons. At the higher photon energies (of several keV) such an effect might be expected to provide a fundamental limitation to the spatial resolution obtainable in the image of a bare-photocathode x-ray converter. The sensitivity of an actual detection element is determined by the largest converter area that might be used for a single resolution element. For reasons to be discussed more fully in the next chapter of this report, the maximum area of a resolution element is here taken to be 1/2 mm x 2 mm = 0.01 cm^2. Consequently, an x-ray-converting photocathode could have an average noise level as high as some twenty spurious counts per resolution element per 2000 seconds. (This particular size of resolution element corresponds to that extent of image plane appropriate for 300 ev photons dispersed by a 2.5 meter long spectrograph like that discussed in the next chapter. Figure 17, in the next chapter, also reveals a rapidly changing spatial resolution requirement as a function of photon energy. As a result, a minimum-area spectrograph resolution element is twenty times smaller than the 0.01 cm^2 just considered and would present the other extreme of photocathode noise level, amounting to only 1 noise electron per 2000 seconds per resolution element. At one of these extremes of resolution element size, spurious counts from primary cosmic ray effects may be comparable to the spurious counts from the photocathodes noise.)

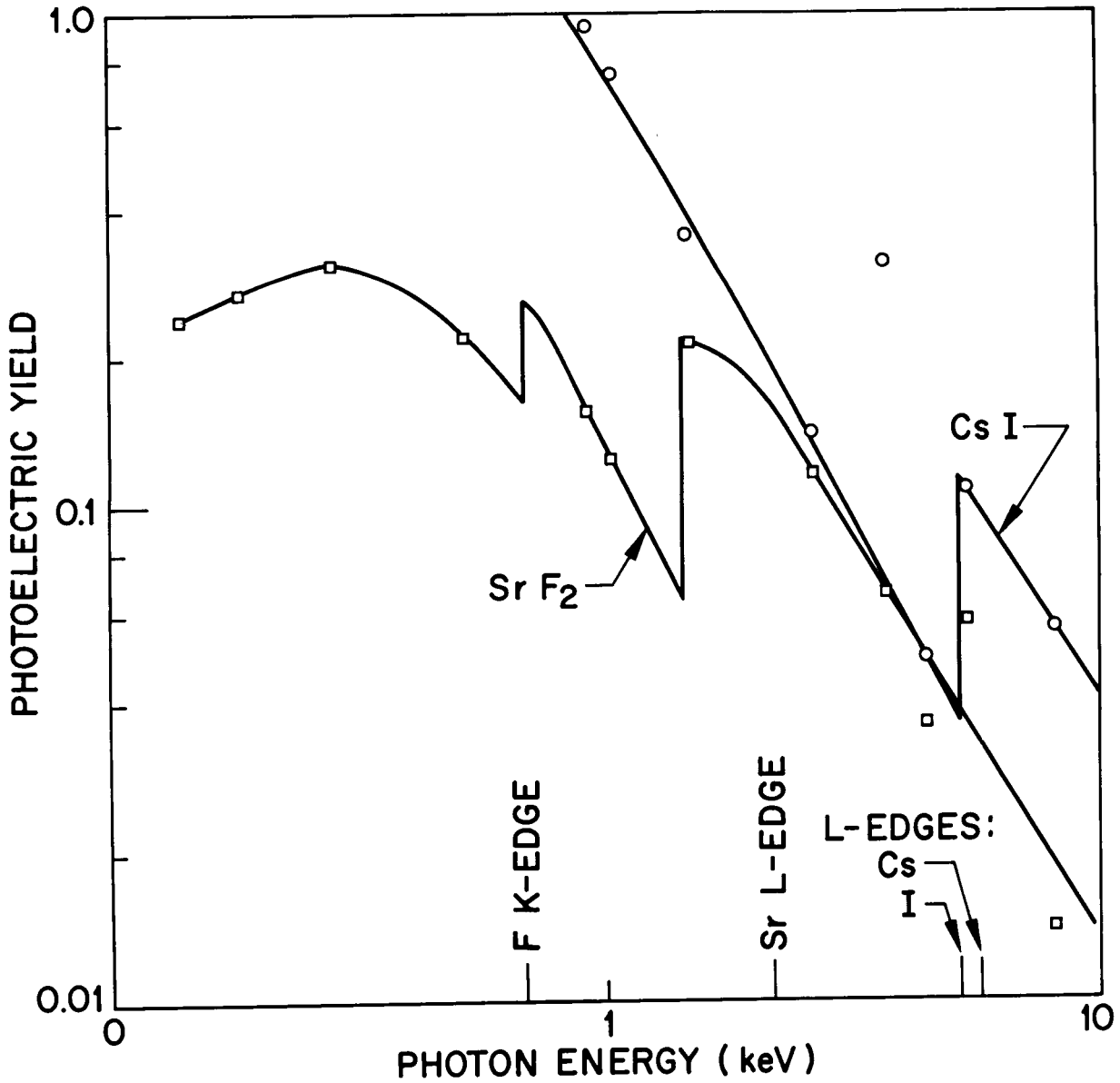

Fig. 8. Fraction of quanta leading to photoemission for soft x-rays incident on two different semiconducting materials. While the data points shown are from Lukirskii et al.[9,10], solid lines have been added between the published data points to suggest an approximate variation of photoelectron yield with photon energy.

(2) A Rocket Test Unit

Figure 9 shows one version (used on the September 1965 flight of NASA Aerobee 4.121) of a bare photocathode detector that was modeled after the system shown schematically in Figure 2. While this unit did not yield an image of the incident x-rays, it did collect most all photoelectrons to a single electron detection element. X-rays entered this detector through the rectangular gridded-aperture at the left of the figure, the grid being used to isolate the photocathode from the plasma surrounding the detector. After filtering by several thin aluminized plastic films (also shown at the left of the figure), x-rays were allowed to enter the electrostatic focusing structure (shown at the right of the figure) and shine on a photocathode at the base of that structure. The resultant photoelectrons were accelerated to a tubular multiplier situated at the apex of the focusing structure. While laboratory operation was successful, no useful flight data were acquired because the detector never outgassed sufficiently.

(3) An Image Amplifier

One particular image amplifier based on the bare photocathode principle is shown schematically in Figure 10. This device is the result of adding a conventional single stage image intensifier to an x-ray conversion stage to try to bring the resultant image up to a brightness level more appropriate for photographic recording. The magnification of each stage is near unity. Although a three-stage device seems to be required for film recording the results of a rocket experiment, the two-stage unit could be a basic ingredient of either a rocket or a satellite experiment. Considerable further experience with this type of apparatus is necessary, but was not obtained as only a portion of the funds originally requested for this feasibility study were made available. Conceivably this experience could lead to combining the conversion stage with a fundamentally different type of amplifying and/or recording system (such as a spark chamber). However, and at the very least, the procedure suggested by Figure 10 is so straightforward that such a device could probably be flown on a rocket within a few years.

In the photon scintillator developed by Rome, Gauthier, and Clausse[11], the high work function of CsI was found to restrict the photocathode's noise

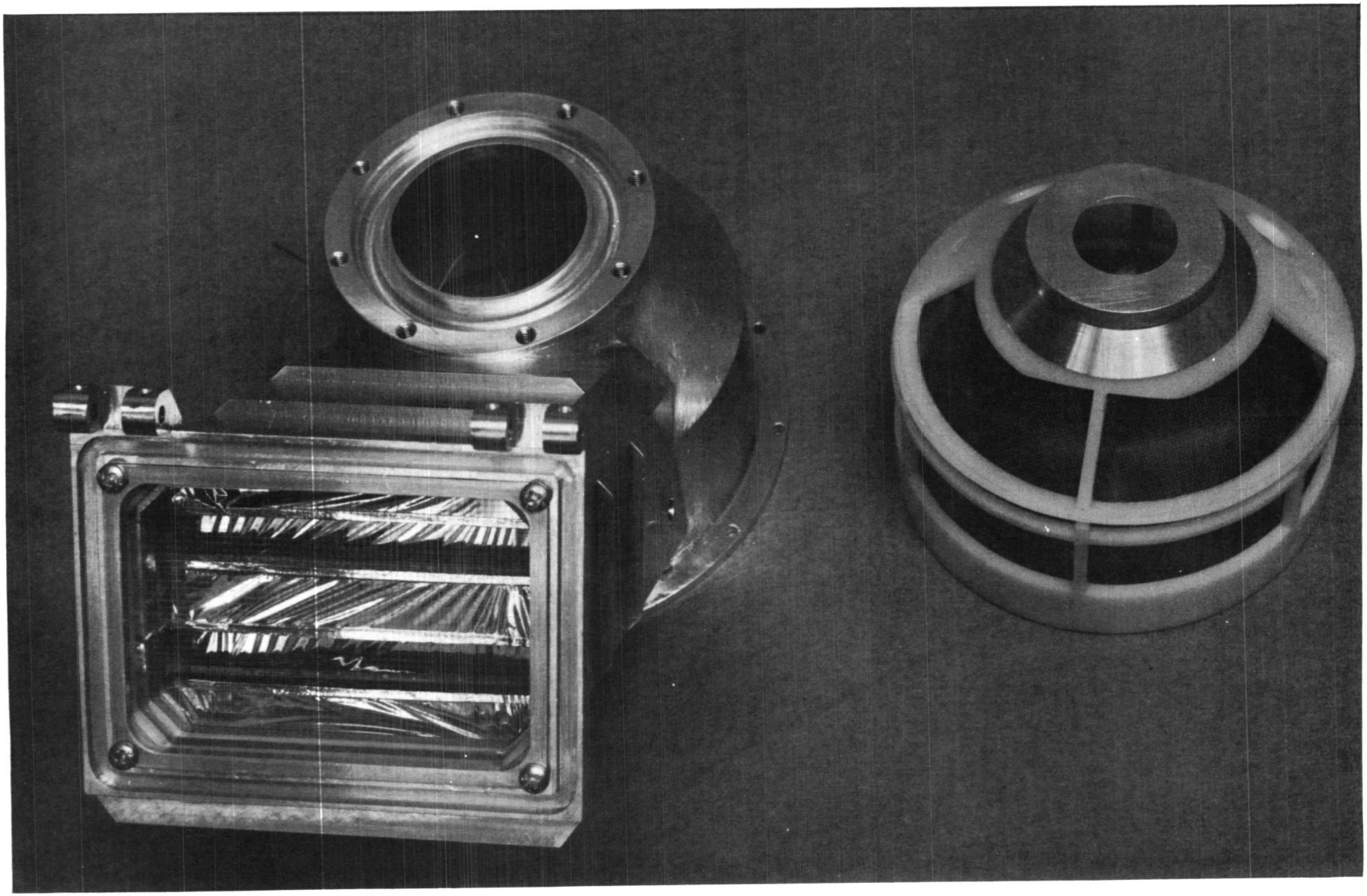

Fig. 9. View of partly-assembled components of a bare photocathode detector flown in September 1965.

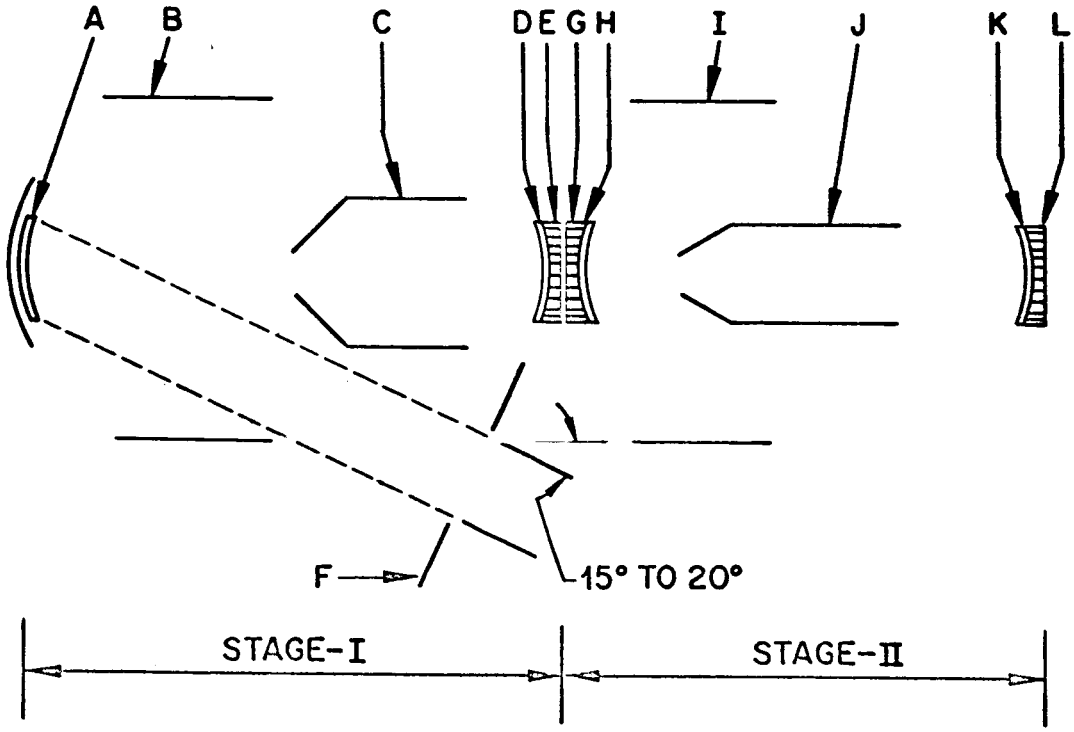

NOMENCLATURE

A. CsI photocathode

B. Cylindrical focus electrode

C. Anode

D. Electron converter

E. Fiber optics interstage coupler, may be integral with Item G

F. Entrance aperture and snout

G. Fiber optics interstage coupler, may be integral with Item E

H. S-20 photocathode

I. Cylindrical focus electrode

J. Anode

K. P-11 phosphor

L. Fiber optics

Fig. 10. Schematic of components of a two-stage image amplifier which might be used as part of the detector for the x-ray spectrograph discussed in the next chapter.

level to $\sim 1/2$ electrons cm^{-2} sec^{-1}. As the x-ray conversion stage of Figure 10 merely substitutes a more accurate focusing field for the simple collecting field of the photon scintillator, presumably the low noise level inherent to that device should be retained in the two-dimensionally-focussed x-ray converter.

To better understand the operation of this type of image amplifier, consider the components of the structure presented in the figure. As only a modest spatial resolution (amounting to a resolution at element L of some 1 to 30 lines per mm) is required, readily available fiber optics can be used to couple the x-ray conversion stage to the second or image-intensifying stage. Upon being released by element A of the conversion stage, individual photoelectrons are accelerated to say 10 keV and then allowed to strike either a phosphor or a scintillator (element D). Photons from this material are in turn converted to photoelectrons by a visible-light-sensitive photocathode (element H). Because of their 10 keV energy, each accelerated photoelectron from the x-ray converter could yield up to 30 photoelectrons from the visible-light-sensitive photocathode (element H). This assumes the photoelectron's energy is converted by element D to 3 ev photons with an efficiency of 10% and that these photons are in turn converted by element H to photoelectrons with an efficiency of 10%. After acceleration to 10 keV, each photoelectron from element H might release some 300 visible photons from the output phosphor, element K. Consequently, an ideal two stage system would yield some 9000 visible photons at the output phosphor per electron from the x-ray photocathode. Experience of others with intensifiers having fiber optics at both input and output surfaces is that the overall gain of a tube might be halved. Under these circumstances, only some 5000 visible photons would be available at the output surface of the image amplifier shown in Figure 10, per electron from photocathode element A.

According to Reynolds[12], some 200 visible photons are needed to produce a developable grain in a fast photographic emulsion. Therefore the 5000 photons produced by each x-ray detected will produce $\sim$ 25 grains in an emulsion. As the maximum size of a resolution element at the x-ray conversion stage is assumed to be $\sim .01$ cm^2, and the image amplifier has unit magnification, each converted x-ray will yield at least 25 developable grains per .01 cm^2 of emulsion. For a density of 0.1, the background fog in the emulsion may correspond to $\sim 10^5$ grains per .01 cm^2 (cf Reynolds[11]). Therefore at least 40

converted x-rays per .01 cm^2 resolution element are required to have a signal that is three standard deviations above the emulsion's background fog. If an additional stage of image intensification had been employed, only 1 or 2 converted x-rays per .01 cm^2 resolution element would have been required for a significant signal. Consequently a three stage image amplifier appears suitable if the effects of (nearly) individual x-rays are to be observed.

In order to test the above assumptions, a small amount of laboratory testing of image amplifier components was done under the contract. One of the basic ingredients of the x-ray conversion stage of Figure 10 is the electrostatic field structure. For the preliminary x-ray converter tests, the shaped field was provided by an adaptation of one of the Rauland Corporation's standard image intensifiers. This structure is shown in Figure 11. The section of the tube which normally contains the photographic plate has been removed, the dome-shaped photocathode surface has been made detachable, and the conventional visible-light-sensitive phosphor has been omitted. The rectangular aperture cut in the side wall of the tube permitted x-rays to shine directly onto the photocathode, which was located near the center of the curved dome at the left of the picture. A complete laboratory conversion stage was obtained by addition of 1) an x-ray converter to the dome-shaped photocathode and 2) a photographic plate in the tube's image plane.

This laboratory apparatus was made in such a manner as to allow a phosphor plus fiber-optics-light-coupler to eventually be substituted for the photographic plate, as this arrangement would preserve the x-ray photocathode's spatial resolution at the input of a conventional image intensifier. A two-stage magnetically-focussed intensifier, equipped with fiber optics at input and output surfaces, was purchased on the contract in order to have a complete image amplifier system. The fiber optics were unclassified and were to be capable of resolving 30 lines per millimeter (corresponding to the smallest resolution element of the spectrograph described in the next chapter). The overall gain of the RCA tube was anticipated to be ~ 1000, equal to one-half the gain quoted for the tube without fiber optics. Due to a number of manufacturing problems, the tube's delivery date was shifted some six months and it is now scheduled to arrive at least several weeks after expiration of the present contract. As a result no tests of a complete image amplifier system were carried out.

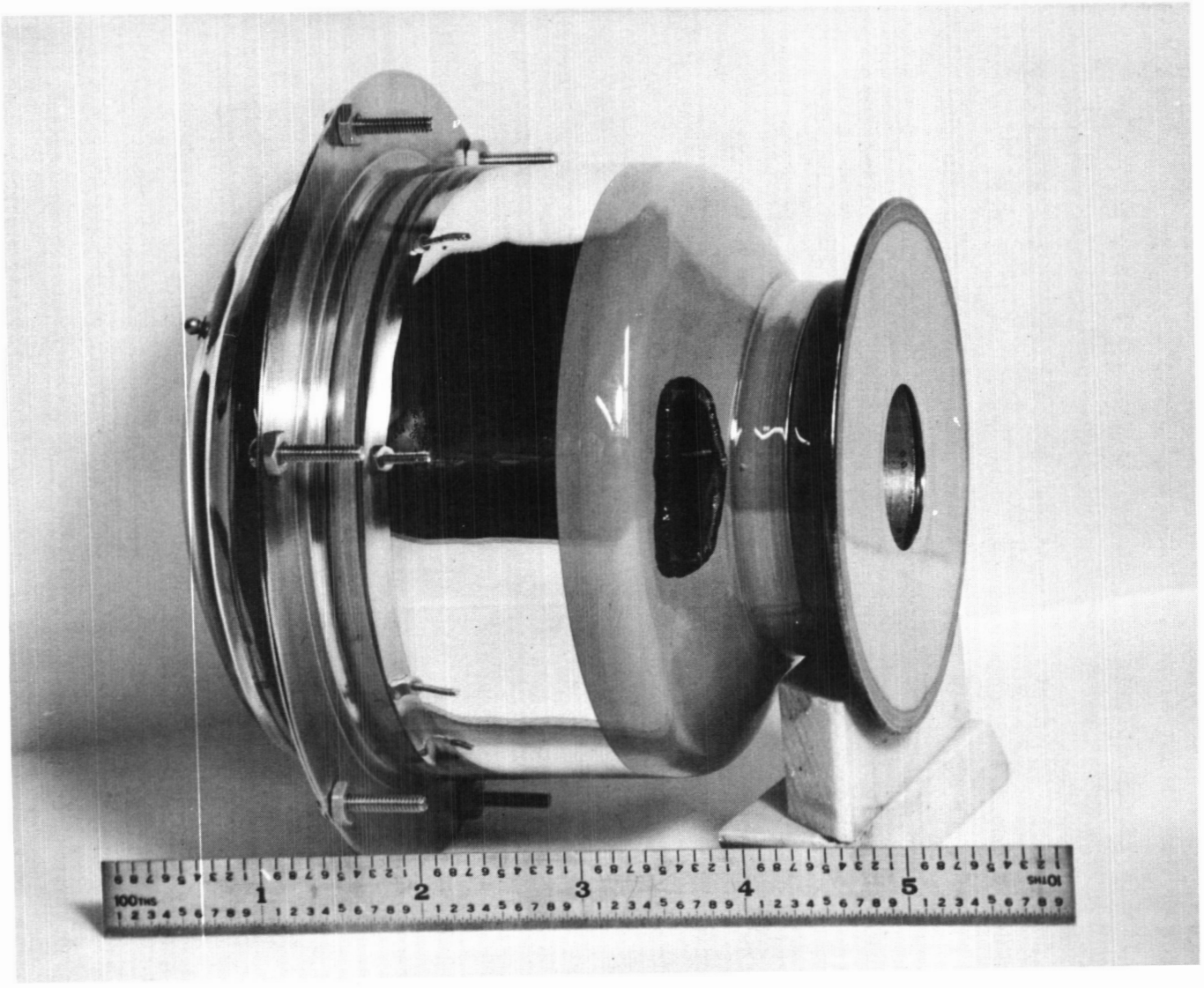

Fig. 11. A major portion of one of the Rauland Corporation's conventional one-stage image intensifiers is shown above. This structure provides a two-dimensional image, as compared to the one-dimensional focus provided by the detectors of Figures 2 and 9.

However, the one test of crucial importance to the image amplifier concept discussed above was performed. This test was made to establish the validity of the low-noise x-ray conversion stage; the results are presented in the next chapter.

Use of a photographic emulsion at the fiber-optics output of a three stage image amplifier like that of Figure 10 is only warranted if the film can be retrieved. For an unmanned Orbiting Astronomical Observatory, the two-stage image amplifier shown in the figure might provide its information to a vidicon.

5. MEDIUM RESOLUTION (~ 1%) SPECTROGRAPH

A. Spectrograph Components

Figure 12 is a current version of Figure 2 (b) and schematically illustrates the spectrograph which is being designed for examination of very weak fluxes of approximately 0.2 to 3 keV x-rays. Although only a single Venetian blind is necessary, two complete instruments are shown in the figure. For a given available geometric aperture, greater reflection efficiencies can be realized with two (instead of one) Venetian blinds. This follows from the permitted reduction in angle of incidence. If the actual configuration is properly chosen, at the higher photon energies each of the two Venetian-blind units can provide an image which has greater contrast (signal to background) than that obtainable from a single Venetian blind of double the entrance dimension. This duplicity permits convenient use of different Z materials for each of the two sets of reflecting and diffracting surfaces, and should permit alleviation of some of the difficulties introduced by the variation of absorption coefficients discussed below. An abstract announcing the potential of this type of spectrograph is given in Appendix B, along with a schematic of the spectrograph's x-ray optics. In addition to the stellar x-ray measurements listed in the abstract, the spectrograph might also be of use in searching for x-rays associated with solar streamers and in improved quality studies of known solar x-ray phenomena. Radiation from a distant angularly small source would be dispersed by a curved grating, which might have to be fabricated as a mosaic of individual diffraction gratings. The resultant spectral lines would be shortened in the dimension parallel to the grating rulings by a Venetian blind, which is composed of a nest of parabolic mirrors similar in form to the collector discussed in Chapter 3 and shown in initial form

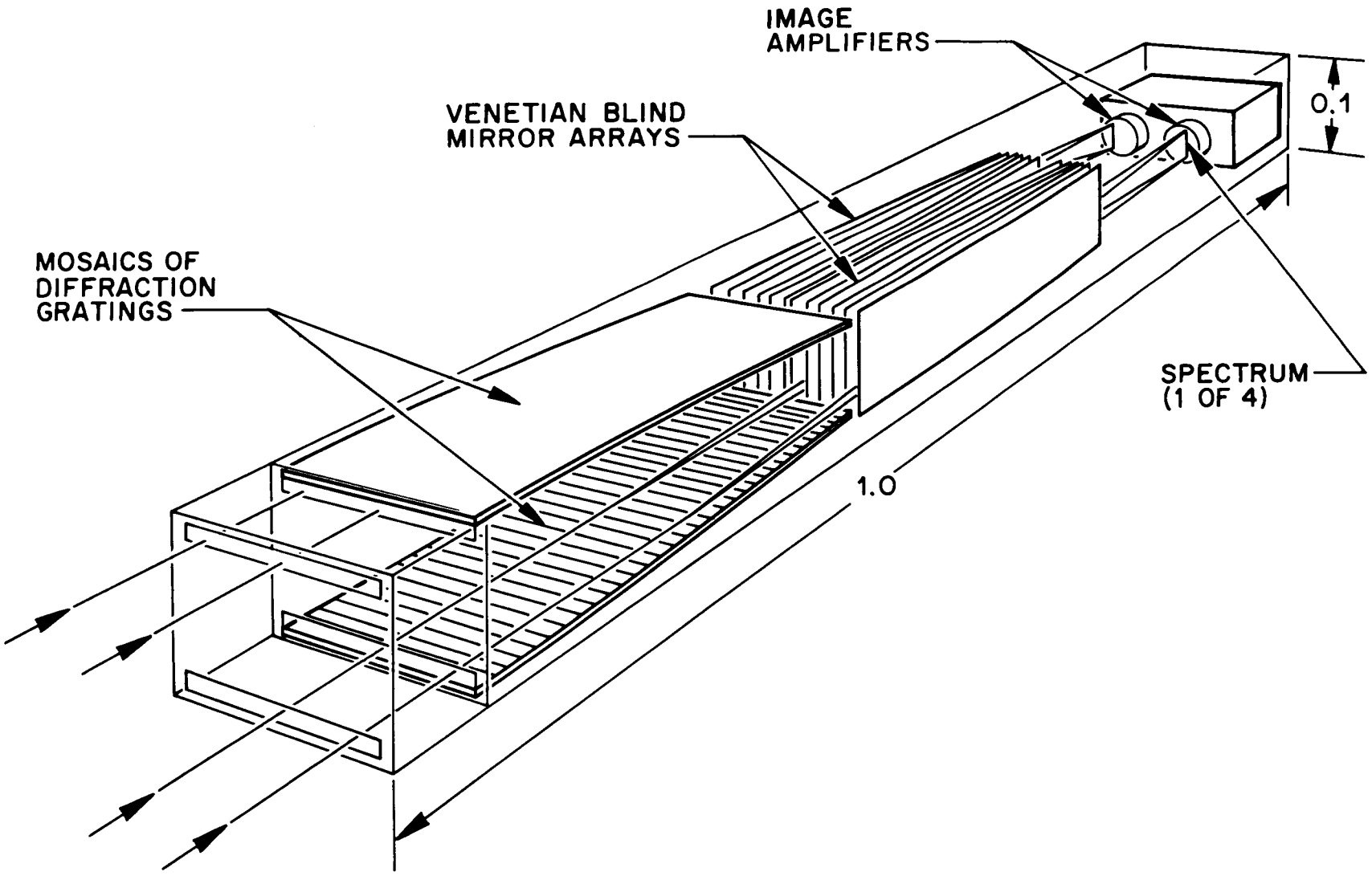

X-RAY SPECTROGRAPH

Fig. 12. Schematic of an x-ray spectrograph possessing an energy resolution of about 1% throughout an 0.2 to 2 keV energy interval. Relative proportions of the instrument's dimensions are given in the schematic.

by the x-ray optics portion of Figure 6. The combined optics produce a line-shaped x-ray image which is converted to a line-shaped visible light image by the first stage of the image intensifier discussed in Chapter 4 and shown schematically in Figure 10. While the components shown in Figure 12 would produce a total of four spectra, only two of these have been shown in the figure. The other two spectra would be adjacent to the pair shown, and would be produced by rays incident on the unused (in the figure) portion of the spectrograph's entrance aperture. The only spectrograph component still to be described is the energy dispersing element. The next part of this report deals with the theoretical design of this element, called a grating mosaic, and is followed by a description of the laboratory measurements which verified the x-ray optic concepts.

B. Resolution of an Idealized Grating Mosaic

The formula which describes diffraction from a plane grating is

$$\frac{n\lambda}{d} = \cos \Phi - \cos \Psi, \text{ where} \qquad (5\text{-}1)$$

n = order of the spectrum,

d = spacing of ruled grooves,

Φ = grazing angle of incidence,

λ = wavelength diffracted, and

Ψ = grazing angle of diffraction.

Most spectrographs rely on a single value of groove spacing and different wavelengths are observed at different angles of diffraction. Cornu showed that by varying the groove spacing across the grating surface, diffracted rays of a single wavelength could be brought to a focus. In January 1963 a grating was proposed which would bring each of two wavelengths to separate foci. This was to be accomplished by introducing curvature to the grating with variable spacing. The effect of curvature can be inserted in equation 5-1 by requiring the flat reflecting surface between successive grating grooves to be tilted at successively greater angles δ with respect to the surface between the initial pair of grooves.

Figure 13 indicates the relation of the pertinent grating-mosaic variables by means of three individual reflecting surfaces of the grating and rays of the two wavelengths selected for perfect focusing. Images of the latter are a pair of parallel lines perpendicular to the plane of the paper; these lines may be used to define an image plane. Although only these two wavelengths are actually in focus in the image plane, there is

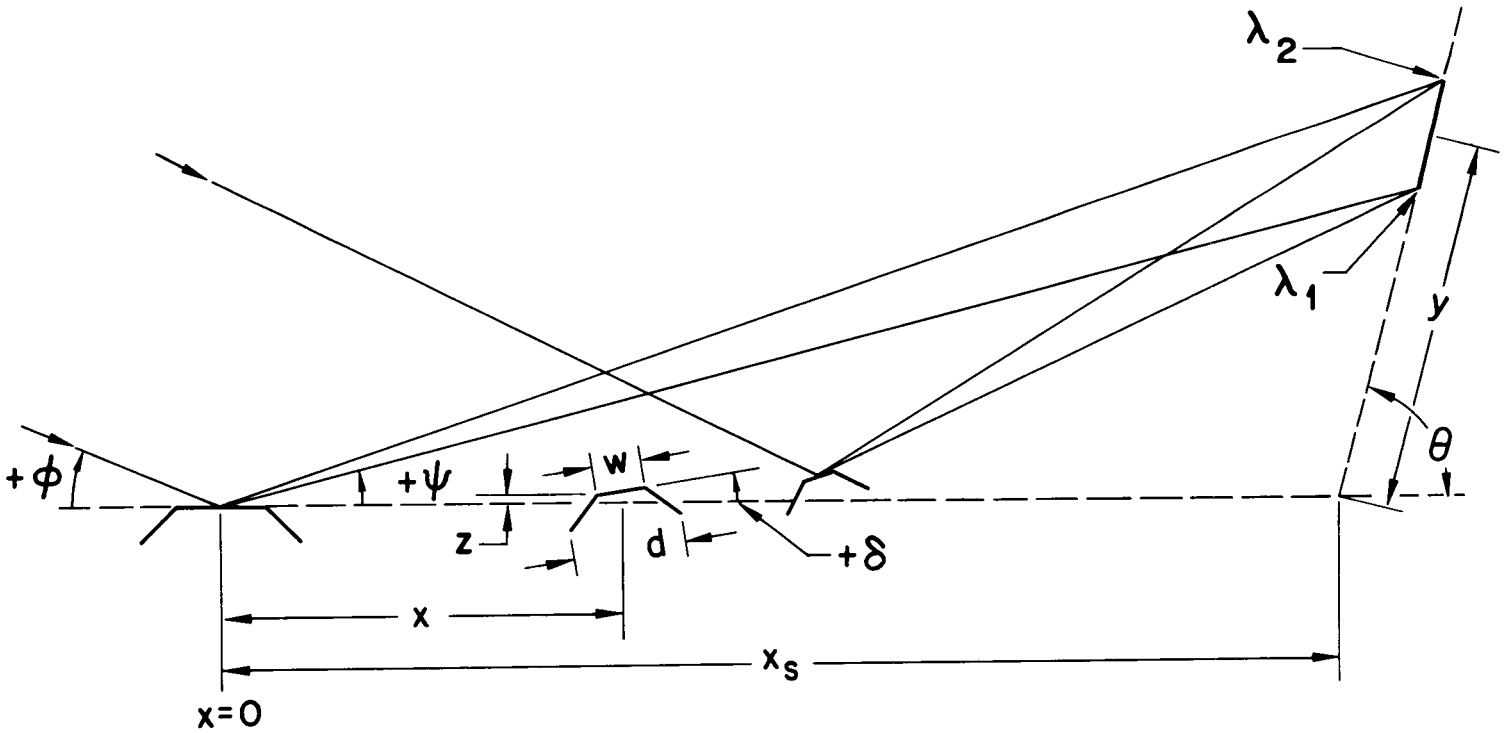

Fig. 13. Ray diagram illustrating diffraction of an incident parallel beam of photons. Perfect focus is achieved for only two selected wave-lengths, λ_1 and λ_2, of the incoming radiation.

only a small spread of wavelengths reaching any similarly oriented intermediate line on this plane. Of the similarly oriented lines in the remainder of the image plane, only those quite near the two foci can be associated with a suitably small spread of wavelengths. Upon allowing for the change of grating characteristics, equation 5-1 becomes:

$$\frac{n\lambda}{d_x} = \cos(\Phi_o + \delta_x) - \cos\left(\tan^{-1}\frac{y}{x_s - x} - \delta_x\right), \text{ where} \qquad (5\text{-}2)$$

Φ_o = grazing angle of incidence relative to the x axis

d_x = spacing of ruled grooves at position x,

δ_x = tilt of elemental grating at position x,

y = position of diffracted beam in image plane,

x_s = overall length of spectrograph, and

x = position along grating where diffraction is being considered.

The remaining symbols are identical to those used in equation 5-1. This formula describes diffraction from a continuous grating like that suggested in Figure 13 when the image plane is normal to the x axis ($\theta = 90^o$) and all reflecting elements of the grating touch the straight base line defined by the x axis. Figure 13 indicates that the lands between pairs of grooves are spaced at progressively further distances from the base line, this spacing being defined by the quantity z in the figure. To allow for this spacing in equation 5-2, the quantity y must be replaced by y-z. A grating mosaic is designed by determining the variation of d_x, δ_x, and z, with x for a given spectrum order and angle of incidence. The mosaic's dispersing ability is completely defined by solution of the pair of simultaneous equations which are available from the requirement that equation 5-2 must be valid at each of the two wavelengths selected for perfect focus at two selected points on the image plane. Appendix C is a listing of the computer program which has been used to investigate the design of an idealized grating mosaic.

All of the calculations cited in this report assume resolution problems arising from the natural width of a spectrum line are negligible. As laboratory measurements of ground-level transitions of low atomic number

elements yield typical line widths of the order of 1% in energy, much better instrumental resolution would be of little use. The 1% resolution specification used here refers only to instrumental effects. To determine whether a particular mosaic is capable of yielding the desired energy resolution over a reasonable energy interval, equation 5-2 must be solved (for several arbitrarily selected positions in the image plane) for a variety of wavelengths. The computer program given as Appendix C does this by determining what wavelength will reach a given image plane line as a function of where on the grating the diffraction occurred. Assuming a flat incident x-ray spectrum, the calculation yields both the maximum spread of photon energies and the mean photon energy reaching a given image plane line. While the ratio of these two quantities is a measure of the energy resolution that a given grating can achieve, in this part of the report that ratio is labeled as a spectral impurity. This nomenclature is used because the calculations of idealized gratings were not sufficiently comprehensive to yield a well-defined energy resolution.

Figure 14 presents some typical results of this type of calculation. The curves labelled C and D in the figure indicate the results obtainable when a grating designed for use with x rays incident at an angle of 1.5° is actually used under these conditions. The anticipated good performance does exist near the photon energies of 0.6 and 2.4 keV, which were selected for perfect focus. The rapid degradation of performance at more extreme photon energies is also apparent. If the two energies chosen for perfect focus had been more nearly equal, the spectral impurity at intermediate energies could have been reduced. However, that improvement would have been obtained at the expense of degraded behavior at other more extreme energies.

The two dashed curves labelled A and B in Figure 14 show the degradation of performance which would have occurred if the grating had been designed for use at angle of incidence of 1.5° but actually was used at an angle of incidence that was larger by 1 min of arc. Degradation of spectral purity is sufficiently severe that the grating could only be used if it can be accurately pointed (to about 1 min of arc) at a very small or point source. To suitably restrict the range of angles of incidence and so retain a high

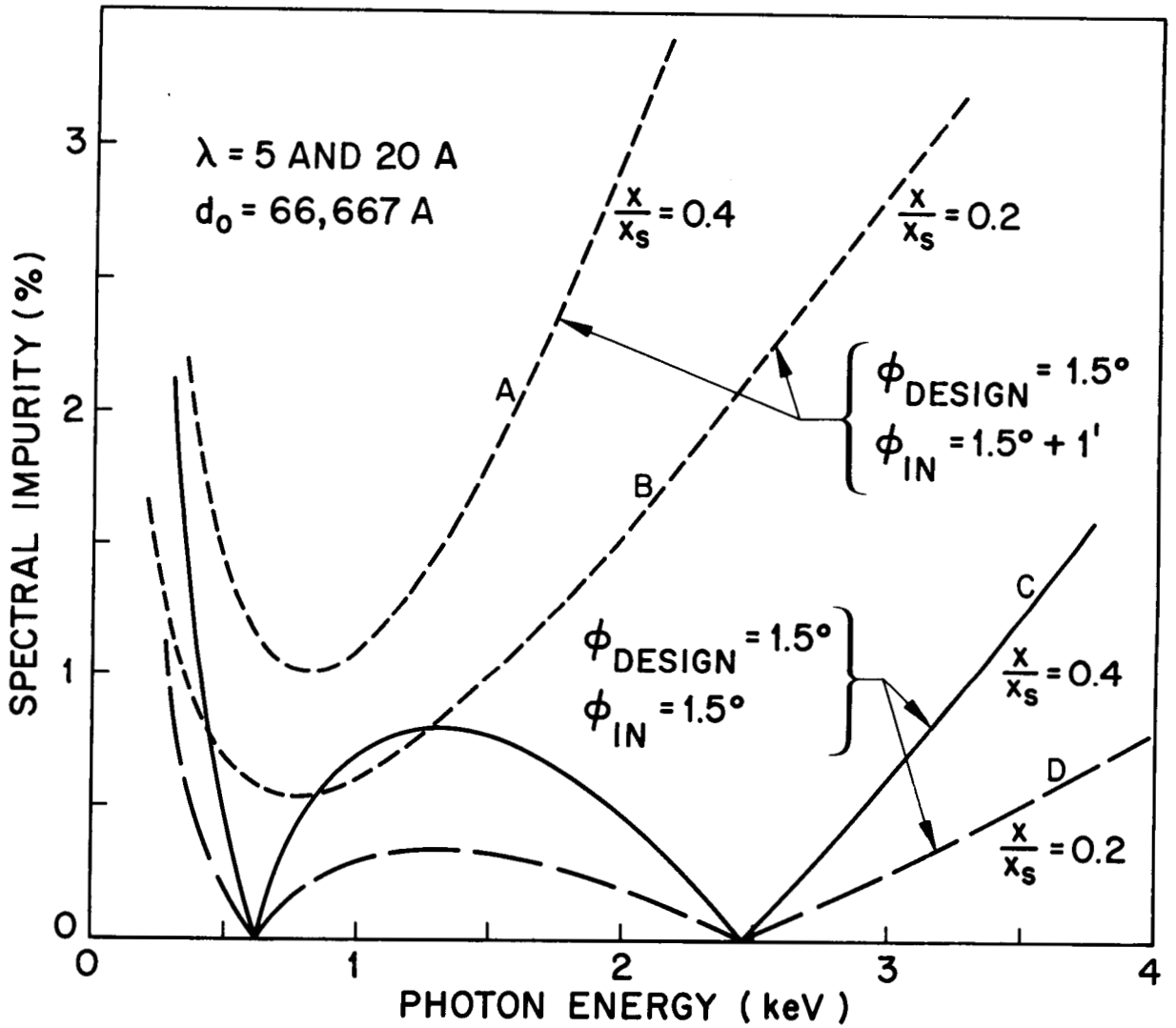

Fig. 14. Variation with photon energy of a quantity related to the energy resolution of an idealized diffraction grating mosaic, designed for perfect focusing of 5 and 20 A photons incident at a grazing angle of 1.5°. The four curves collectively represent the behavior of mosaics of two different lengths (maximum values of x/x_s) for photons arriving either on or one minute of arc off the spectrograph's design axis.

spectral resolution for a source larger than several minutes of arc in diameter, a Soller slit would be required at the entrance to the grating. Comparison of curves B and D to curves A and C of Figure 14 shows the reduction of spectral impurity that can be obtained by reducing the overall grating length by a factor of two. Although the spectral purity can be improved by decreasing the relative extent of the grating, the largest possible grating area is required if the highest possible sensitivity is to be attained.

C. Resolution of a Practical Grating Mosaic

The idealized situation which underlies the results presented in Figure 14 may not be achievable in practice if the groove spacing d_x and tilt angle δ_x are not continuous variables. It seems likely that an actual grating may have to be constructed from an array of individual elements each of which has only a single value of groove spacing. Therefore a series of calculations was carried out to evaluate the influence exerted on the mosaic's energy resolution by other characteristics of the grating, and the resolution itself was more carefully determined than in the case of the idealized mosaic just discussed.

Although the suitability of a large area array of flat grating elements has been considered, the quantization of both groove spacing and tilt angle which exists in such an array is sufficient to prevent the desired resolution from being attained. A significant, though still insufficient, improvement in resolution was found to occur when several different groove spacings were used on each grating element having a single tilt angle. As the best way to achieve the desired large-area good-resolution grating is to utilize curved (concave) grating elements, the computer program listed in Appendix D was written to include the effects of curved grating elements.

Because of the more comprehensive calculations performed, the behavior of the mosaic can be described in terms of an approximate resolution rather than the spectral impurity previously used. This resolution was found by accounting for the variety of wavelengths diffracted to a given line in the image plane from successive portions of the grating, just as had been done for the idealized mosaic with continuously variable groove spacing. By dividing the complete grating mosaic into several hundred elements, and determining the number of elements which would diffract

photons in a given wavelength interval to a given image plane position, distributions of the relative number of rays diffracted into several wavelength intervals versus wavelength were obtained. Figure 15 summarizes the approximate resolution for a typical grating as determined by such calculations. While a continuous variation of resolution with photon energy exists, the principle concern here was a determination of the photon energy interval within which a resolution $\sim$ 200 could be obtained. Consequently, the high resolution portion of the three Figure 15 curves has been omitted in the figure. Approximate resolution is defined here as the ratio of the average photon energy in the distribution at an image plane line divided by the spread of photon energies which embraces two thirds of all rays diffracted to that line. For the results given in Figure 15, the mosaic was considered to have 64 elements possessing different radii of curvature and each element was ruled with three different values of groove spacing. The computer program used to obtain these results assumed that z (see Figure 13) was equal to zero. If all the grating's reflecting surfaces touched the base line, then one grating element might partially shadow the next grating element. Although the aperture of the grating mosaic might be reduced, energy resolutions calculated with the aid of Appendix D are valid. It should be noted that the elemental gratings were originally considered to be composed of plane segments, each possessing a single value of tilt angle. Consequently, the radius of curvature of each element was determined by finding the intersection of the lines normal to the centers of the first and last pair of plane segments of each grating element.

D. A Practical Grating Mosaic

A resolution as high as 200 was sought in most of the grating's intermediate energy range in order to leave some margin of error for imperfect construction of an actual mosaic. The approximate resolutions that have been calculated usually do not attain this resolution throughout the desired range but appear to be adequate throughout a reasonable energy interval. Therefore the mosaic whose resolution is indicated by Figure 15 would be adequate for a flight spectrograph. The behavior shown in the figure seems to result from a nearly constant wavelength interval being required to encompass two-thirds of the photons arriving at a single image plane line. Consequently, the resolution is best for a range of relatively low photon energies. Figure 16 gives the approximate variation with position

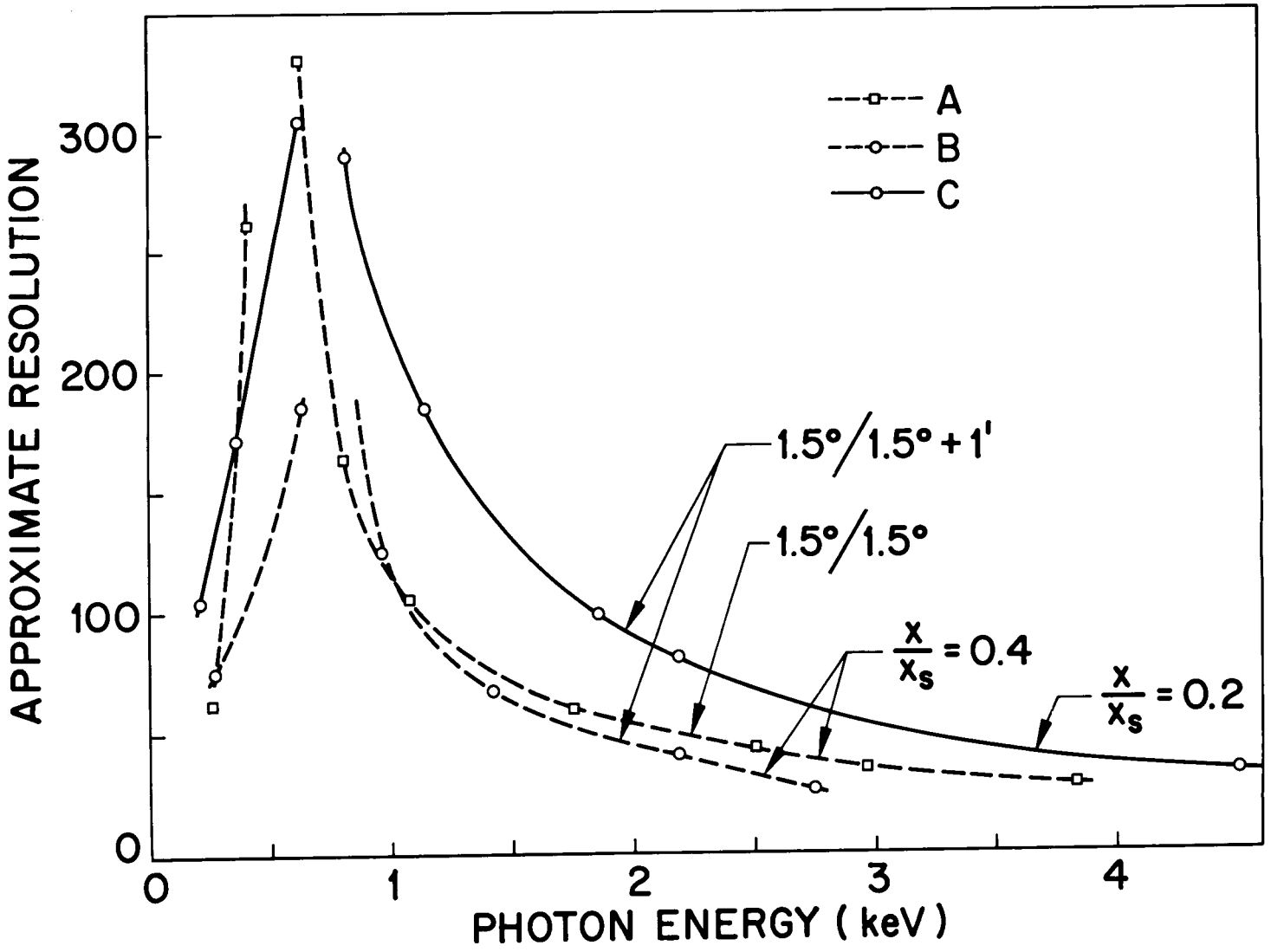

Fig. 15. Variation with photon energy of the resolution of a practical approximation to the idealized grating mosaic whose behavior was described in Figure 14. The groove spacings and curvatures of the elemental gratings of this particular mosaic have been restricted to a smaller number of values. The effects of changing both the overall length of the grating (maximum value of x/x_s) and the angle of incidence are shown.

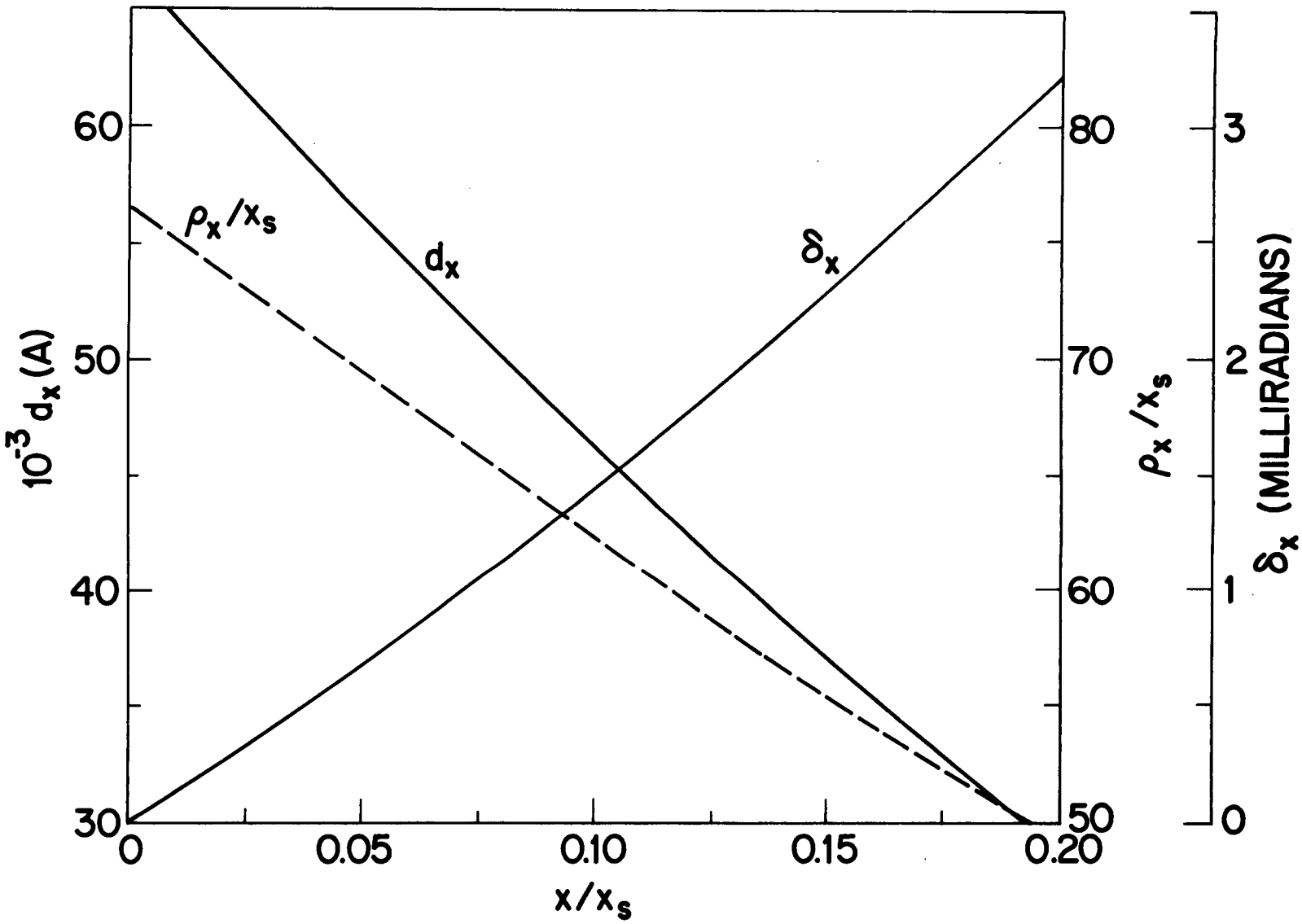

Fig. 16. Change with position along the grating of groove spacing d_x, curvature ρ_x/x_s, and tilt angle δ_x, of one particular mosaic design.

along the grating, x/x_s, of groove spacing, tilt angle, and radius of curvature, (expressed in units of x_s) of the mosaic whose approximate resolution is given by Figure 15. The variations are not precise because the array is actually a set of many discontinuous elements and these discontinuities have been smoothed over in the figure. The location off the reference plane ($y = o$, when $\theta = 90^o$) of diffracted photons of various energies is given by Figure 17.

While the results of Figures 15 through 17 do indicate that a suitable spectrograph can be designed, not all of the parameters used in understanding the behavior of the idealized mosaic have been allowed for in these calculations. In particular, the computer code of Appendix D does not calculate values of the quantity z shown in Figure 13. Experience with results from the idealized grating computations showed that about the same spectral impurity occured when different z were allowed for as when all z were set equal to zero. That situation is believed to also exist here. Therefore while the performance of the grating mosaic has been fairly correctly assessed, the precise shape of the actual grating still must be specified. While the rudiments of a computer program which would include such second order effects in the code of Appendix D have been considered, the results of Figures 15 through 17 were obtained without these additional refinements and so must be considered of a preliminary nature. In actual practice, errors arising from the grating curvature being a discontinuous function of position along the grating would be reduced as well as those errors which might be traced to the diffracting surfaces all being tangent to the base line.

So far, no results have been discussed for image planes oriented at other than 90° to the base line. A few calculations have been made with image planes tilted at angles of 45° and 135° to the reference plane ($y = o$) and the results indicate an energy resolution comparable to that found for an orientation of 90°. No improvement of resolution via deformation of the shape of the image plane has been attempted here, and no consideration has yet been given to the (potential) blaze of the grating. About a one percent spread in photon energy is inherent in transitions involving the K shell of a low Z elements and this natural line width has been consistently neglected in the calculations. Finally, it may be worth noting that the 0.2 to 3 keV energy interval should be quite free of mixed first and second order spectra.

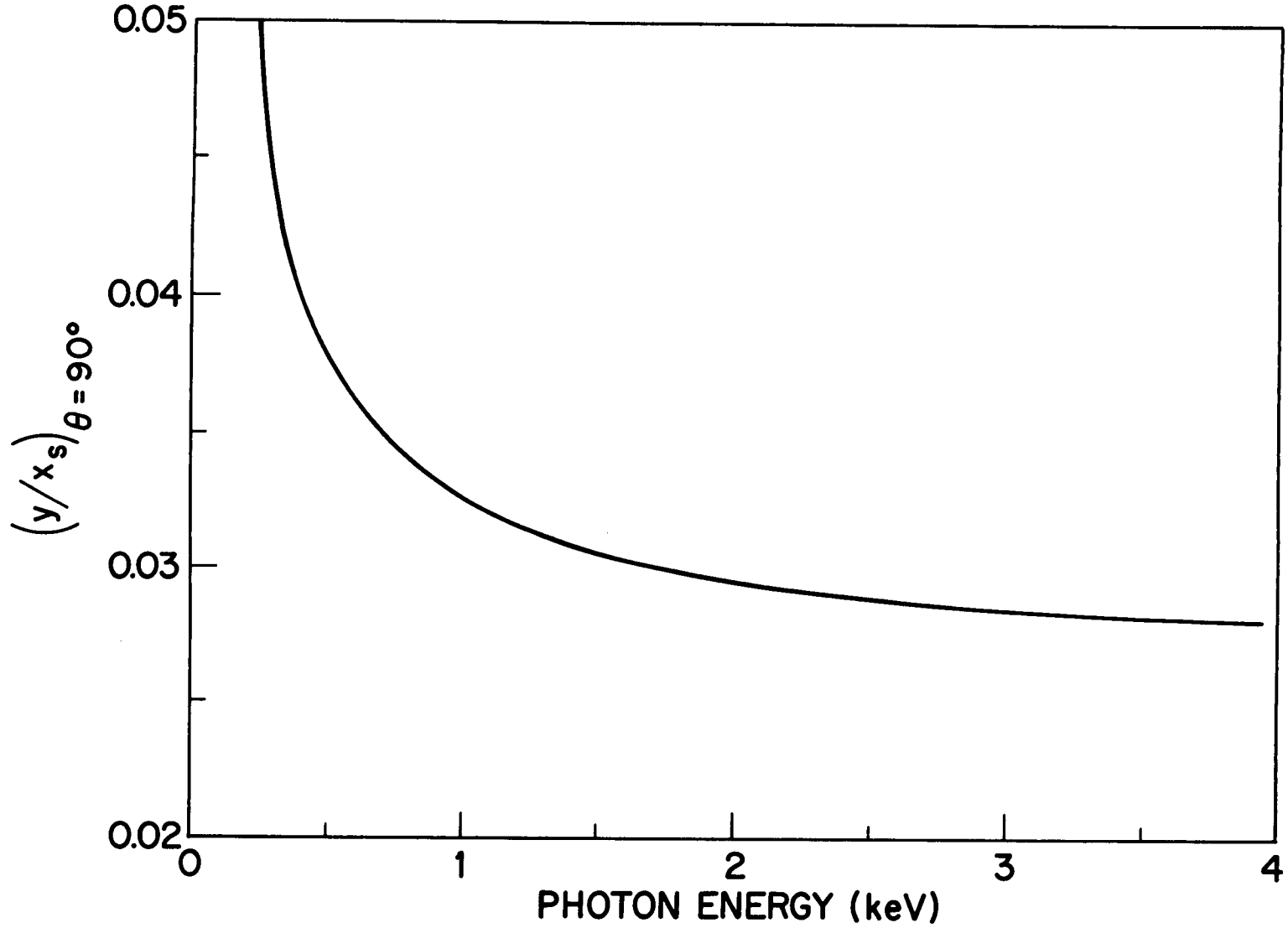

Fig. 17. Relative position on the spectrograph's image plane of photons of various energies. Once the actual length x_s of a spectrograph has been defined, this curve can be used to determine the resolution (say in lines per mm) required of the spectrograph's x-ray detector.

E. Estimated Efficiency of a Practical Grating Mosaic

The immediately preceding discussion has been primarily devoted to describing the design of a grating mosaic possessing desirable energy dispersing properties. In addition to dispersive ability, a useful grating must possess a reasonably high diffraction efficiency. To arrive at an optimum efficiency, the various permissible orders of diffraction, the critical wavelength of the diffracting material, the absorption coefficient of the diffracting material, the shape of the ruled grooves, and the effects of blaze of the grating, must all be considered and properly allowed for.

All the preceding results have assumed the spectrum in the first outside order was to be examined. However, calculations and measurements of Lukirskii and Savinov[13] show that for a given angle of incidence, a greater diffraction efficiency can prevail if the relatively shorter wavelengths are observed in the first inside (rather than first outside) order. The first inside order would appear between the zero order spectrum and the grating's surface. To date, the improvement of diffraction efficiency available via use of inside orders has not been considered worth the hazard of the greater scattering effects which might be anticipated. Although a quantitative measurement of these scattering effects can be made, this may only be meaningful for gratings of an actual flight mosaic.

It is assumed here that a necessary, though not sufficient, condition for obtaining a high diffraction efficiency is that the angle of incidence be restricted to a value smaller than the critical angle. A large critical angle is obviously beneficial as the effective aperture of the mosaic is directly proportional to the angle of incidence, which is limited by the critical angle permissible. Large critical angles are associated with grating surfaces of high-density high-Z materials. The critical wavelength for the outside orders can be calculated as a function of angle of incidence and groove spacing by using a formula for total external reflection cited by Sprague, Tomboulian, and Bedo[14].

$$\delta \lambda_c^2 - \frac{n \lambda_c}{d} - (1 - \cos \Phi) = 0, \text{ where} \qquad (5\text{-}3)$$

Φ = grazing angle of incidence,

d = groove spacing,

λ_c = critical wavelength,

n = spectrum order (+1 for the first outside order), and

δ = (1 - index of refraction) / (wavelength)^2

$= \frac{\rho}{2\pi} \frac{e^2}{mc^2}$ where ρ is the number of relatively free electrons per unit volume.

The quantity δ(wavelength)^2 is photon energy dependant so that accurate evaluation of equation 5-3 is difficult. In addition, there could well be errors in the few existing experimental values of δ at very low photon energies that are traceable to contamination of the reflecting surface by foreign (low Z air) atoms. Interpolation of results of Lukirskii et al.[2] and Hildenbrand (cf Cosslett and Nixon[15]) for gold surfaces, and allowance for discontinuities at the N II and N III absorption edges of gold, leads to the curves shown in Figure 18. The curves are for photons incident at grazing angles of incidence of 1.5° and 2.5° on gold-coated diffraction gratings. As few data exist, no curves are given for photons less energetic than (the absorption edges near) 0.3 keV. The region below each curve indicates the circumstances required for efficient diffraction, greater efficiency being obtainable at photon energies significantly below the relevant curve. Measurements like those related to Figures 18 and 19 indicate that equation 5-3, which specifies conditions for high reflection efficiency, is only a rough guide to the highest energy photon which might be diffracted under given conditions. The run of photon energies diffracted into the first inside order could also have been given in the figure. It would then have been apparent that to diffract photons less energetic than a given limiting value, either a small angle of incidence on a relatively sparsely ruled grating, or a slightly larger angle of incidence on a more finely ruled grating, was permissable. Because of the potential background from scattering mentioned earlier, and a concern over the detailed shape of the grating surface, effort so far has been directed toward use of outside orders and sparsely ruled gratings.

Experimental verification of the discontinuities which can occur near absorption edges of a grating material is given in Figure 19. This figure shows the ratio of the intensities of the zero and first order

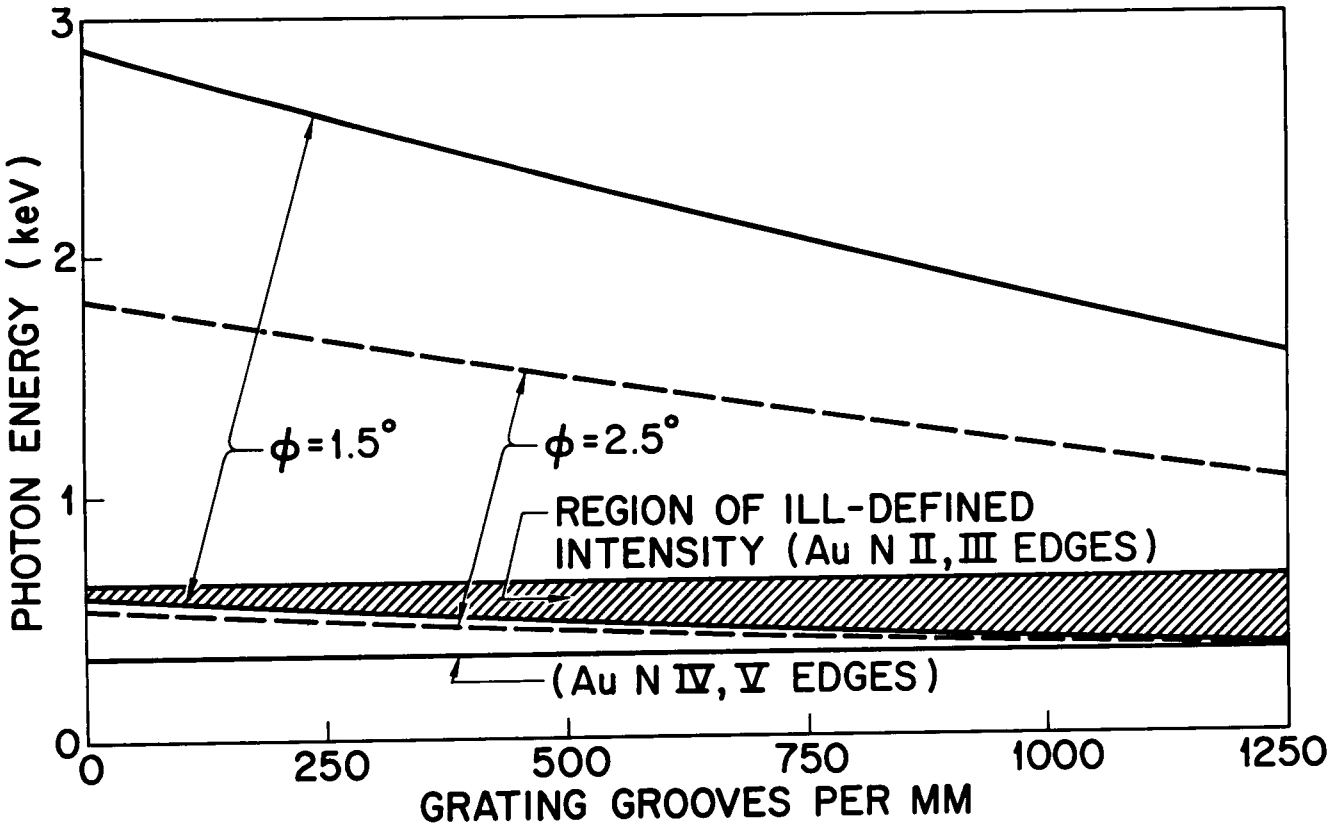

Fig. 18. The portion of this diagram below any particular curve indicates the range of photon energies at which efficient diffraction into the first outside order may occur for a particular grating spacing, angle of incidence Φ, and material.

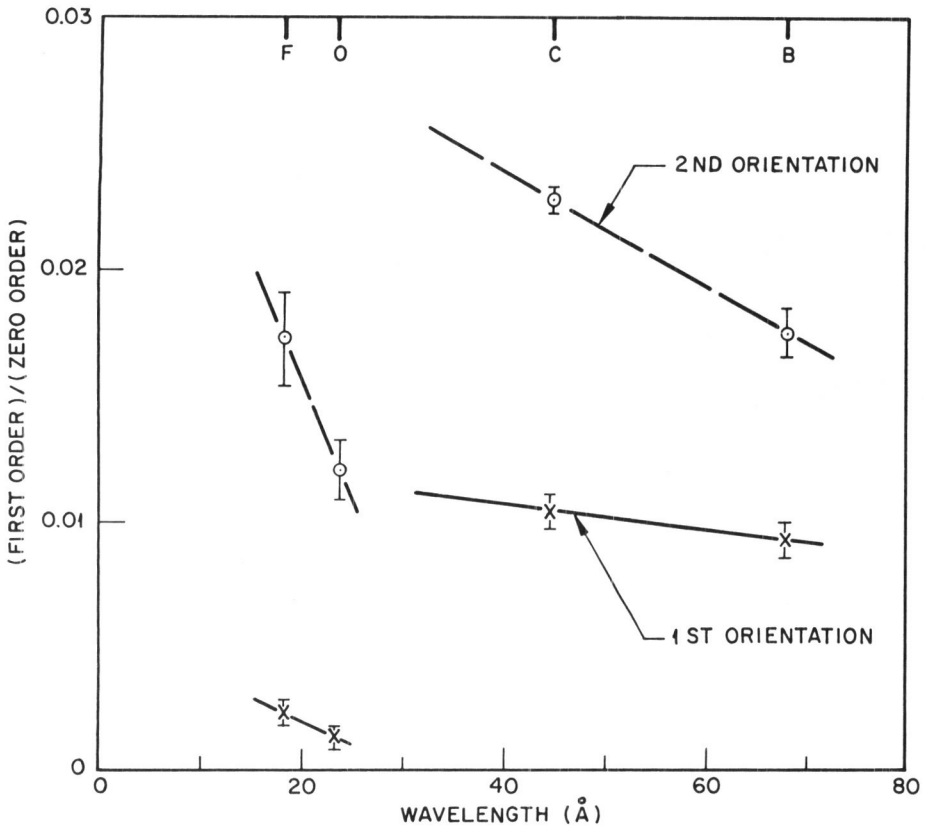

(a)

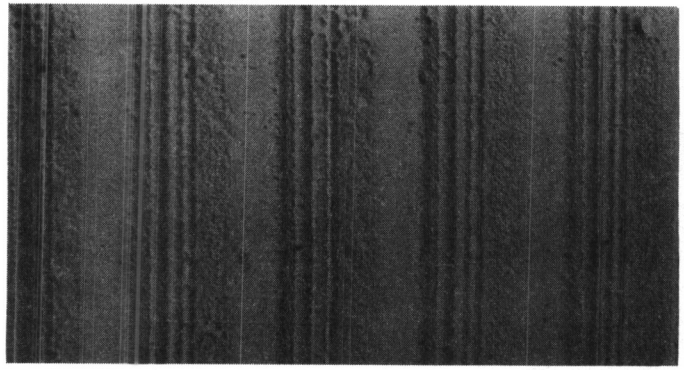

(b)

Fig. 19. Unpublished results of some 1963 measurements of the relative efficiency of a Siegbahn-type diffraction grating. Part (a) gives measured efficiencies obtained before and after reversal of the grating's orientation (with respect to the incident beam of photons). Data taken in the two orientations have been denoted by the symbols X and ⊙. Part (b) is an electron microscope view showing the plowed-up edge of each ruled groove which caused the results of part (a).

images as determined by 1963 measurements in this laboratory of monochromatic photons incident at a grazing angle of $\sim 4^{\circ}$ on a grating advertised to be of the Siegbahn (or non-blazed) type. The discontinuity near the oxygen K-edge arises because of the oxygen in the glass (i.e. silicon dioxide) grating. The grating had a one meter radius of curvature and was part of a "Rowland circle" monochromator described by Fisher, Kirkpatrick, and Meyerott[16]. Dispersed spectra were analyzed as a function of both angle of diffraction and photon energy, a thin-window gas flow proportional counter like that described by Fisher et al.[17] being used for the latter measurement. The error bars on the experimental points are arithmetic errors resulting from simply averaging the results of four to five experimental determinations of each datum. As only a few photon energies were used, the results for the two grating orientations are given as a pair of line segments covering photon energies on either side of the discontinuity from the oxygen absorption edge. Data given in Figure 19 also show that the grating was in fact blazed, and this evidence was corroborated by the electron microscope picture of the groove profiles shown in part (b) of Figure 19.

The detailed geometric shape of the grating's surface is the final item to be noted. The ratio of reflecting surface to groove spacing must be $\sim\frac{1}{2}$ (cf Sprague, Tomboulian, and Bedo[14]) for high efficiency diffraction into the first outside order. In addition to this, the grating must either be unblazed or deliberately blazed for the wavelength region of interest. Considerable pains must be taken to preserve a desirable grating surface during the fabrication of an actual grating mosaic. While Figure 19 indicates that even some Siegbahn-type gratings possess a blaze, Sayce and Franks[18] have shown how simple it is to obtain truly unblazed gratings.

F. Laboratory Verification of Spectrograph Behavior

(1) X-ray Optics

The x-ray optics of the spectrograph were mocked up in the laboratory as shown schematically in Figure 20 and in reality in Figure 21. Characteristic x-rays of aluminum (at 1.5 keV) and oxygen (at 0.5 keV) were allowed to illuminate portions of a pair of flat platinum-coated diffraction gratings. The grating closer to the source was ruled with

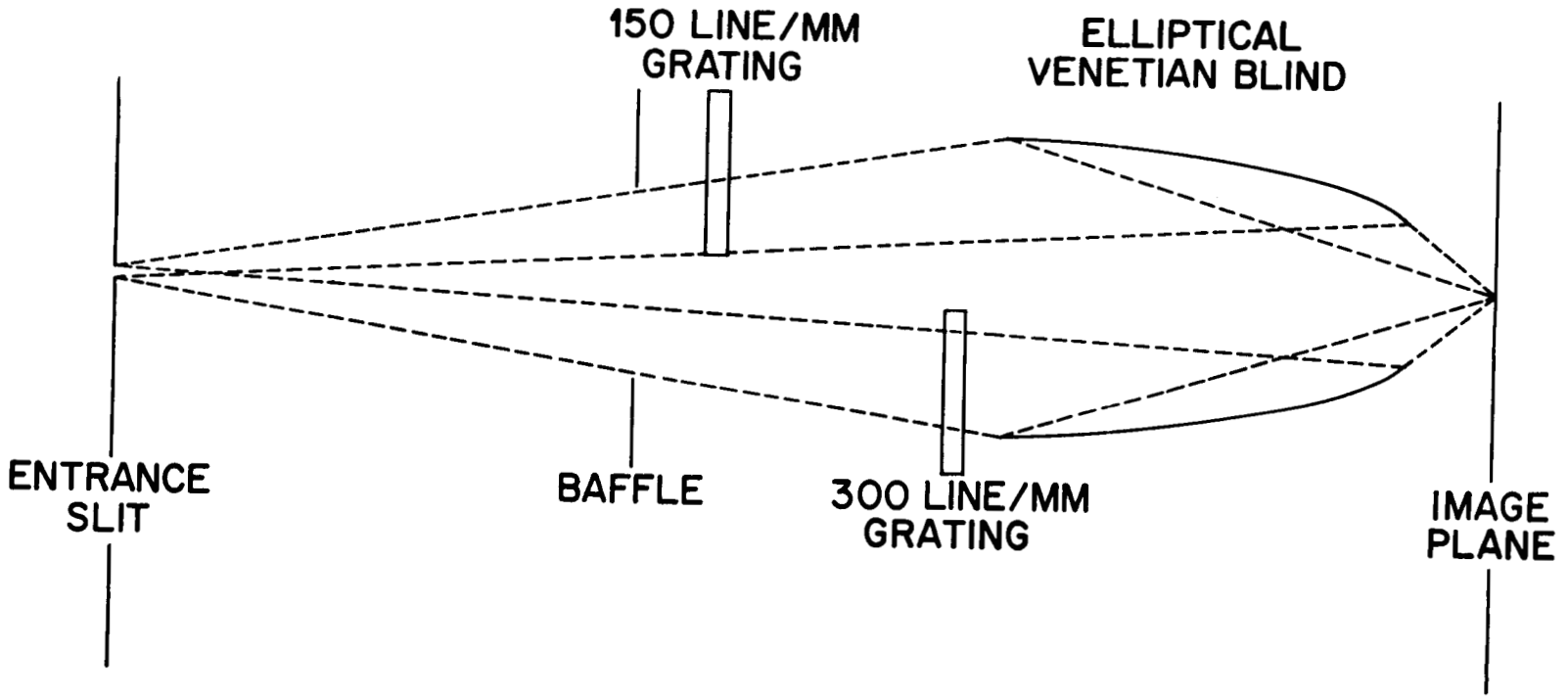

Fig. 20. Schematic of laboratory mockup used to verify the spectrograph's x-ray optical concepts. The reduction of scale in the direction of the radiation is ten times that of the reduction in the transverse direction.

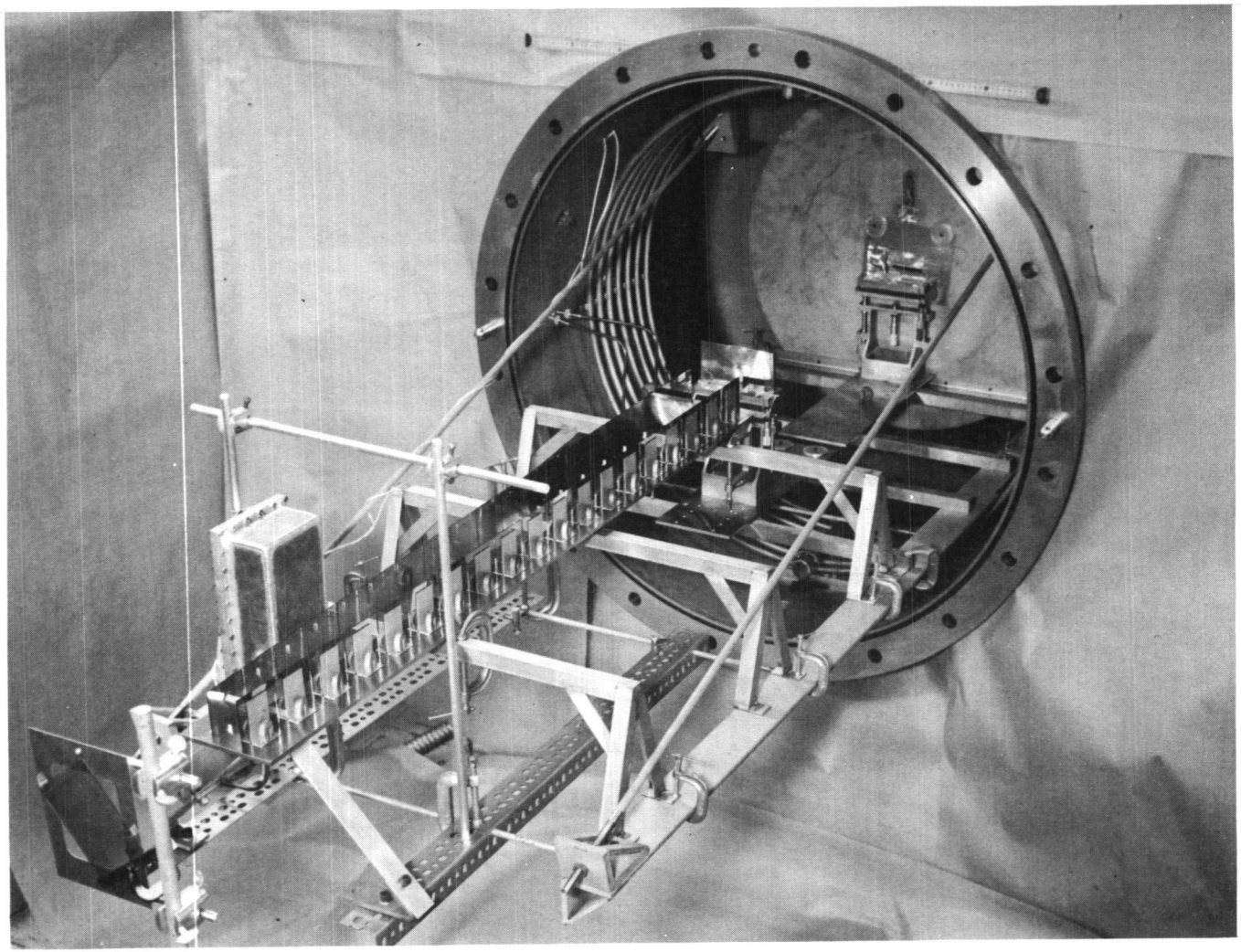

Fig. 21. Photograph showing apparatus used to mock up the spectrograph of Figure 12. X rays entered the system through a narrow rectangular slit at the far right of the system, and then shone on gratings in the pair of holders to the right of the rather rudimentary Venetian blind. A photographic plate at the far left of the system was used to record the results of each test.

150 lines/mm while the grating further from the source was ruled with 300 lines/mm. The locations of the gratings and their inclinations to the incident x-ray flux were chosen so as to produce superposition at the image plane (in the coordinate for dispersion), of the spectra from the two gratings. Appreciable first outside order diffraction of aluminum K-radiation was secured by using grazing angles of incidence of $\sim 1^{\circ}$. Because of the divergent nature of the x-ray source, the half centimeter long entrance slit was situated at one focal point of an ellipse and the Venetian blind was given an appropriate elliptical (rather than parabolic) curvature. The elliptical reflecting surface was approximated by 2" x 2" x 0.06" gold-coated pieces of glass (which eventually were found to possess notably wavy surfaces). Spectra appeared at the second focal point of the design ellipse and were recorded by Kodak type SWR photographic emulsions.

In order to indicate the amount of dispersed radiation that could be collected, and to prove correct relative orientation of the two gratings, the initial photographic exposures were taken without the Venetian blind of Figures 20 and 21 in place. The final exposure of this nature is presented here as Figure 22. While spectra from the 150 line/mm grating are easily distinguished at the left of the figure, spectra from the apparently less efficient 300 line/mm grating at the right of the figure are just barely recognizable. The short black line near the center of the figure is a reflection from the 300 line/mm grating holder, while the solarized image at the bottom right is from x-rays which passed directly over (and so were unaffected by) the 300 line/mm grating. A majority of the large amount of blackening of the photographic plate between the oxygen K-radiation and the zero order spectrum from a given grating is due to x rays scattered by imperfections of the grating surfaces. The existance of such imperfections can be inferred from the zero order spectra. Both of the gratings used for the tests were blazed at an angle of 8° 38' for their intended use in infra-red studies. As the x rays shone on the gratings from a direction opposite to that specified for the infra-red situation and at grazing incidence angles of $\sim 1^{\circ}$, the advertised grating groove shape should have prevented the existance of any zero order spectra. That such spectra do exist and are also intense is attributed to departures of the real grating surface profile from the idealized representation.

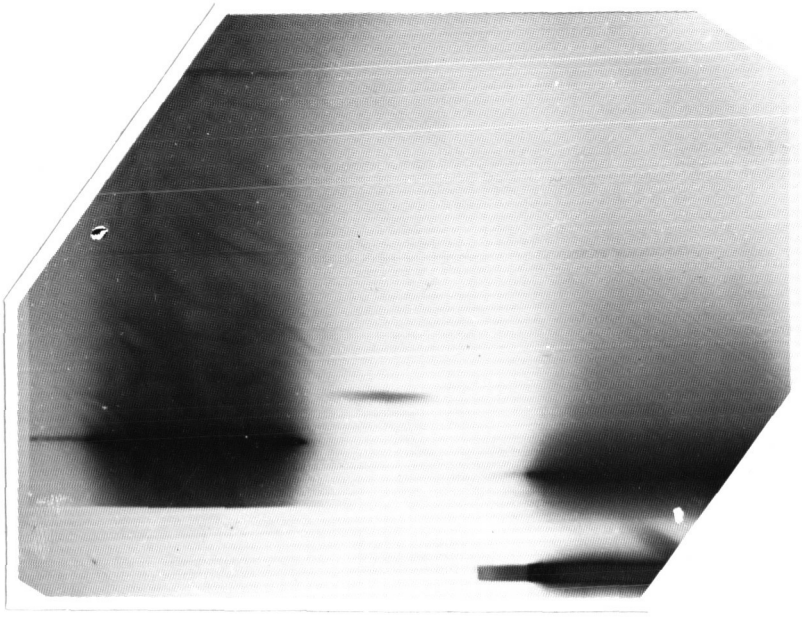

Fig. 22. Full scale reproduction of spectra of aluminum and oxygen K-radiations in the first outside order, and zero order, dispersed by gratings arranged like those of Figures 20 and 21. Spectra of oxygen appear near the top of the figure. In this particular situation, the different angles of incidence and the different orientations of the two gratings resulted in the zero order spectra not being lined up although the first order spectra were.

Addition of the Venetian blind image compressor behind the two gratings completed the mockup of the x-ray optics and lead to the images shown in Figure 23 (a) and (b). The spectra at either side of each of these pictures are from diffracted x-rays which proceeded directly to the photographic plate and so were unaffected by the presence of the Venetian blind. The central spectrum is from x-rays which have been both dispersed (by the gratings) and reflected (by the Venetian blind). Both oxygen and aluminum radiations are noticeable in the Figure 23 (a) spectrum associated with the 150 line/mm grating. However, the lower reflection efficiency of the Venetian blind for 1.5 keV photons as compared to 0.5 keV photons has resulted in no obvious image of the aluminum line in the central spectrum. The low diffraction efficiency of the 300 line/mm grating was the cause of no spectrum from that grating appearing at the side of Figure 23 (a) (although affects of oxygen K-radiation are barely discernable on the original photographic plate).

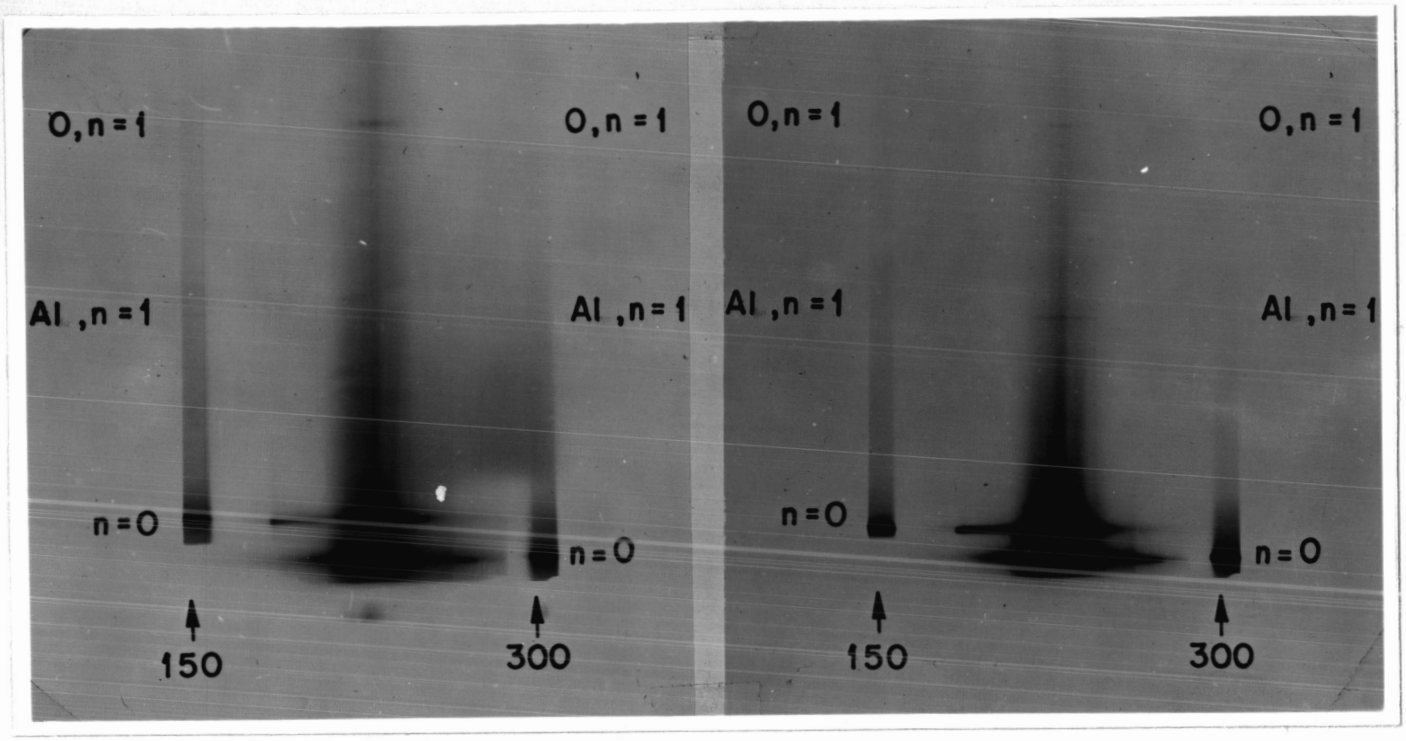

(a) (b)

Fig. 23. First order spectra of aluminum and oxygen K-radiations and separate zero orders taken with x-ray optical setup of Figures 20 and 21. The exit end of the Venetian blind was sufficiently open that a portion of each dispersed spectrum proceeded to the image plane unaffected by the Venetian blind. These spectra appear immediately above the number denoting the grooves/mm of the grating. The different features have been labelled according to the order of diffraction n and the chemical symbol for the element emitting the radiation. The different exposure times used to obtain the various spectra are discussed in the text.

To compensate for the different diffraction efficiencies of the two gratings, an exposure for a spectrum from the 150 line/mm grating was made for only one fourth the time that was used to obtain the spectrum from the 300 line/mm grating. Figure 23 (b) shows the result of such an experiment. The much shorter exposure (as compared to the times used in obtaining the Figure 22 and 23 (a) results) for the spectrum from the 150 line/mm grating has lead to its spectrum showing effects of only the aluminum K-radiation. Obviously the Venetian blind has functioned as intended as both oxygen and aluminum K-radiations are present in the central image. The significant length of the various central image features in the direction parallel to the grooves

of the gratings is a result of the finite size of the source slit, the imperfect nature of the Venetian blind reflecting surface, and the fact that the photographic plate was displaced several inches from the spectrograph's true focal plane. Although the effect can not be seen in Figure 23, this displacement was of use in verifying that each grating contributed to the central spectrum. The imperfections already mentioned, plus the fact that the vertical dimension of the individual 2" x 2" glass flats of the Venetian blind were only parallel to within a few degrees of the image coordinate representing energy, combined to degrade the spectrograph's resolution by a factor of about two.

In spite of the various difficulties noted above, a grating mosaic evidently can be used to disperse x rays as postuated, and the combined x-ray optics does function as intended. Because of these difficulties, fabrication of the desired quality x-ray optics for a flight spectrograph now appears to be a relatively straightforward task.

(2) Electron Optics

As noted in Chapter 4, the primary electron-optics problem of the x-ray spectrograph is the first stage where x rays must be converted to a different form of radiation. The simple collection system for rocket use shown in Figure 9 was patterned after the schematic of Figure 2. Because the spectrograph requires a low noise imaging system, the device of Figure 11 was used. The 150 line/mm grating used for Figures 22 and 23 was repositioned so that dispersed radiation from it would fall on to a one inch diameter layer of CsI that had been evaporated onto the image intensifier's photocathode. Preliminary tests of the behavior of this x-ray conversion system were carried out with a CsI scintillator and a low-noise photomultiplier. Distributions were taken of pulse heights (out of the photomultiplier) that were produced by photo-electrons accellerated to 20 keV. These distributions indicated the tube's noise events occurred at a significantly lower rate than did the x-ray related events. Due to the physical size and orientation of the different elements involved, it was only possible to shine two of the three available radiations from the grating on to the CsI photocathode.

Figure 24 presents the results of the second successful exposure of an emulsion in the intensifier's image plane. Effects of the first-order aluminum K-radiation appear as the short line near the middle of the figure, while the effects of zero-order radiation form the brighter line near the bottom of the figure. The spectral lines appear against a background of x rays scattered from the grating, the approximately rectangular area of

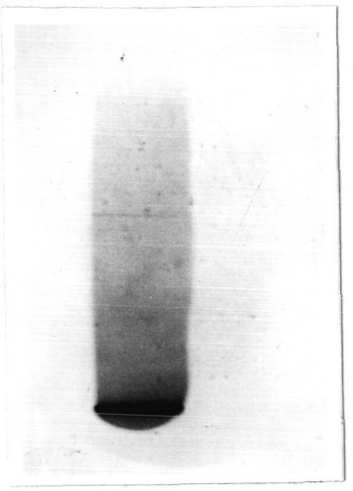

Fig. 24. Spectra from a 150 line/mm diffraction grating recorded on a photographic plate placed at the image plane of the device shown in Figure 11. The original photographic image has been magnified by a factor of two for the reproduction given here.

this background region being defined by the entrance aperture shown in Figure 11. The above features lie within a much weaker ill-defined background region whose limits correspond to those of the intensifier's CsI converter. Although extensive measurements could not be made under this contract, the low noise feature of this system is apparent as the background from the CsI photocathode is nearly insignificant even though the exposure was of two hour duration. The exposure time was a factor of six shorter than that used for obtaining the similar results of Figure 22. The fiber optic-equipped RCA intensifier will be subjected to similar tests when it is received, but the background noise probably will be large compared to that of the bare-photocathode results shown above. As seems true of the x-ray optics discussed earlier, it does not appear possible to make significant further progress without constructing a complete spectrograph, testing it, and then flying it on a rocket.

G. Anticipated Performance of a Satellite Spectrograph

Combination of an x-ray optical system having components based on those shown in Figure 12 with an electron optical system patterned after that of Figure 10 appears to provide a satisfactory basis for the spectrograph first proposed in January 1963.

The efficiency of an actual flight unit will be a product of the conversion efficiency of x rays to photoelectrons as given by Figure 8 (if a bare photocathode is used), the collection efficiency of the Venetian blind as shown in Figure 7, and the grating's efficiency for diffraction into the first outside order (the grating's effective aperture is here arbitrarily taken to be 5% of the grating's projected aperture). The product of these three efficiencies

is given in Figure 25, which assumes CsI was used for the x-ray converter. The projected aperture of the grating mosaic of a single 2.5 meter long instrument, such as could be fitted into an OAO, might be some 10 cm^2. On the basis of Figure 25, the instrument's effective aperture is found to vary from a minimum of $\sim 1/50$ cm^2 at a photon energy of ~ 2 keV to a maximum of $\sim 1/4$ cm^2 at photon energies ~ 0.5 keV. Consequently, an exposure time of some three hours would be required to measure as many as 1000 photons (assuming no significant spectral features) from a source having a flux of ~ 0.6 photons cm^{-2} sec^{-1} keV^{-1} near one keV. Only about four minutes of observing time would be required to measure the same number of photons from the brightest x-ray source in Scorpius.

By resorting to the instrument design of Figure 12, where 4 complete spectra are acquired simultaneously, twofold weaker sources might be observed. Other improvements in spectrograph design, might lead to a still larger aperture by a factor of five. Furthermore, ability to fly an instrument of scaled up size would permit the aperture to be increased by at least the scale factor. Contemporary gas proportional counter measurements of the spectra of discrete x-ray sources may well suggest that efficient examination of the flux of 0.2 to 0.5 keV x rays is less important than efficient examination of 2 to 3 keV x rays. Should this prove true, it may be more appropriate to use a scintillator than a bare photocathode as the x-ray conversion element of the several-stage image amplifier of a satellite spectrograph. A relatively modest improvement (decrease) of the noise level of existing photocathodes might render feasible this type of converter. The dashed curve in Figure 25 indicates the limiting efficiency which might be obtained if a CsI or NaI scintillator (rather than the CsI converter) had been used for the initial stage of the x-ray detector.

With the limited calculation procedures employed, the approximate energy resolution of 100 appears attainable for a point source no more than one arc minute off-axis for an energy range of about 0.2 to 1.8 keV. While it was not possible to achieve the desired resolution of 200 throughout the 0.3 to 3 keV range, it is believed that a more accurate calculation of an actual grating mosaic would show that a wavelength resolution of 200 is obtainable for about an 0.3 to 1.5 keV energy interval. If a grating with continuously variable spacing can actually

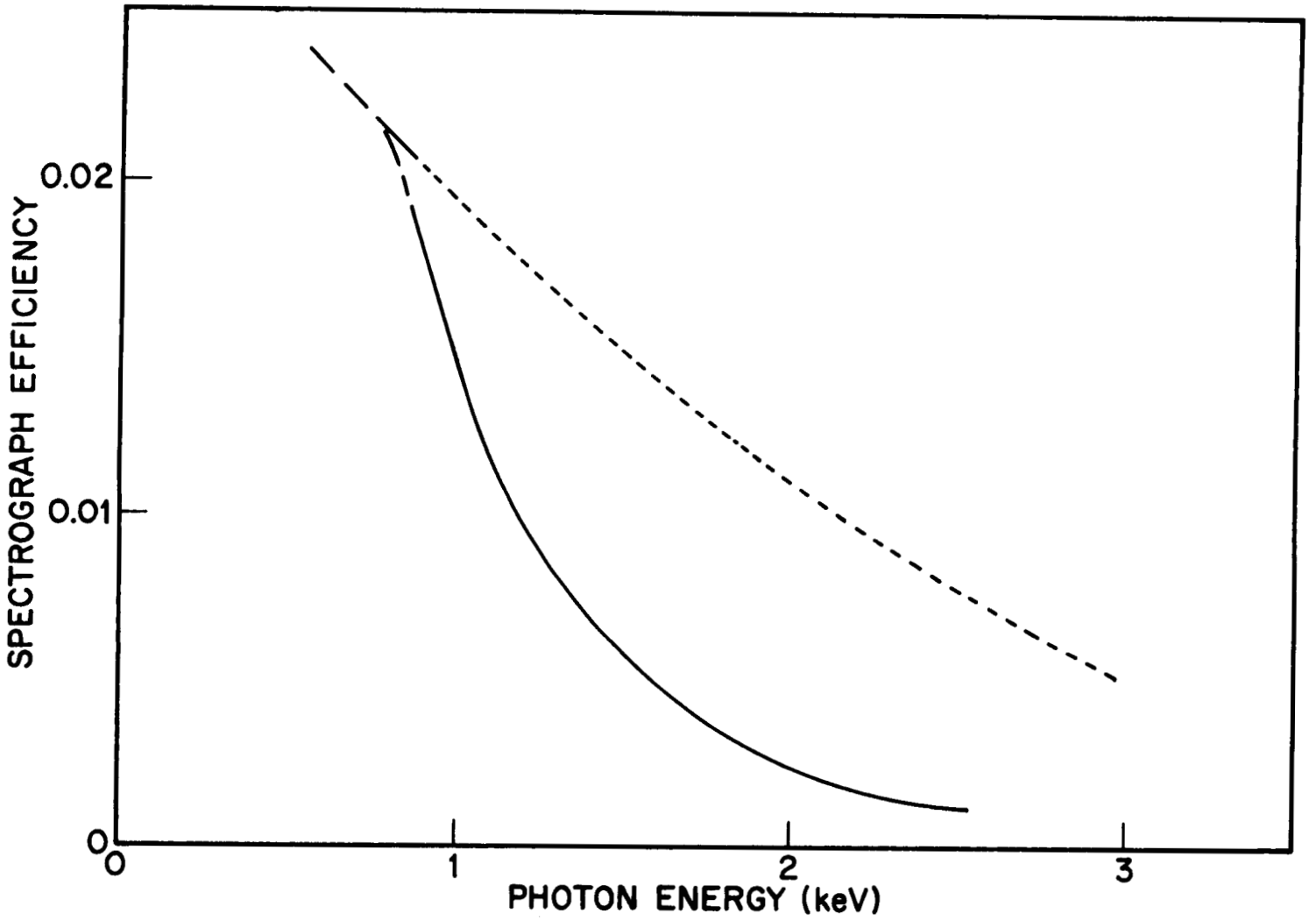

Fig. 25. The estimated efficiency of a complete spectrograph (as given by the solid curve) is the product of the efficiencies of the CsI converter, the Venetian blind, and the diffraction grating. The dotted curve indicates the efficiency which might be obtained from a spectrograph employing an x-ray converter of unit efficiency.

be fabricated, the .3 to 3 keV energy range originally desired might actually be obtained. Resolution of features of stellar spectra should be comparable to that obtained with the solar spectrograph of Blake et al[19].

6. SUMMARY OF STUDY RESULTS

A. Problems Solved

1) On the basis of laboratory tests, the x-ray optical concepts of a medium resolution ($\sim 1\%$) spectrograph have been proved valid.
2) The electron-optical concepts of one type of x-ray converter which could be used with the above spectrograph have undergone cursory laboratory testing, and the general procedure is suitable for incorporation into either rocket or satellite experiments.
3) Both a Venetian blind mirror array and one version of a bare photocathode detector have been constructed. While both units were flown on an Aerobee rocket in 1965, several difficulties resulted in no useful data being obtained. The Venetian blind, which has been used in an x-ray spectrograph to collect and form a line-shaped image of the dispersed x-rays, may well find application as one of several components in other x-ray optical devices.
4) A large area gas proportional counter array (for OAO-A1) was constructed and successfully maintained its calibration during a year of extensive pre-launch environmental tests.

B. Problems Still to be Solved

1) A capacity to fabricate suitable gratings for a flight spectrograph should be developed, and the detailed x-ray characteristics (with regard to effective blaze, diffraction efficiency, background from scattering, and ghosts) of these gratings must be established.
2) While difficulties in the operation of simple bare photocathode and scintillation devices have been experienced and overcome in the laboratory, the flight use of very low noise image amplifiers based on such x-ray converters may not yet be well understood. Further experimental evaluation of the low energy

($\lesssim$ 2 keV) portion of the spectra of discrete x-ray sources is needed before a well-founded choice can be made of whether to use a bare photocathode or a scintillator in the x-ray conversion stage of an image amplifier for satellite use.

3) Although the usefulness of both the Venetian blind system for high sensitivity survey work and the x-ray spectrograph for spectral measurements seems obvious, successful rocket demonstrations of these instruments' value has not yet been made.

7. RECOMMENDATIONS AND CONCLUSIONS

1) Pre-flight behavior of the OAO-A1 array of gas proportional counters was sufficiently straightforward that some excellent reason must be established if a satellite experiment based on large-area gas counters and detection of few-keV x rays is to be operated in the Geiger rather than in the proportional region.
2) While neither the high-sensitivity Venetian blind system nor the medium-resolution x-ray spectrograph have yet been proven in flight, they both appear sufficiently promising as to merit inclusion in tentative plans for future space astronomy experiments (of both solar and stellar phenomena).
3) In view of scheduling difficulties, a small-scale effort for developing grating ruling techniques should be separately and immediately funded if flight of the x-ray spectrograph described in this report is approved in principle. The quality of currently available conventional gratings for use at x-ray energies is so low that a significant attempt at improvement of ruling techniques seems worth the effort.
4) In situ evaluation of the behavior and background problems of both bare photocathode and scintillator-equipped image amplifiers should be performed where convenient. Potential satellite use of spark chambers for recording soft x-ray information should be examined.
5) A rocket version of the medium resolution ($\sim$ 1%) spectrograph should be constructed, exhaustively tested in the laboratory, and then flown.

REFERENCES

1. L. M. Rieser, Jr., J. Opt. Soc. of Amer., 47, 987 (1957)
2. A. P. Lukirskii, E. P. Savinov, O. A. Ershov, and Yu. F. Shepelev, Optics and Spectroscopy, 16, 168 (1964)
3. P. Kirkpatrick, X-Ray Optics and X-Ray Microanalysis (Academic Press, New York) 247 (1963)
4. R. Giacconi and B. Rossi, J. Geophys. Res., 65, 773 (1960)
5. A. V. Baez, J. Geophys. Res., 65, 3019 (1960)
6. R. L. F. Boyd, Space Science Reviews, 4, 35 (1965)
7. R. Giacconi, N. F. Harmon, R. F. Lacey, and Z. Szilagyi, J. Opt. Soc. Amer., 55, 345 (1965)
8. A. Lansiart, J. P. Morucci, and G. Roux, Proc. of the 10th Scintillation and Semiconductor Counter Symposium (1966) to be published
9. A. P. Lukirskii, M. A. Rumsh, and I. A. Karpovich, Optics and Spectroscopy, 9, 343 (1960)
10. A. P. Lukirskii, M. A. Rumsh, and L. A. Smirnov, Optics and Spectroscopy, 9, 265 (1960)
11. M. Rome, R. V. Gauthier, and J. P. Causse, IEEE Trans. on Nuc. Sci., NS-11, 120 (1964)
12. G. T. Reynolds, Applied Optics, 5, 577 (1966)
13. A. P. Lukirskii and E. P. Savinov, Optics and Spectroscopy, 14, 147 (1963)
14. G. Sprague, D. H. Tomboulian, and D. E. Bedo, J. Opt. Soc. Amer., 45, 756 (1955)
15. V. E. Cosslett and W. C. Nixon, X-Ray Microscopy, (Cambridge University Press, Cambridge) 89 (1960)
16. P. C. Fisher, P. Kirkpatrick, and A. J. Meyerott, Production of Photons in the 0.05 to 1.0 keV Energy Interval, Report No. AFSWC-TDR-61-98 to the Air Force Special Weapons Center, Kirtland Air Force Base, New Mexico (November 1961)
17. P. C. Fisher, A. J. Meyerott, H. A. Grench, R. A. Nobles, and J. B. Reagan, IEEE Trans. on Nuclear Science, NS-10, 211 (1963)
18. L. A. Sayce and A. Franks, Proc. Roy. Soc. A., 282, 353 (1964)
19. R. L. Blake, T. A. Chubb, H. Friedman, and A. E. Unzicker, Astrophys. J., 142, 1 (1965)

APPENDIX A

HIGH SENSITIVITY DETECTORS FOR FEW-KEV X-RAYS*

P. C. Fisher and A. J. Meyerott

Lockheed Missiles and Space Company
Palo Alto, California

ABSTRACT

Three different types of instrumentation with high detection sensitivity for investigation of cosmic x-ray sources are considered in some detail. The first instrument is designed for detection of photons in the 2 to 20 keV energy interval. Large aperture is achieved by ganging together the outputs of many individual gas proportional counters. An x-ray experiment with a total aperture of ~0.1 m^2 has been constructed for use on the first Orbiting Astronomical Observatory. The overall nature of this package is discussed and some details of the behavior of the gas counters and their associated electronics are given. Data from flight of similar well-collimated counters on Aerobee rockets suggests the background counting rate is proportional to the wall area of the gas counter. Therefore, instruments combining x-ray optics with a smaller detector are of value. Systems using both aplanatic and Venetian blind optics are considered. Some details are given of a rocket-sized Venetian blind detector that was flown for investigation of 0.2 to 3 keV photons.

INTRODUCTION

High detection sensitivity for observations of extra-terrestrial sources of soft x-rays in the 0.1 to 20 keV energy range can be obtained with a gas proportional counter whose output pulses can be pulse-height analyzed. The background counting rate in such a counter can be reduced by an anticoincidence shield and the collecting area of the counter can be increased by an x-ray collection device.[1] This paper is in part devoted to consideration of the influence of the background counts on the detection sensitivity of the counter. Measured pulse-height distributions of background events obtained with gas proportional counters flown on several Aerobee rockets are presented and several different geometries which successfully preserve the counter's inherent energy resolution are described. Then the general features of an x-ray experiment designed for investigation of 2-20 keV photons for the first Orbiting Astronomical Observatory are discussed.

Finally the behavior of a complementary system for 0.1 to 6 keV photons, utilizing x-ray optics which focus in only one dimension, is considered. While an imagining system with two-dimensional focusing has already successfully photographed the sun,[2] its restricted field of view is a serious handicap in survey work. Therefore the characteristics of the recently developed one-dimensional focusing system, which overcomes this disadvantage, are discussed. Although a comparison of the effective collection apertures of the Venetian blind and paraboloidal collectors has been made,[3] an appraisal of the actual detection sensitivity of related detector systems has not yet appeared and so is given here.

COUNTER BACKGROUND AND SENSITIVITY

Two distinct types of background counts have been observed during several rocket flights of gas proportional counters. While the majority of the background counts in a well-collimated (~.03 ster field of view) detector appear to arise from energetic charged particle and gamma effects, a small portion is due to a diffuse (background) flux of x-rays originating in sources other than the one under study. Comparison of flight results obtained with two quite different gas counter configurations indicates the penetrating radiation component of the background count in a well-collimated detection system is proportional to the counter wall area rather than to the counter volume, window area, or solid angle. Table I illustrates this dependence. As used here, wall area means the surface encompassing the counter's sensitive volume (between the inner ends of the field tubes noted in the next section). For these well-collimated 1963-1964 era counters, the 4-8 keV counting rate due to the diffuse (background) x-ray flux was only ~10% of the total background counting rate. The magnitude of this diffuse x-ray flux was determined by subtracting the counts obtained when the detector was looking down (at the earth) from the counts obtained when the detector was looking up (away from the well recognized concentrated x-ray sources in the night sky). While only meager information is available concerning the diffuse x-ray flux, the October 1964 flight yielded a value of the order of 0.8 photons cm^{-2} sec^{-1} $ster^{-1}$ keV^{-1} for photon energies in the range of 4 to 8 keV.

Further insight on background problems was derived from the March 1963 measurements[4] in which a plastic scintillator anticoincidence shield was used. Although the geometry was rather poor, the shield reduced the counter background by a factor of two. While too few counts

TABLE 1

Comparison of background rates obtained with different well-collimated counter configurations. The counter wall area and volume are for the region between the counter field tubes as discussed in the text.

Results from	Clear Window Aperture (cm^2)	Counter Wall Area (cm^2)	Counter Volume (cm^3)	X-Ray Solid Angle (sq. deg.)	Average In-flight[a] Counts/sec in 4-8 keV Interval
October 1, 1964	260	1100	1200	2.9 x 25	75
March 20, 1963	8	90	70	5 x 10	7.8
Ratio of above numbers	~30	~12	~17	~1.5	~10

a. For each counter, the effective wall thickness including rocket structure was at least 0.8 cm of magnesium. About one half of the counter used on the March 20, 1963 flight was also covered by an 0.8 cm thick plastic (anticoincidence) shield. The net effect (on background counts from energetic particles) of this difference in absorbing material is believed to be small.

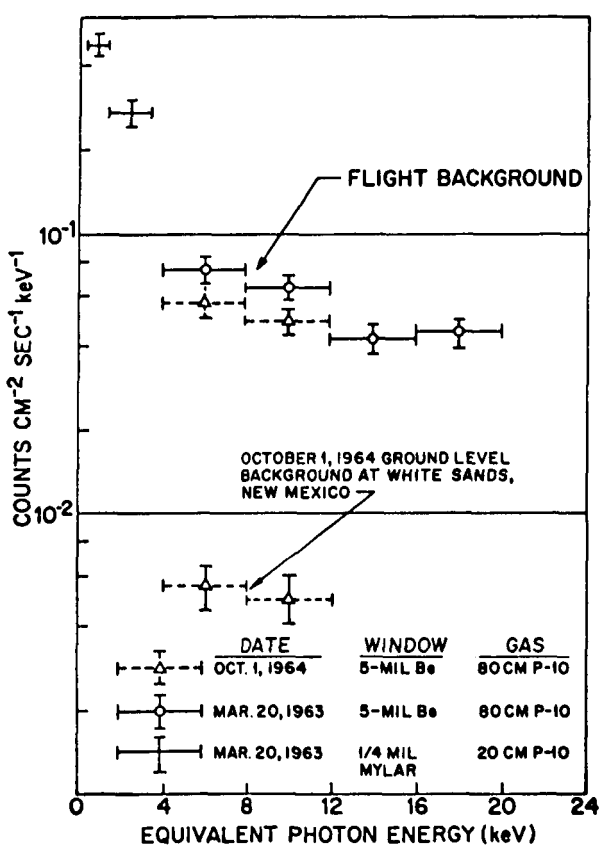

Fig. 1—Distribution of background counts as a function of equivalent photon energy obtained with several different gas proportional counters. The text defines the area of each counter used to derive values of counts cm^{-2} sec^{-1} keV^{-1}.

were obtained during the flight to yield precise background pulse height distributions, the energy distribution of gas counter pulses not associated with scintillator pulses was indistinguishable in shape or absolute magnitude from the distribution of gas counter pulses associated with scintillator pulses. This was true of pulses from both a 1/4-mil mylar-window counter which was for detection of 0.5-3.5 keV x-rays, and a similarly shaped beryllium-window counter which was used to detect 4-20 keV x-rays. The March 1963 counter pulse-height distributions (obtained without anticoincidence) are given in Figure 1, which also presents the corroborating measurements of 4-8- and 8-12-keV pulses found on October 1, 1964. To obtain the count rate per unit area given in Figure 1, an "effective" counter cross section was required. Adequate accuracy for the purpose at hand was obtained by defining the "effective" area as one-sixth of the counter's wall area. The vertical error bars of Figure 1 refer solely to statistical errors in counts in each energy interval while the horizontal lines correspond to the length of each energy interval. The two points at pulse heights corresponding to photon energies below 4 keV (from the 1/4-mil mylar-window counter) indicate a much higher background count rate than was found for pulses above 4 keV. As no corroborating evidence exists, it is not clear whether this higher level is real or spurious. As indicated in Table 1, each counter gas compartment was surrounded by roughly comparable amounts of absorbing material so that effects of mass and its distribution on the two rockets can not be accurately judged. However, the absolute level of count rate in Figure 1 for the beryllium window counters is believed to be in error by no more than a factor of three.

Consider the counter sensitivity required for acceptable detection of an x-ray source. The

minimum flux detectable might be simply derived from an arbitrary requirement that the number of counts from the source be at least three standard deviations greater than the average count. The penetrating radiation produces counts in the detector at the rate of I_b in counts cm^{-2} sec^{-1} per pulse height interval equivalent to one keV of photon energy. Allowance must also be made for the diffuse x-ray flux I_x, expressed in photons cm^{-2} sec^{-1} $ster^{-1}$ keV^{-1}, which is observed through the entrance area A_x of the detection system and through the solid angle Ω_x defined by the detector's collimation system. The photon flux from the point source is designated Φ_x and is in units of photons cm^{-2} sec^{-1} keV^{-1}. Then for an observing time t, photons from a detectable point source producing pulse heights within the energy interval ΔE (in keV) must satisfy the relation

$$\Phi_x K_x A_x t\Delta E \geq 3\sqrt{I_b(1-K_b)A_b t\Delta E + I_x \Omega_x K_x A_x t\Delta E}. \quad (1)$$

The factor $1-K_b$ represents the fraction of counts from energetic radiation that were not eliminated by the detector's anticoincidence system. K_x is the counter's efficiency for detection of photons of the particular energy being considered.

In the absence of a significant background count (the quantity under the radical of Equation 1 being less than unity), the minimum detectable flux Φ_x defined by Equation 1 is without meaning and Φ_x must be determined from the relation

$$\Phi_x K_x A_x t\Delta E \geq N. \quad (2)$$

This inequality merely states that at least N source-related events must be noted in the observing time interval t. Equation 1 fails to be significant when the angular resolution of the detector is so high that its sensing element has negligible area and therefore observes no background events during the observing time. Unfortunately, only a subjective decision can fix the numerical value for N. For computing the weakest observable source strength, N is set equal to 3 in the following discussion. While this is really too small a signal count to provide much confidence, such a criterion does indeed indicate the faintest source that might be detected in a minimum of observing time.

Anticoincidence equipped detection systems of large aperture must be employed if faint x-ray sources are to be detected and located. Several extreme but feasible systems are worth considering. These include: a) well-collimated detectors with no focusing for investigation of 2-20 keV photons, b) detectors equipped with cylindrically symmetric x-ray optics focusing in two dimensions for 1/2-2 keV photons, and c) detectors equipped with Venetian blind x-ray optics focusing in only one dimension for 1/2-6 keV photons. Although several other arrangements might be used, they are not discussed here because they are considered to be less extreme forms of the configurations just listed. A reasonable evaluation of these configurations can be attained by considering their sensitivity for detection of ~2-keV photons in a one keV wide energy interval, as this is the only photon energy range accessible to all three systems. The evaluation presented below is specifically directed at determining the minimum source strength detectable by a system with a prescribed maximum dimension.

Solution a) is equivalent to a shallow detector sandwiched between an anticoincidence shield and a passive collimation system. Assuming unit efficiency in the x-ray detector, and $A_x t$ values of 10^5 to 10^9 cm^2 sec believed to be compatible with Aerobee- and Saturn-sized launch vehicles, $\Phi_x \Delta E$ values in the range of 10^{-3} to 10^{-5} photons cm^{-2} sec^{-1} can be found. The minimum detectable source strength is limited by background effects and so Equation 1 is used to evaluate sensitivity. The limits just given were based on $A_x \approx A_b$, a field of view of 10^{-3} ster, a one keV wide energy interval, an anticoincidence shield efficiency of 95%, the penetrating particle effects of Figure 1 and the diffuse x-ray flux quoted earlier. For this choice of constants, the two causes of background were of comparable importance in fixing Φ_x for the one keV wide energy interval at $\approx 0.2/\sqrt{A_x t}$.

If the detector's energy sensitivity were rather poor, as would be the case if Geiger counters or bare photocathode detectors were used in place of proportional counters, all penetrating particle events would contribute to the background count. Therefore, if the source's x-rays occurred in only a small portion of the energy range covered by the background distribution, the limiting detection sensitivity of a given sized system could not be as large as the value just computed.

Solution b) is for imaging x-ray optics and involves a very different geometry from that of the large area detector just considered. Aplanatic optics involving matched parabolic-hyperbolic reflection surfaces of revolution have been discussed by Giacconi et al.[5,6] Kirkpatrick and Pattee,[7] and Kirkpatrick.[3] Unfortunately, efficient reflection of 1.5, 3, and 6 keV x-rays can only occur for grazing angles of incidence θ no larger than about 1.5°, 1°, and 1/2° respectively. With the maximum angle of reflection fixed, the aperture (A_x of Equations 1 and 2) for collecting radiation with an approximately conical collecting surface is proportional to L^2, where L is the overall length of the detector system in centimeters. For the prototype high-efficiency imaging telescope described by Giacconi et al.,[6] the constant of proportionality (allowing for a 50% efficient reflection at each of the two reflecting surfaces) appears to be $\sim 10^{-4}$. As a refined version of this telescope might have an aperture as high

as $\sim 5 \times 10^{-4}$ L^2 for 1.5 keV x-rays, the more optimistic aperture has been used for the present calculations. Therefore the minimum detectable source strength in a one keV wide energy interval as derived from Equation 2 occurs at a Φ_x of $\approx 6 \times 10^3/L^2t$.

Assuming unit efficiency in the x-ray counter, and L^2t values of 10^5 to 10^{11} cm^2 sec for Aerobee- and Saturn-sized launch vehicles, values of $\Phi_x \Delta E$ in the range of 10^{-1} to 10^{-7} photons cm^{-2} sec^{-1} could be observed. Because of the two dimensional focusing of the x-ray optics, the limiting detectable source strength is not determined by the penetrating particle or diffuse x-ray background effects but by the requirement that the minimum number of three events be detected. With the reflection angle fixed by the highest energy photon to be detected, a large effective collection aperture can only be achieved by resort to an optical system of large overall length. It should be noted that high angular resolution is inherent in this type of optical system and really must be utilized to keep the background effects negligible if the quoted limiting sensitivity is to be attained.

Intermediate to the two extremes just discussed is solution c) in which incoming flux from the distant point source is converged to a line rather than to a point as in case b). Consider a symmetrical parabolic cylinder or sheet with radiation approaching in a direction parallel to the axis of the parabola and normal to the focal line. The radiation reflected from the two cylindrical surfaces can be received through an entrance slit of a linearly extended counter. The overall length of this instrument (focal plane to entrance end) is taken as L and θ is the angle of grazing incidence which it would be useless to exceed. It may be shown[3] that the broadest beam which may be reflected under these circumstances has a width θL. If the collecting surface has a linear extent B in the direction normal to the incoming photon flux, the cross-sectional area of the intercepted beam is found to be proportional to θLB.

To facilitate intercomparison of solutions b) and c), the maximum entrance dimensions of the aplanatic and Venetian blind systems are here required to be equal. Admittedly this restriction of B to a value no larger than θL severely limits the Venetian blind aperture. The advantage gained from the restriction is that a single cylindrical envelope describes the overall dimensions of each optical system. Under these circumstances, the collection aperture, A_x, of the Venetian blind is proportional to L^2. Characteristics of the prototype Venetian blind system described in Section V of this article appear to be typical and yield a collection aperture (allowing for a 50% efficient reflection) of $\sim 10^{-3}$ L^2 for 1.5 keV x-rays. Because of the Venetian blinds focusing action, the counter cross section A_b may be taken to be $\lesssim 0.1$ of the x-ray collection aperture. Therefore the limiting detectable flux in a one keV wide energy interval corresponds to a Φ_x of $\sim 0.6/\sqrt{L^2t}$. This sensitivity assumed a 95% efficient anticoincidence shield. The relation derived for Φ_x applies to values of $L^2t \gtrsim 10^6$ cm^2 sec where particle background effects do indeed limit the sensitivity.

Evaluation of the desired angular resolution, the permissible detector length, and the total time available to examine a given sky area for sources of a given strength determine which type of x-ray optics should be used. For example, consider a fixed time interval were available for examination of a five to ten square degree portion of sky for faint point sources. For moderately large systems arranged to observe photon energies of the order of two keV, the nearly one square degree fields of view of both kinds of focusing optics indicate comparable times will be required by each system at each orientation needed to examine all of the sky area of interest. As noted above, the image-plane or particle-background-sensitive-area of the Venetian blind system for 0.1^o wide swath of sky is about a factor of ten less than the x-ray aperture. Comparable limiting detection sensitivities can be obtained from the two types of focusing system at a value of $L^2t \sim 10^9$, although the position accuracy from the Venetian blind measurements will be expressed as a fraction of a degree as compared to the fraction of a minute attainable and necessary (for maximum sensitivity) with the double focusing optics.

Table 2 indicates the sensitivity of some of the configurations considered above. For progressively higher photon energies than considered in Table 2, the collection aperture and field of view of the two-dimensional focusing system become progressively smaller. The resultant decrease in each of these quantities therefore requires correspondingly longer time intervals to observe a given sky area. This limitation is sufficiently severe that for values of L^2t or $A_xt \lesssim 10^9$ cm^2 sec, both the Venetian blind and the large area detector systems can observe at least tenfold weaker 6 keV sources than the imaging optical system.

It must be remembered, that in deriving the results given in Table 2, the detection efficiency of all x-ray counters has been assumed to be 100% and no consideration has been given to the practical difficulties of either obtaining or successfully flying some of the particular features assumed!

COUNTER CROSS SECTION AND RESPONSE

A special high-voltage feed-through insulator equipped with both a guard tube and a field tube has been used in the three counter configurations shown in Figure 2. To within the measuring errors of a few percent, it has been

TABLE 2

Approximate ultimate sensitivity in photons cm^{-2} sec^{-1} of several types of x-ray detection systems for ~2 keV photons falling in a 1 keV wide energy interval. Assumptions underlying these calculations are given in the text.

Configuration[a]	10^5	10^7	10^9	10^{11}	Inherent Angular
Observing time (sec)	10^1	10^2	10^3	10^4	Resolution (deg.)
Detector					
Large area	10^{-3}	10^{-4}	10^{-5}	10^{-6}	~1
2 dimensional focus	10^{-1}	10^{-3}	10^{-5}	10^{-7}	$\sim 10^{-3}$
1 dimensional focus	10^{-2}	10^{-4}	10^{-5}	10^{-6}	$\sim 10^{-1}$

a. Configuration refers to the assumed value of $A_x t$ (large area counter) or $L^2 t$ (focusing system). A_x and L^2 are in cm^2 and t is in sec.

possible to obtain constant gas gain and energy resolution for all three geometries for the entire length of the central wire, or collecting electrode, lying between the field tubes. The optimum ratio of center wire voltage to field-tube voltage in each instance was empirically determined. As can be noted in the figure, rectangular cross-section counters have been employed. Such a geometry is permissible because the gas multiplication of these proportional counters occurs essentially at the center wire.

X-RAY EXPERIMENT FOR OAO-A

A schematic view of the Lockheed x-ray experiment for OAO-A is given by Figure 3, while Figure 4 is a photograph of the portion of the package containing the x-ray detectors. The system consists of an array of gas proportional counters sandwiched between cellular

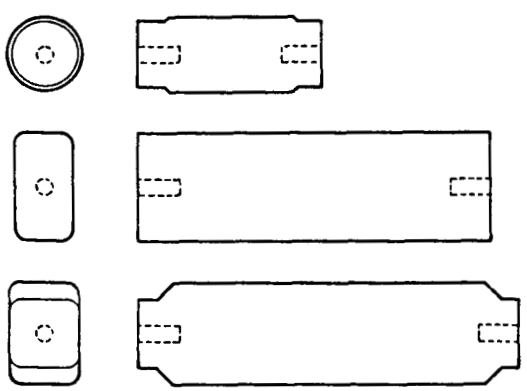

Fig. 2—Cross sections of gas chambers of proportional counters used for x-ray measurements. The dotted outline represents the field tube of the high-voltage feed-through insulator.

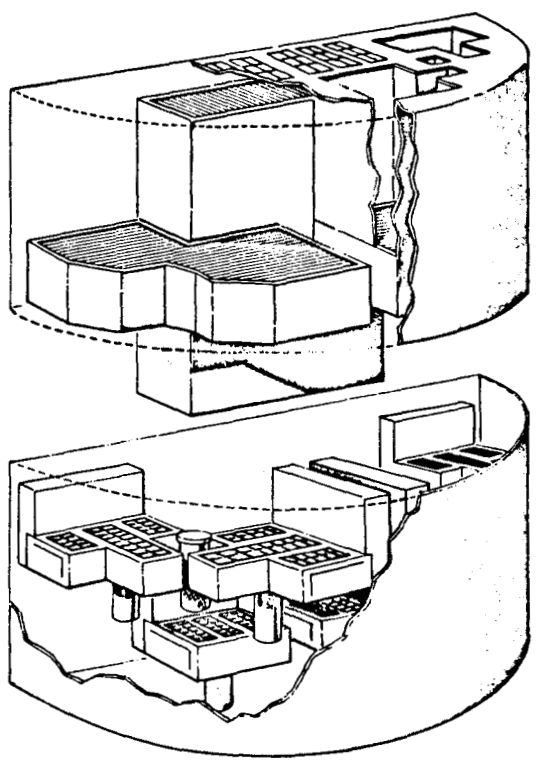

Fig. 3—Schematic of OAO-A x-ray experiment. The upper portion of the sketch contains two differently configured cellular aluminum collimators, while the lower portion of the sketch contains six gas-counter-anticoincidence-unit detectors. The gas counter windows in the lower portion of the package have been given the darkest shade of gray and subdivided into small squares.

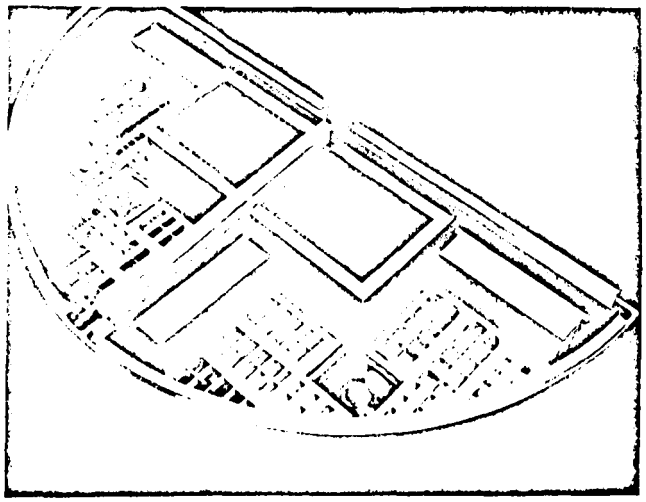

Fig. 4—View into lower half of flight package. Four separate pyramid-shaped survey-counter systems surround a portion of collimator which obscures the two separate pointed-counter systems mounted on a lower lying shelf.

collimators (which prescribe the field of view of the x-ray counters) and scintillator-photomultiplier anticoincidence units (which reject some of the background counts from the gas counters). One ideal form of large area detector would have an x-ray sensitive length (parallel to the path of the x-ray to be detected) that was negligible in comparison to the average diameter (perpendicular to the x-ray's path) of both the anticoincidence unit and the x-ray counter aperture. In the OAO-A experiment, the ratio of length to average diameter for each individual detector is only about 1:3 and so the anticoincidence shield's efficiency is much less than that obtainable from the ideal arrangement. Six completely separate detection systems are indicated in Figure 3. Table 3 lists characteristics of the four pyramid-shaped detectors shown in Figure 4, which have been labeled "survey" detectors. The two "pointed" detectors not visible in Figure 4 are shown at the bottom-most layer of Figure 3. The complete experiment was designed and finally calibrated in a four-month time interval.

Figure 5 is a block diagram of part of the electronics and shows one of the two identical halves of the survey detector system. Normal operation is illustrated by the solidly drawn output signal lines to the memory and results in a single four-channel analysis of pulses from all survey gas counters connected in parallel. On those few occasions when the spacecraft's attitude may be determined by the x-ray experiment, a greater amount of storage is available and the dotted output signal lines become useful. On these occasions an eight-channel analysis of all survey counter pulses may be acquired as well as a four-channel analysis of all pulses from the pointed counters, not shown in Figure 5. As indicated in Figure 3, the line-shaped fields of view of the two detector systems are orthogonal. Therefore more precise position information may also be obtained when spacecraft control is permitted.

The variation of counter efficiency with energy is given in Figure 6. The low efficiency for photon energies below 2 keV is due to the counter window which is equal to 6 mils of beryllium plus 1/2 mil of mylar. All counters are filled with a gas mixture consisting of 69.5% argon, 20% xenon, 10% methane, and 0.5% helium. The xenon extends the counter's useful range to higher photon energies as compared to the range obtainable with the P-10 (90% argon-10% methane) gas used previously (see Figure 6). The argon-xenon mixture also minimized argon escape peak effects arising from photons more energetic than the argon K-edge. It was felt that if xenon were the principal x-ray absorber, the combination of the small path length of the gas and L-M shell x-ray transitions in the xenon might produce an escape peak effect which would unnecessarily complicate interpretation of the lower-energy portion of any spectral data obtained.

When as much as eight-channel coverage of a moderate range of pulse height is desired, there is a choice to be made between use of stacked discriminators and conventional clock-controlled analyzers. To provide redundancy while keeping

TABLE 3
Characteristics of detectors in OAO-A x-ray experiment

	Survey Counters	Pointed Counters
Effective area (cm^2)	50 to 700	70 to 400
Field of view (sq. deg.)	2 x 8 ≈ 15	1/2 x 4 ≈ 2
Possible position accuracy (deg.)	~0.3	~0.1
Energy range (keV)	2 to ≈ 25	2 to ~25
Intervals in energy range	4 (8 if in pointed mode)	4 if in pointed mode

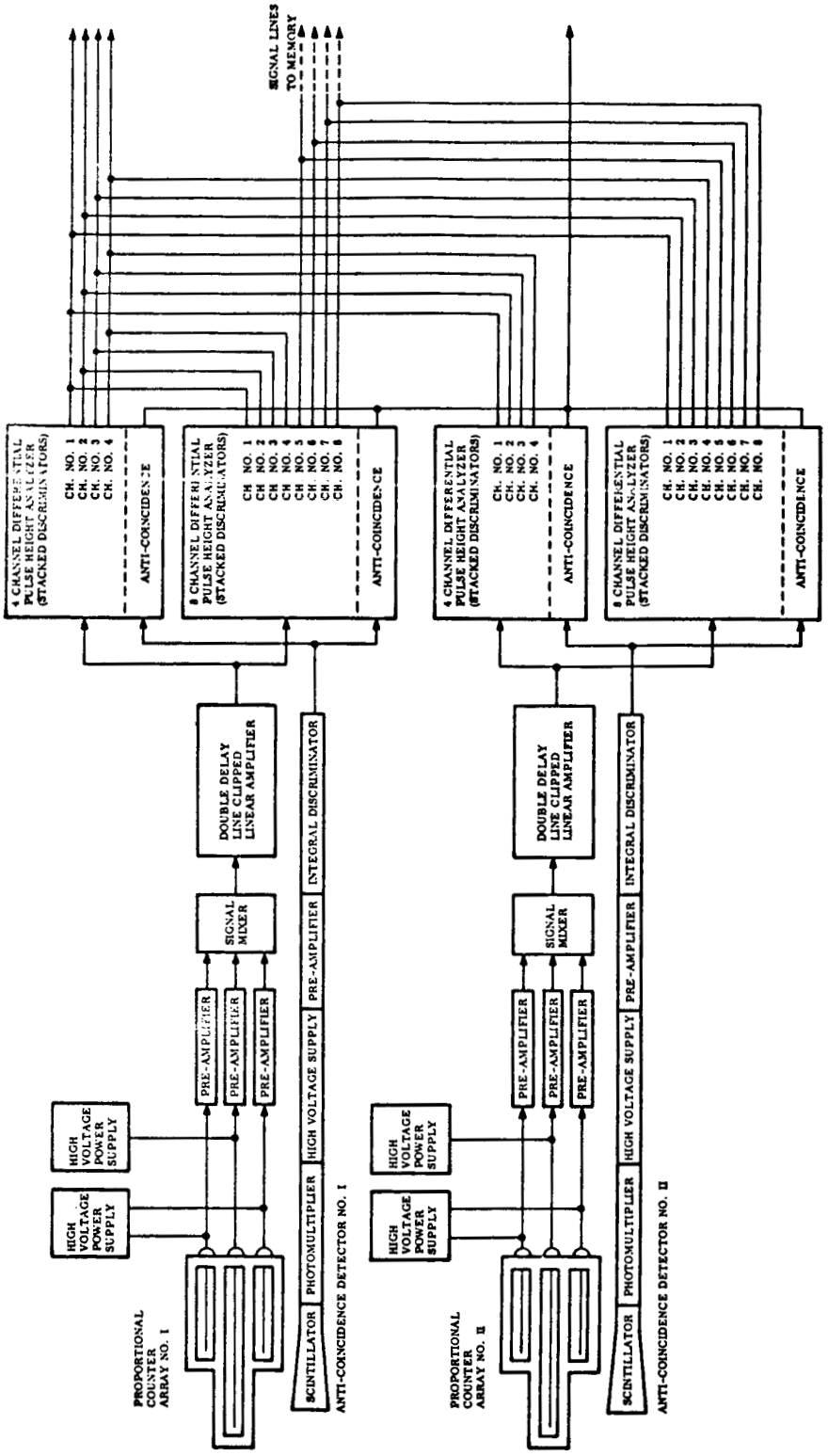

Fig. 5—Block diagram showing signal processing electronics for one-half of the survey detector system.

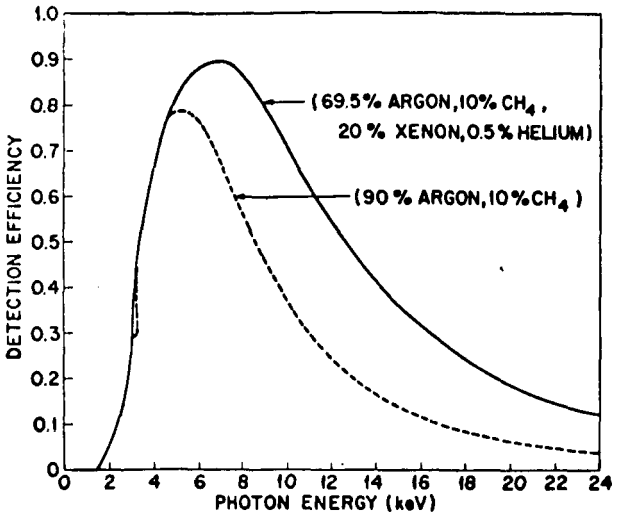

Fig. 6—X-ray counter efficiency versus photon energy for two different counter gases. The discontinuity near 3.2 keV arises from the K absorption edge of argon.

the quantity of electronics low, stacked discriminators were chosen here. The resolution obtained is indicated in Figure 7 which shows how portions of the spectrum from a Co^{57} calibration source (as measured by a 100-channel analyzer) are allocated to the eight channels of the flight electronics. At the higher photon

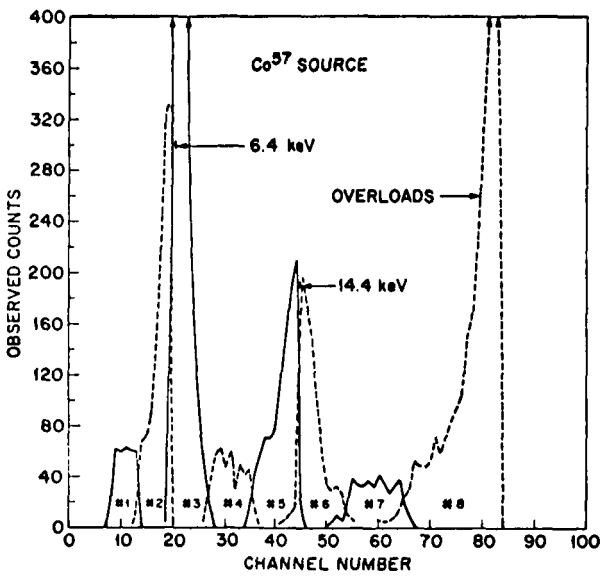

Fig. 7—Manner of division of spectrum of Co^{57} calibration source by 8-channel flight electronics. The portion of the spectrum appearing in each of the eight flight channels was displayed on a 100-channel analyzer.

energies, the width of a flight channel is about twice the inherent resolution associated with the statistics involved in the detection process itself.

While stacked discriminators are well suited to analysis of the source spectra anticipated, experience with this apparatus indicates that parallel use of four sets of eight-channel systems is a practical limit for this general procedure. The most important difficulties which arose were 1) measuring errors in establishing four sets of discriminator biases, 2) temperature shifts in counters, their electronics, and the discriminator biases (over the +40° to -40°C temperature range anticipated) and 3) the inherent resolution of the gas counter itself.

A ROCKET-SIZED VENETIAN BLIND SYSTEM

Figure 8 schematically illustrates the configuration of a one-dimensional focusing instrument flown on an Aerobee rocket on September 30, 1965. The system was 0.9 meters long and the total effective collection aperture was about 60 cm^2 at photon energies below 1.5 keV. Although the reflecting surfaces providing this aperture could have been arranged for use with a single detector, a combination of the small size of the system and the high angular resolution of the x-ray optics made it physically impossible to place two gas counters (desired for redundance) in the focal plane. For this reason, the system actually contained two complete 30 cm^2 aperture Venetian blind units as indicated. Parabolic curvature was approximated in the Venetian blind itself by subdividing each of the four reflection surfaces into a number of identical slats. Each of these slats was optically polished and then gold overcoated. The estimated variation of collection aperture with photon energy shown in Figure 9 is predicated on an ideal gold-coated optical system. No allowance was made for gold absorption effects and below about one-half keV, the efficiency estimate could be in serious error because of a) low density of the evaporated gold, or b) low-atomic-number contaminants accumulated from exposure of the optical system to air. The angular field of view of this particular instrument was about 1/2° x 12°.

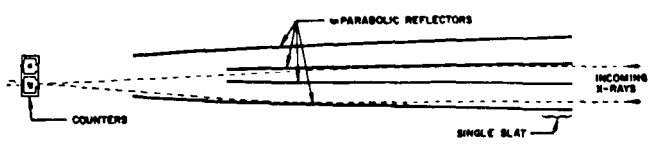

Fig. 8—Schematic of dual Venetian blind system flown on an Aerobee rocket on September 30, 1965.

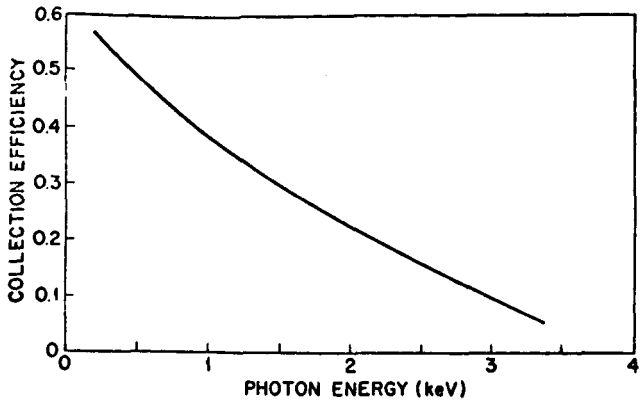

Fig. 9—Fraction of incident flux collected by the gold coated Venetian blind system of Figure 8.

SUMMARY

Large aperture x-ray detectors of different angular resolution have been considered. It appears that x-ray sources 10^5 times fainter than those currently being observed from rockets, could be detected by scaled up versions of todays instrumentation. At least the angular resolution, the detection sensitivity, and the x-ray energy interval to be examined determine the apparatus to be selected. Because the experimental sensitivity for the next decade will probably be severely limited by the observing time available, all three types of x-ray detectors discussed here should prove useful.

ACKNOWLEDGMENTS

The continued encouragement and advice of J. E. Kupperian, Jr. of NASA's Goddard Space Flight Center has been of fundamental importance to the experiments described above. The invaluable assistance of P. Kirkpatrick in the design and evaluation of x-ray optical systems is gratefully acknowledged. Comparison of the sensitivities of the different types of detectors was made following a procedure formalized by W. L. Kraushaar for large area counters. We wish to acknowledge the extensive contributions of W. C. Jordan and L. W. Acton to the OAO-A x-ray experiment. We also wish to thank A. S. Knapp, V. A. Olivier, D. T. Roethig, and K. L. Smith for assistance in design and calibration of the various detectors, and J. B. Reagan and W. G. Soltwedel for design and calibration of the electronics.

*Portions of this work have been supported by the National Aeronautics and Space Administration under Contracts NAS 5-1174, NASw-909, NASw-1073, and by the Lockheed Independent Research Program.

REFERENCES

1. P. C. Fisher, A. J. Meyerott, H. A. Grench, R. A. Nobles, and J. B. Reagan, IEEE Trans. Nuclear Science NS-10, 211, 1963.

2. R. Giacconi, private communication.

3. P. Kirkpatrick, Third International Symposium on X-Ray Optics and X-Ray Micro-Analysis, 247, 1964 (Academic Press, Inc., New York).

4. P. C. Fisher, D. B. Clark, A. J. Meyerott, and K. L. Smith, Ann. d'Astrophys. 27, 809, 1964.

5. R. Giacconi and B. Rossi, J. Geophys. Res. 65, 773, 1960.

6. R. Giacconi, N. R. Harmon, R. F. Lacey, and Z. Szilagyi, J. Opt. Soc. Am. 55, 345, 1965.

7. P. Kirkpatrick and H. H. Pattee, Jr., Handbuch der Physik 30, 304, 1957 (Springer-Verlag, Berlin).

APPENDIX B

Abstract of paper presented at the July 1966 meeting of the American Astronomical Society, to be published in the Astronomical Journal

MEASUREMENT OF STELLAR X-RAY SPECTRA

Philip C. Fisher and Paul Kirkpatrick
Lockheed Palo Alto Research Laboratories
Palo Alto, California

As has proven true for the sun, ~ 1% energy resolution studies of the spectra of stellar x-ray sources may lead to determinations of elemental abundances and the variation with time of these abundances. By evaluation of absorption effects on the lower-energy portion of a source's x-ray spectrum, information relative to distance and/or the interstellar medium might also be obtained. Fisher and Meyerott (Ap. J. 139, 123, 1964) had such investigations and a concept for an appropriate spectrograph in mind when they pointed out that a 4-8 keV x-ray flux of the order of 0.3 photons cm^{-2} sec^{-1} seemed sufficiently high to encourage attempting detailed spectral measurements. Tests to investigate the validity of this spectrograph's design are currently being made. Continuous sensitivity to photons throughout the 0.2 to 2 keV range is maintained by combining a special curved diffraction grating with a Venetian blind x-ray collector. These optics provide a line image, position along the line being a measure of the energy of the dispersed x-ray. Utilizing several spectrograms obtained from a laboratory mockup of the instrument, a brief description will be given of the spectrograph's characteristics. A conservative estimate indicates that a complete 3-meter long instrument may possess a minimum effective aperture (allowing for the inefficiency of all of the vital components) of at least 1/6 cm^2 for photons less energetic than one keV. Improvements might conceivably increase this aperture by a factor of ten.

* Between January 1963 and April 1964, this work was supported by the Lockheed Independent Research Program. Since the latter time, most all of the effort has been under contract NASw-917 of the National Aeronautics and Space Administration.

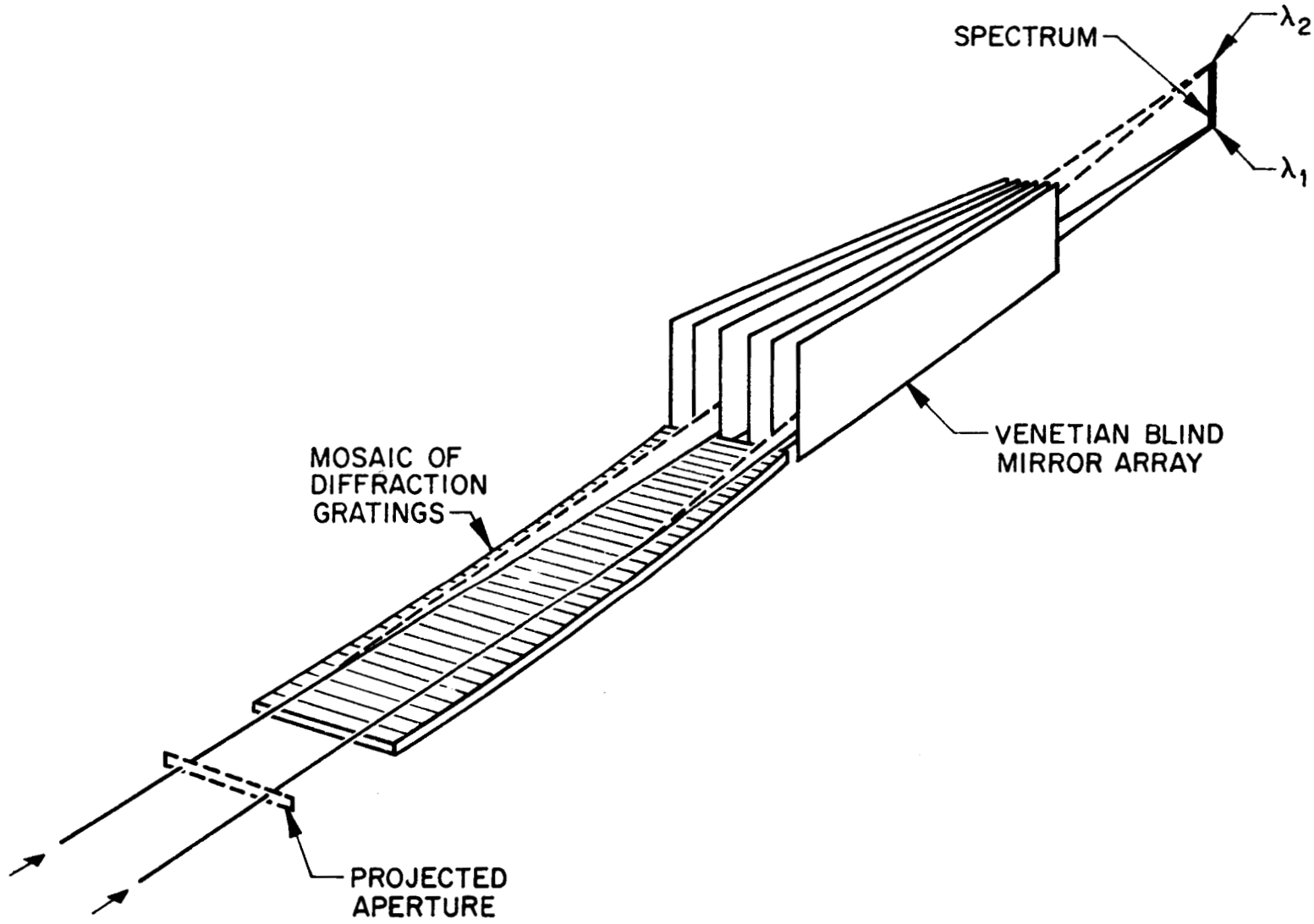

Fig. 1. Schematic of the x-ray optics of a spectrograph which utilizes a diffraction grating mosaic to produce a dispersed spectrum of an infinitely distant point source. A Venetian blind array of nested parabolic mirrors is used to compress the areal extent of the spectrum.

APPENDIX C

LISTING OF FORTRAN PROGRAM FOR IDEALIZED-GRATING CALCULATIONS

The more significant expressions used in the program are identified below, the symbols of Figure 13 of the report being used wherever possible.

PHIN	=	Φ of grating design
PHI	=	Φ actually used
WN	=	λ_1
WP	=	λ_2
DN	=	d_x at $x = 0$
ORDR	=	diffraction order actually used
DORDR	=	diffraction order of grating design
TLG	=	total length of grating surface in units of x_s
NPG	=	number of positions on each grating from which rays were traced
THETA	=	θ
RN	=	value of s/x_s for λ_1
RP	=	value of s/x_s for λ_2
RX	=	x/x_s
TNDELX	=	tangent of δ_x
DELX	=	δ_x
DX	=	d_x
ZX	=	z/x_s at position x
LAMBDA	=	arbitrary λ
s/x_s	=	image plane position wavelength λ diffracted to, $= y/x_s$ if $\theta = 90^\circ$

```
$EXECUTE        IBJOB
$IBJOB          GO
$IBFTC FXS      LIST
C     F. X. S.   CONTINUOUS-ARRAY DESIGN PARAMETER ANALYSIS
C     D. T. ROETHIG  PROGRAM THIRTEEN  9-17-64
C     THIS PROGRAM USES AN ITERATITIVE METHOD TO PERFORM PERFECT FOCUSSING
C     IF THE GRATING IS CONTINUOUS AND RAISED FROM THE DETECTOR PLANE WITH
C     INCREASING X.
      DIMENSION B(80), C(80), D(80), E(80), RX(80), TNDELX(80), DELX(80)
     1         , ZX(80), DX(80), H(80,12), RS(80,12), SR(24), XLMDA(80,24
     2           ), W(12), RLMDA(24), RRS(12), G(80)
      DOUBLE PRECISION PHIN, DN, WP, WN, RN, RP, B, C, D, E, TNDELX,
     1                  DELX, DX, DSQRT, DCOS, DSIN, DATAN, W, SR, XLMDA
     2                  , H, RS, RX, DELN, RRS, RLMDA, ORDR, DORDR, SUM,
     3                  PHI, STORE, THETA, HN, HP, G, AA,BB, CC, DD,
     4                EE, GG, ZX, UXZ, TLG, RW
   14 READ (5,15) PHIN, PHI, WN, WP, DN, ORDR, DORDR, TLG, NPG, DATE1,
     1     DATE2, THETA, (SR(K), K=3, 24), W
   15 FORMAT (2D16.9, 2D9.1, D12.1, 2D9.1/ D10.4/ I2/ A6, A2/ D16.9/
     1        8D10.3/ 8D10.3/ 6D10.3/ 6D10.2/ 6D10.2)
      LL = NPG
      DELN = 0.0D0
C     POSITIONS OF PERFECT FOCUS
      HN = DCOS(PHIN) - DORDR * WN/DN
      HP = DCOS(PHIN) - DORDR * WP/DN
      IF (1.0D0 - HP*HP)  950, 17, 17
   17 RN =(DCOS(THETA)*(HN*HN-1.0D0)+HN*DSIN(THETA)*DSQRT(1.0D0-HN*HN))/
     1    (HN*HN-DCOS(THETA)**2.0D0)
      RP =(DCOS(THETA)*(HP*HP-1.0D0)+HP*DSIN(THETA)*DSQRT(1.0D0-HP*HP))/
     1     (HP*HP-DCOS(THETA)**2.0D0)
      DO 25 I = 1, LL
   25 RX(I) = DBLE(FLOAT(I-1))*TLG/DBLE(FLOAT(NPG-1))
      AA = (WP/WN - 1.0D0)*DCOS(PHIN)
      BB = (WP/WN - 1.0D0)*DSIN(PHIN)
      CC =  (1.0D0/BB)*(DSQRT(RP**2.0D0+1.0D0) -(WP/WN)*DSQRT(RN**2.0D0+
     1      1.0D0))
      RW = WP/WN
      ZX(1) = 0.0D0
      DO 40 I= 2, LL
      DD = AA/BB*RX(I)-1.0D0/BB*DSQRT(RP**2.0D0+(1.0D0-RX(I))**2.0D0)+RW
     1     /BB*DSQRT(RN**2.0D0+(1.0D0-RX(I))**2.0D0)+CC
      EE = AA/BB*RX(I)-1.0D0/BB*DSQRT((RP-DD)**2.0D0+(1.0D0-RX(I))**2.0D
     1      0)+RW/BB*DSQRT((RN-DD)**2.0D0+(1.0D0-RX(I))**2.0D0)+CC
      GG = (DD**2.0D0)/(2.0D0*DD-EE)
   34 IF(GG) 950, 35, 35
   35 UXZ = AA/BB*RX(I)-1.0D0/BB*DSQRT((RP-GG)**2.0D0+(1.0D0-RX(I))**2.0
     1     D0)+RW/BB*DSQRT((RN-GG)**2.0D0+(1.0D0-RX(I))**2.0D0)+CC
      IF(ABS(GG-UXZ) - 1.0D-11) 40, 40, 37
   37 GG= (UXZ + GG)/2.0D0
      GO TO 35
   40 ZX(I) = GG
C     CIRCULAR FUNCTION-OF-BETA ARRAYS FOR SUCCEEDING X POSITIONS
      DO 110 I=1, LL
      B(I) = (1.0D0-RX(I)-(RN-ZX(I))*DCOS(THETA))/DSQRT((1.0D0-RX(I))**2
     1       .0D0+(RN-ZX(I))**2.0D0-2.0D0*(1.0D0-RX(I))*(RN-ZX(I))*DCOS(
     2       THETA))
      C(I) = (1.0D0-RX(I)-(RP-ZX(I))*DCOS(THETA))/DSQRT((1.0D0-RX(I))**2
     1       .0D0+(RP-ZX(I))**2.0D0-2.0D0*(1.0D0-RX(I))*(RP-ZX(I))*DCOS(
```

```
     2        THETA))
      D(I) = ((RN-ZX(I))*DSIN(THETA))/DSQRT((1.0D0-RX(I))**2.0D0+(RN-ZX(
     1        I))**2.0D0-2.0D0*(1.0D0-RX(I))*(RN-ZX(I))*DCOS(THETA))
      E(I) = ((RP-ZX(I))*DSIN(THETA))/DSQRT((1.0D0-RX(I))**2.0D0+(RP-ZX(
     1        I))**2.0D0-2.0D0*(1.0D0-RX(I))*(RP-ZX(I))*DCOS(THETA))
C     TANGENT OF DELTA X MATRIX AS A FUNCTION OF X POSITION                 49
      TNDELX(I) = ((WP/WN)*(DCOS(PHIN)-B(I))-(DCOS(PHIN)-C(I)))/((WP/WN)
     1            *(DSIN(PHIN)+D(I))-(DSIN(PHIN)+E(I)))
C     DELTA X MATRIX
      DELX(I) = DATAN(TNDELX(I))
C     GRATING SPACING MATRIX AS A FUNCTION OF X POSITION
      DX(I) = (DORDR*WP)/((1.0D0/DSQRT(1.0D0+TNDELX(I)**2.0D0))*(DCOS(PH
     1         IN)-C(I)-TNDELX(I)*(DSIN(PHIN)+E(I))))
      DO 110 J=1, 12
      G(I) = DCOS(THETA)*DCOS(DELX(I)) - DSIN(THETA)*DSIN(DELX(I))
      H(I,J) = DCOS(PHI  + DELX(I))- ORDR * W(J)/DX(I)
  110 RS(I,J)=(H(I,J)*H(I,J)*DCOS(THETA)-G(I)*DCOS(DELX(I))+H(I,J)*
     1           DSQRT(DCOS(DELX(I))**2.0D0+ G(I)*G(I) - 2.0D0*G(I)*
     2           DCOS(DELX(I))*DCOS(THETA) - H(I,J)*H(I,J)*DSIN(THETA)*
     3 *2.0D0))*(1.0D0-RX(I))/(H(I,J)*H(I,J)-G(I)*G(I))+ZX(I)
      DO 114 J = 1, 12
      STORE = 0.0D0                                                         99
      SUM = 0.0D0                                                          100
      DO 113 I = 1, LL
      STORE = SUM + RS(I,J)
  113 SUM = STORE
  114 RRS(J) = DBLE(FLOAT(LL)) *(RS(LL,J) - RS(1,J))/SUM
      SR(1) = RN
      SR(2) = RP
      DO 115 I = 1, LL
      DO 115 K = 1, 24
  115 XLMDA(I,K) = (DX(I)/ORDR)*(DCOS(PHI+DELX(I))-(((1.0D0-RX(I)-(SR(K)
     1              -ZX(I))*DCOS(THETA))*DCOS(DELX(I))+(SR(K)-ZX(I))*DSIN
     2              (THETA)*DSIN(DELX(I)))/DSQRT((1.0D0-RX(I))**2.0D0+(SR
     3              (K)-ZX(I))**2.0D0-2.0D0*(1.0D0-RX(I))*(SR(K)-ZX(I))*
     4              DCOS(THETA))))
      DO 120 K=1, 24
      STORE = 0.0D0                                                        106
      SUM = 0.0D0                                                          107
      DO 116 I = 1, LL
      STORE = SUM + XLMDA(I,K)
  116 SUM = STORE
  120 RLMDA(K) = DBLE(FLOAT(LL))*(XLMDA(1,K)-XLMDA(LL,K))/SUM
      WRITE (6,200) DATE1, DATE2
  200 FORMAT (1H1, 36X, 46HFXS CONTINUOUS-ARRAY DESIGN PARAMETER ANALYSI
     1S, // 54X, 16HPROGRAM THIRTEEN//51X, 15HD. T. ROETHIG  , A6, A2///
     2)
      WRITE (6, 210) PHIN, PHI, WN, WP, DN, ORDR, DORDR, TLG, NPG, THETA
     1               , RN, RP
  210 FORMAT (51X, 8HPHIN  = 1PD15.8/
     3        51X, 8HPHI   = 1PD15.8/
     1        51X, 8HWN    = 1PD15.8/
     2        51X, 8HWP    = 1PD15.8/
     3        51X, 8HDN    = 1PD15.8/
     4        51X, 8HORDR  = 0PF3.0 /
     5        51X, 8HDORDR = 0PF3.0 /
     6        51X, 8HTLG   = 1PD15.8/
     7        51X, 8HNPG   = I2/
```

```
   8          51X, 8HTHETA = 1PD15.8//
   9          51X, 8HRN    = 1PD15.8/
   1          51X, 8HRP    = 1PD15.8////)
    WRITE (6, 220) (RX(I), TNDELX(I), DELX(I), DX(I),  ZX(I), I=1, LL)
220 FORMAT (11X, 2HRX, 18X, 6HTNDELX, 14X, 4HDELX, 16X, 2HDX, 18X,
   1          3HZX // (10X, 1PD15.8, 5X, 1PD15.8, 5X, 1PD15.8, 5X, 1PD15
   2          .8, 5X, 1PD15.8))
    WRITE (6,349)
349 FORMAT (1H1, 21X, 75H POSITIONS OF DETECTOR INTERCEPTS FOR PARTICU
   1LAR LAMBDAS AS A FUNCTION OF X       ///)
    WRITE (6, 350) W(1), W(2), W(3), W(4), (RX(I), (RS(I,J), J= 1,4)
   1                , I = 1, LL)
350 FORMAT (6X, 4HRX =, 5X, 10HLAMBDA =  2PD10.2, 5X, 10HLAMBDA =  2PD
   1         10.2, 5X, 10HLAMBDA =  2PD10.2, 5X, 10HLAMBDA =  2PD10.2 //
   2         /(5X, 0PF6.3, 4X, 1PD21.14, 4X, 1PD21.14, 4X, 1PD21.14, 4X,
   3         1PD21.14))
    WRITE (6,351) (RRS(J),J=1, 4)
351 FORMAT (/6X,  7HRESOLTN ,  2X  , 1PD21.14, 4X, 1PD21.14, 4X, 1PD21
   1          .14, 4X, 1PD21.14)
    WRITE (6, 400) W(5), W(6), W(7), W(8), (RX(I), (RS(I,J), J= 5,8)
   1                , I = 1, LL)
400 FORMAT (///6X, 4HRX =, 5X, 10HLAMBDA =  2PD10.2, 5X, 10HLAMBDA =
   1         2PD10.2, 5X, 10HLAMBDA =  2PD10.2, 5X, 10HLAMBDA =  2PD10.2
   2         ///(5X, 0PF6.3, 4X, 1PD21.14, 4X, 1PD21.14, 4X, 1PD21.14,
   3         4X, 1PD21.14))
    WRITE (6,401) (RRS(J),J=5, 8)
401 FORMAT (/6X, 7HRESOLTN, 2X, 1PD21.14, 4X, 1PD21.14, 4X, 1PD21.14,
   1         4X, 1PD21.14)
    WRITE (6, 450) W(9), W(10), W(11), W(12), (RX(I), (RS(I,J), J=9,12
   1               ) , I = 1, LL)
450 FORMAT (///6X, 4HRX =, 5X, 10HLAMBDA =  2PD10.2, 5X, 10HLAMBDA =
   1         2PD10.2, 5X, 10HLAMBDA =  2PD10.2, 5X, 10HLAMBDA =  2PD10.2
   2         ///(5X, 0PF6.3, 4X, 1PD21.14, 4X, 1PD21.14, 4X, 1PD21.14,
   3         4X, 1PD21.14))
    WRITE (6,451) (RRS(J), J=9,12)
451 FORMAT (/6X, 7HRESOLTN, 2X, 1PD21.14, 4X, 1PD21.14, 4X, 1PD21.14,
   1         4X, 1PD21.14)
    WRITE (6,500)
500 FORMAT (1H1, 27X, 63HVALUES OF LAMBDA FOR PARTICULAR S INTERCEPTS
   1AS A FUNCTION OF X      ///)
    WRITE (6, 550) SR(1), SR(2), SR(3), SR(4), (RX(I), (XLMDA(I,K),
   1                 K = 1, 4), I = 1, LL)
550 FORMAT (3X, 4HRX =, 10X, 6HS/XS =, D14.7, 5X, 6HS/XS =, D14.7, 5X,
   1         6HS/XS =, D14.7, 5X, 6HS/XS =, D14.7 ///(2X, 0PF6.3, 10X,
   2         1PD20.13, 5X, 1PD20.13, 5X, 1PD20.13, 5X, 1PD20.13))
    WRITE (6,551) (RLMDA(K), K=1, 4)
551 FORMAT (/3X, 10HRESOLUTION, 5X, 1PD20.13, 5X, 1PD20.13, 5X, 1PD20.
   1         13, 5X, 1PD20.13)
    WRITE (6, 600) SR(5), SR(6), SR(7), SR(8), (RX(I), (XLMDA(I,K),
   1               K = 5, 8), I = 1, LL)
600 FORMAT (///3X, 4HRX =, 10X, 6HS/XS =, D14.7, 5X, 6HS/XS =, D14.7,
   1         5X, 6HS/XS =, D14.7, 5X, 6HS/XS =, D14.7 ///(2X, 0PF6.3, 10
   2         X, 1PD20.13, 5X, 1PD20.13, 5X, 1PD20.13, 5X, 1PD20.13))
    WRITE (6,601) (RLMDA(K), K=5, 8)
601 FORMAT (/3X, 10HRESOLUTION, 5X, 1PD20.13, 5X, 1PD20.13, 5X, 1PD20.
   1         13, 5X, 1PD20.13)
    WRITE (6, 650) SR(9), SR(10), SR(11), SR(12), (RX(I), (XLMDA(I,K)
   1                 , K = 9, 12), I = 1, LL)
```

```
650 FORMAT (///3X, 4HRX =,  10X, 6HS/XS =, D14.7, 5X, 6HS/XS =, D14.7,
   1        5X, 6HS/XS =, D14.7, 5X, 6HS/XS =, D14.7 ///(2X, 0PF6.3, 10
   2        X, 1PD20.13, 5X, 1PD20.13, 5X, 1PD20.13, 5X, 1PD20.13))
    WRITE (6,651) (RLMDA(K), K=9, 12)
651 FORMAT (/3X, 10HRESOLUTION, 5X, 1PD20.13, 5X, 1PD20.13, 5X, 1PD20.
   1        13, 5X, 1PD20.13)
    WRITE (6, 700) SR(13),SR(14), SR(15), SR(16), (RX(I), (XLMDA(I,K),
   1                K=13, 16), I=1, LL)
700 FORMAT (1H1, 3X, 4HRX =, 10X, 6HS/XS =, D14.7, 5X, 6HS/XS =,D14.7,
   1        5X, 6HS/XS =, D14.7, 5X, 6HS/XS =, D14.7 ///(2X, 0PF6.3, 10
   2        X, 1PD20.13, 5X, 1PD20.13, 5X, 1PD20.13, 5X, 1PD20.13))
    WRITE (6,701) (RLMDA(K), K=13, 16)
701 FORMAT (/3X, 10HRESOLUTION, 5X, 1PD20.13, 5X, 1PD20.13, 5X, 1PD20.
   1        13, 5X, 1PD20.13)
    WRITE (6, 750) SR(17),SR(18), SR(19), SR(20), (RX(I), (XLMDA(I,K),
   1                K=17, 20), I=1, LL)
750 FORMAT (///3X, 4HRX =, 10X, 6HS/XS =, D14.7, 5X, 6HS/XS =, D14.7,
   1        5X, 6HS/XS =, D14.7, 5X, 6HS/XS =, D14.7 ///(2X, 0PF6.3, 10
   2        X, 1PD20.13, 5X, 1PD20.13, 5X, 1PD20.13, 5X, 1PD20.13))
    WRITE(6,800) (RLMDA(K), K=17, 20)
800 FORMAT (/3X, 10HRESOLUTION, 5X, 1PD20.13, 5X, 1PD20.13, 5X, 1PD20.
   1        13, 5X, 1PD20.13)
    WRITE (6,850)  SR(21), SR(22), SR(23), SR(24), (RX(I),(XLMDA(I,K),
   1                K= 21, 24), I=1, LL)
850 FORMAT (///3X, 4HRX =, 10X, 6HS/XS =, D14.7, 5X, 6HS/XS =, D14.7,
   1        5X, 6HS/XS =, D14.7, 5X, 6HS/XS =, D14.7///(2X, 0PF6.3, 10
   2        X,  1PD20.13, 5X, 1PD20.13, 5X, 1PD20.13, 5X, 1PD20.13))
    WRITE (6,900) (RLMDA(K), K=21, 24)
900 FORMAT (/3X, 10HRESOLUTION, 5X, 1PD20.13, 5X, 1PD20.13, 5X, 1PD20.
   1         13, 5X, 1PD20.13)
    GO TO 14
950 WRITE (6, 955) DATE1, DATE2, PHIN, PHI, WN, WP, DN, ORDR, DORDR,
   1                TLG, NPG, THETA
955 FORMAT (1H1, 41X, 42HCONTINUOUS-ARRAY DESIGN PARAMETER ANALYSIS /
   1         55X, 16HPROGRAM THIRTEEN /51X, 15HD. T. ROETHIG   , A6,
   2         A2 ////
   2         51X, 8HPHIN  = 1PD15.8/
   3         51X, 8HPHI   = 1PD15.8/
   4         51X, 8HWN    = 1PD15.8/
   5         51X, 8HWP    = 1PD15.8/
   6         51X, 8HDN    = 1PD15.8/
   7         51X, 8HORDER = 0PF3.0/
   8         51X, 8HDORDER= 0PF3.0/
   9         51X, 8HTLG   = 1PD15.8/
   1         51X, 9HNPG   =  I2/
   2         51X, 8HTHETA = 1PD15.8//
   5         10X, 67HTHE INPUT PARAMETERS LISTED ABOVE DO NOT CORRESPON
   6D TO A PHYSICALLY  /  10X, 66HREALIZABLE CONFIGURATION, OR THE FIR
   9ST VALUE OF Z/XS WAS NEGATIVE.)
    WRITE (6, 956) AA, BB, CC, DD, EE, GG, I
956 FORMAT (//10X, 4HAA =1PD27.20/
   1           10X, 4HBB =1PD27.20/
   2           10X, 4HCC =1PD27.20/
   3           10X, 4HDD =1PD27.20/
   4           10X, 4HEE =1PD27.20/
   5           10X, 4HGG =1PD27.20/
   6           10X, 4HI  =I6)
    GO TO 14
```

APPENDIX D

LISTING OF FORTRAN PROGRAM FOR PRACTICAL-GRATING CALCULATIONS

The more significant expressions used in the program are identified below, the symbols of Figure 13 of the report being used wherever possible.

PHIN	=	Φ of grating design
PHI	=	Φ actually used
WN	=	λ_1
WP	=	λ_2
DN	=	d_x at $x = 0$
CHECKD	=	computer check to see that δ_x $(\frac{x}{x_s} = 0)$ is correct
ORDER	=	diffraction order actually used
DORDER	=	diffraction order of grating design
GEL	=	length of grating element in units of x_s
NEL	=	number of grating elements
NSUB	=	number of different groove spacings per grating element
THETA	=	θ
RN	=	value of s/x_s for λ_1
RP	=	value of s/x_s for λ_2
BDELX	=	δ_x
BDX	=	d_x
RHO	=	radius of grating element, in units of x_s
LAMBDA	=	arbitrary λ
s/x_s	=	image plane position wavelength λ diffracted to, $= y/x_s$ if $\theta = 90^\circ$

```
$EXECUTE        IBJOB
$IBJOB          GO
$IBFTC FXS      LIST
C       F.X.S.  DISCONTINUOUS-ARRAY DESIGN PARAMETER ANALYSIS                    5
C      D. T. ROETHIG  PROGRAM TWELVE  9-1-64
C      THIS PROGRAM APPROXIMATES THE CONTINUOUS CASE BY DIVIDING THE ARRAY INTO
C      CONCAVE SEGMENTS OF A PARTICULAR RADIUS OF CURVATURE THE DETERMINATION FOR
C      WHICH THERE ARE THREE IPTIONS. OPTION (1) GIVES THE 'INFINITE' RHO AT THE
C      ENDS OF THE ELEMENTS. OPTION (2) MAKES ALL THE RHO'S THE AVERAGE RHO.
C      OPTION (3) ALLOWS THE RHOS TO BE READ IN. EACH ELEMENT IS DIVIDED INTO
C      SUBELEMENTS EACH HAVING THE INFINITE CASE SPACING. DX IS CHOSEN FROM THE
C      CENTER OF EACH SUBELEMENT.
       DIMENSION  RX(193), TNDELX(193), RHO(193), BRX(193),
      1            DELX(193), DX(193), BDX(193),              BDELX(193),
      2           SR(24), XLMDA(193,24), RLMDA(24), RS(193,12), RRS(12),
      3           W(12)
       DOUBLE PRECISION   HN, HP, RN, RP, DSIN, DSQRT, DCOS, RX, Z, GEL,
      1                   B, C, D, E, TNDELX, PHIN, DELX, DX, BDX, CDELX
      2          ,BDELX, STORE, SUM, DN, WP, WN, DATAN, ORDR, DORDR, THETA
      3          , SR, XLMDA, RLMDA, G, H, RS, RRS, W, PHI, DELN, CHECKD
      4           , CONST, BRX, RHO
   14 READ (5,16)   OPTION,    NOPT,          PHIN, PHI, WN, WP, DN, ORDR
      1            , DORDR, GEL, DATE1, DATE2, THETA, NSUB, NEL, (SR(K),
      2             K=3, 24), W
   16 FORMAT (A6, I2/ 2D16.9, 2D9.1, D12.1, 2D9.1/ D11.4/ A6, A2/ D16.9/
      1        I10, I10/ 8D10.3/ 8D10.3/ 6D10.3/ 6D10.2/ 6D10.2)
       DELN = 0.0D0                                                            18
C      POSITIONS OF PERFECT FOCUS
       HN = DCOS(PHIN) - DORDR * WN/DN
       HP = DCOS(PHIN) - DORDR * WP/DN
       IF (1.0D0 - HP*HP)  950, 17, 17
   17 RN =(DCOS(THETA)*(HN*HN-1.0D0)+HN*DSIN(THETA)*DSQRT(1.0D0-HN*HN))/
      1    (HN*HN-DCOS(THETA)**2.0D0)
       RP =(DCOS(THETA)*(HP*HP-1.0D0)+HP*DSIN(THETA)*DSQRT(1.0D0-HP*HP))/
      1     (HP*HP-DCOS(THETA)**2.0D0)
       MAX = NEL*NSUB*2 + 1
       DO 55 I = 1, MAX
       RX(I) = (DBLE(FLOAT(I))-1.0D0)*GEL/(DBLE(FLOAT(NSUB))*2.0D0)
       Z = RX(I)                                                               39
C      CIRCULAR FUNCTION-OF-BETA MATRICIES FOR SUCEEDING X POSITIONS           40
       B     = (1.0D0 -Z -RN*DCOS(THETA))/DSQRT((1.0D0-Z)**2.0D0+RN*RN-2.0
      1        D0*(1.0D0-Z)*RN*DCOS(THETA))
       C     = (1.0D0 -Z -RP*DCOS(THETA))/DSQRT((1.0D0-Z)**2.0D0+RP*RP-2.0
      1        D0*(1.0D0-Z)*RP*DCOS(THETA))
       D     = (RN*DSIN(THETA))/DSQRT((1.0D0-Z)**2.0D0+RN*RN-2.0D0*(1.0D0
      1        -Z)*RN*DCOS(THETA))
       E     = (RP*DSIN(THETA))/DSQRT((1.0D0-Z)**2.0D0+RP*RP-2.0D0*(1.0D0
      1        -Z)*RP*DCOS(THETA))
C      TANGENT OF DELTA X MATRIX AS A FUNCTION OF X POSITION                   49
       TNDELX(I) = ((WP/WN)*(DCOS(PHIN)-B    )-(DCOS(PHIN)-C    ))/((WP/WN)
      1            *(DSIN(PHIN)+D    )-(DSIN(PHIN)+E    ))
C      DELTA X MATRIX                                                          52
       DELX(I) = DATAN(TNDELX(I))                                              53
C      GRATING SPACING MATRIX AS A FUNCTION OF X POSITION                      54
   55 DX(I) = (DORDR*WN)/((1.0D0/(DSQRT(1.0D0+TNDELX(I)**2.0D0)))*((DCOS       55
      1         (PHIN)-B    )-(TNDELX(I)*(DSIN(PHIN)+D    ))))
       CHECKD = DX(1)
C      INDEXING OF BRX UNDER L
```

```
      BRX(1) = RX(1)
      NN= MAX - 1
      BRX(NN) = RX(MAX)
      K = MAX - 2
      DO 66 L=3, K, 2
      BRX(L) = RX(L)
      N = L-1
   66 BRX(N) = RX(L)
C     INDEXING OF BDX UNDER L
      DO 67  L=2, NN, 2
      N = L - 1
      BDX(L) = DX(L)
   67 BDX(N) = DX(L)
      GO TO (68, 68, 75), NOPT
C     START OPTION ONE -- CALCULATION OF RHO FOR EACH L
   68 M = 1
      J = 2*NSUB
      N = 2*NSUB + 1
      NN = 2*NEL*NSUB
   69 CONST = GEL*DCOS(DELX(N))/DSIN(DELX(N)-DELX(M))
      DO 70  L=M, J
   70 RHO(L) = CONST
      IF (J - NN)  705, 71, 71
  705 M = M + 2*NSUB
      N = N + 2*NSUB
      J = J + 2*NSUB
      GO TO 69
   71 GO TO ( 82, 72, 75),NOPT
C     START OPTION TWO -- CALCULATION OF AVERAGE RHO
   72 STORE = 0.0D0
      N = 2*NSUB
      NN= 2*NSUB*NEL
      DO 73  L=N, NN, N
   73 STORE = STORE + RHO(L)
      STORE = STORE/DBLE(FLOAT(NEL))
      DO 74  L=1, NN
   74 RHO(L) = STORE
      GO TO 82
C     START OPTION THREE -- READING IN OF A RHO FOR EACH ELEMENT AND
C         DEFINING IT UNDER L
   75 N = 2*NSUB
      NNN = 2*NSUB*(NEL-1) + 1
   76 READ(5,77)  (RHO(L), L = 1, NNN, N)
   77 FORMAT (4D20.10)
   78 M = 1
      MM = 2
   79 CONST = RHO(M)
      DO 80  L = MM, N
   80 RHO(L) = CONST
      IF( N - NNN) 81, 82, 82
   81 M = M + 2 * NSUB
      MM = MM + 2*NSUB
      N  =  N + 2*NSUB
      GO TO 79
   82 M = 1
      N = 2*NSUB
      NN= 2*NSUB*NEL
  825 DO 83 L = M, N
```

```
   83 BDELX(L) = DATAN((BRX(L)-BRX(M))/(RHO(L)*DCOS(DELX(M)))+TNDELX(M))
      IF (N - NN) 84, 85, 85
   84 M = M + 2*NSUB
      N = N + 2*NSUB
      GO TO 825
C     START MAIN CALCULATIONS
   85 NN = 2*NSUB*NEL
      LL = 2*NSUB*NEL
      DO 88  L= 1, NN
      G = DCOS(THETA)*DCOS(BDELX(L))-DSIN(THETA)*DSIN(BDELX(L))
      DO 88  J=1, 12                                                    85
      H = DCOS(PHI+BDELX(L))-ORDR*W(J)/BDX(L)
   88 RS(L,J) = (H*H*DCOS(THETA) - G*DCOS(BDELX(L)) + H*DSQRT(DCOS(BDELX
     1           (L))**2.0D0 + G*G - 2.0D0*G*DCOS(BDELX(L))*DCOS(THETA) -
     2           H*H*DSIN(THETA)**2.0D0))*(1.0D0 - RX(L))/(H*H - G*G)
      DO 104 J=1, 12                                                    98
      STORE = 0.0D0                                                     99
      SUM = 0.0D0                                                      100
      DO 103 L=1, LL                                                   101
      STORE = SUM +RS(L,J)                                             102
  103 SUM = STORE                                                      103
  104 RRS(J) = DBLE(FLOAT(LL)) *(RS(LL,J) - RS(1,J))/SUM
      SR(1) = RN
      SR(2) = RP
      DO 94 L = 1, NN
      DO 94  K=1, 24                                                    92
   94 XLMDA(L,K) =(BDX(L)/ORDR)*(DCOS(PHI+BDELX(L))-(((1.0D0- RX(L)-SR(K
     1              )*DCOS(THETA))*DCOS(BDELX(L))+SR(K)*DSIN(THETA)*DSIN(   95
     2              BDELX(L)))/DSQRT((1.0D0- RX(L))**2.0D0+SR(K)*SR(K)-2.   96
     3              0D0*(1.0D0- RX(L))*SR(K)*DCOS(THETA))))
      DO 111 K=1, 24                                                   105
      STORE = 0.0D0                                                    106
      SUM = 0.0D0                                                      107
      DO 110  L=1, LL                                                  108
      STORE = SUM + XLMDA(L,K)                                         109
  110 SUM = STORE                                                      110
  111 RLMDA(K) = DBLE(FLOAT(LL))*(XLMDA(1,K)-XLMDA(LL,K))/SUM
      WRITE (6,114) DATE1, DATE2, OPTION, NOPT
  114 FORMAT (1H1, 39X, 45HDISCONTINUOUS-ARRAY DESIGN PARAMETER ANALYSIS
     1       /56X, 14HPROGRAM TWELVE /51X, 15HD. T. ROETHIG  , A6, A2////
     2        59X, A6, I2//)
      WRITE (6, 115) PHIN, PHI, WN, WP, DN, CHECKD, ORDR, DORDR, GEL,
     1              NEL, NSUB, THETA, RN, RP
  115 FORMAT (51X,  8HPHIN   = 1PD15.8/
     3         51X,  8HPHI    = 1PD15.8/
     4         51X,  8HWN     = 1PD15.8/
     5         51X,  8HWP     = 1PD15.8/
     6         51X,  8HDN     = 1PD15.8/
     5        51X,  8HCHECKD= 1PD15.8/
     7         51X,  8HORDER = 0PF3.0/
     8         51X,  8HDORDER= 0PF3.0/
     9         51X,  8HGEL    = 1PD15.8/
     1        51X,  9HNEL    =  I2/
     2        51X,  9HNSUB   =  I2/
     2         51X,  8HTHETA = 1PD15.8//
     3         51X,  8HRN     = 1PD15.8/
     4         51X,  8HRP     = 1PD15.8////)
      WRITE (6, 121) (BRX(L), BDELX(L), BDX(L),  RHO(L), L=1, LL)
```

```
121 FORMAT (11X, 3HBRX, 27X, 5HBDELX, 25X, 3HBDX, 27X, 3HRHO//
   1        (5X, 1PD20.8, 10X, 1PD20.8, 10X, 1PD20.8, 10X, 1PD20.8))          122
    WRITE (6,349)
349 FORMAT (1H1, 21X, 75H POSITIONS OF DETECTOR INTERCEPTS FOR PARTICU
   1LAR LAMBDAS AS A FUNCTION OF X      ///)
    WRITE (6,350) W(1), W(2), W(3), W(4), (BRX(L), (RS(L,J), J=1,4)
   1                , L=1, LL)
350 FORMAT (6X, 4HRX =, 5X, 10HLAMBDA =  2PD10.2, 5X, 10HLAMBDA =  2PD
   1        10.2, 5X, 10HLAMBDA =  2PD10.2, 5X, 10HLAMBDA =  2PD10.2 //
   2        /(5X, 0PF6.3, 4X, 1PD21.14, 4X, 1PD21.14, 4X, 1PD21.14, 4X,
   3        1PD21.14))
    WRITE (6,351) (RRS(J),J=1, 4)
351 FORMAT (/6X,  7HRESOLTN ,  2X  , 1PD21.14, 4X, 1PD21.14, 4X, 1PD21
   1         .14, 4X, 1PD21.14)
    WRITE (6,400) W(5), W(6), W(7), W(8), (BRX(L), (RS(L,J), J=5,8)
   1                , L=1, LL)
400 FORMAT (///6X, 4HRX =, 5X, 10HLAMBDA =  2PD10.2, 5X, 10HLAMBDA =
   1        2PD10.2, 5X, 10HLAMBDA =  2PD10.2, 5X, 10HLAMBDA =  2PD10.2
   2        ///(5X, 0PF6.3, 4X, 1PD21.14, 4X, 1PD21.14, 4X, 1PD21.14,
   3        4X, 1PD21.14))
    WRITE (6,401) (RRS(J),J=5, 8)
401 FORMAT (/6X, 7HRESOLTN, 2X, 1PD21.14, 4X, 1PD21.14, 4X, 1PD21.14,
   1        4X, 1PD21.14)
    WRITE (6,450) W(9), W(10),  W(11), W(12), (BRX(L), (RS(L,J),J=9,12
   1               ), L=1, LL)
450 FORMAT (///6X, 4HRX =, 5X, 10HLAMBDA =  2PD10.2, 5X, 10HLAMBDA =
   1        2PD10.2, 5X, 10HLAMBDA =  2PD10.2, 5X, 10HLAMBDA =  2PD10.2
   2        ///(5X, 0PF6.3, 4X, 1PD21.14, 4X, 1PD21.14, 4X, 1PD21.14,
   3        4X, 1PD21.14))
    WRITE (6,451) (RRS(J), J=9,12)
451 FORMAT (/6X, 7HRESOLTN, 2X, 1PD21.14, 4X, 1PD21.14, 4X, 1PD21.14,
   1        4X, 1PD21.14)
    WRITE (6,500)
500 FORMAT (1H1, 27X, 63HVALUES OF LAMBDA FOR PARTICULAR S INTERCEPTS
   1AS A FUNCTION OF X      ///)
    WRITE (6,550)  SR(1), SR(2), SR(3), SR(4), (BRX(L), (XLMDA(L,K),
   1                K=1, 4), L=1, LL)
550 FORMAT (3X, 4HRX =, 10X, 6HS/XS =, D14.7, 5X, 6HS/XS =, D14.7, 5X,
   1        6HS/XS =, D14.7, 5X, 6HS/XS =, D14.7 ///(2X, 0PF6.3, 10X,
   2        1PD20.13, 5X, 1PD20.13, 5X, 1PD20.13, 5X, 1PD20.13))
    WRITE (6,551) (RLMDA(K), K=1, 4)
551 FORMAT (/3X, 10HRESOLUTION, 5X, 1PD20.13, 5X, 1PD20.13, 5X, 1PD20.
   1        13, 5X, 1PD20.13)
    WRITE (6,600)  SR(5), SR(6), SR(7), SR(8), (BRX(L), (XLMDA(L,K),
   1               K=5,8), L=1, LL)
600 FORMAT (///3X, 4HRX =, 10X, 6HS/XS =, D14.7, 5X, 6HS/XS =, D14.7,
   1        5X, 6HS/XS =, D14.7, 5X, 6HS/XS =, D14.7 ///(2X, 0PF6.3, 10
   2        X, 1PD20.13, 5X, 1PD20.13, 5X, 1PD20.13, 5X, 1PD20.13))
    WRITE (6,601) (RLMDA(K), K=5, 8)
601 FORMAT (/3X, 10HRESOLUTION, 5X, 1PD20.13, 5X, 1PD20.13, 5X, 1PD20.
   1        13, 5X, 1PD20.13)
    WRITE (6,650)  SR(9), SR(10), SR(11), SR(12), (BRX(L), (XLMDA(L,K)
   1                , K=9, 12), L=1, LL)
650 FORMAT (///3X, 4HRX =,  10X, 6HS/XS =, D14.7, 5X, 6HS/XS =, D14.7,
   1        5X, 6HS/XS =, D14.7, 5X, 6HS/XS =, D14.7 ///(2X, 0PF6.3, 10
   2        X, 1PD20.13, 5X, 1PD20.13, 5X, 1PD20.13, 5X, 1PD20.13))
    WRITE (6,651) (RLMDA(K), K=9, 12)
651 FORMAT (/3X, 10HRESOLUTION, 5X, 1PD20.13, 5X, 1PD20.13, 5X, 1PD20.
```

```
   1        13, 5X, 1PD20.13)
    WRITE (6,700)  SR(13), SR(14), SR(15), SR(16), (BRX(L), (XLMDA(L,
   1               K), K=13, 16), L=1, LL)
700 FORMAT (1H1, 3X, 4HRX =, 10X, 6HS/XS =, D14.7, 5X, 6HS/XS =,D14.7,
   1        5X, 6HS/XS =, D14.7, 5X, 6HS/XS =, D14.7 ///(2X, 0PF6.3, 10
   2        X, 1PD20.13, 5X, 1PD20.13, 5X, 1PD20.13, 5X, 1PD20.13))
    WRITE (6,701) (RLMDA(K), K=13, 16)
701 FORMAT (/3X, 10HRESOLUTION, 5X, 1PD20.13, 5X, 1PD20.13, 5X, 1PD20.
   1        13, 5X, 1PD20.13)
    WRITE (6,750)  SR(17), SR(18), SR(19), SR(20), (BRX(L), (XLMDA(L,
   1               K), K=17, 20), L=1,LL)
750 FORMAT (///3X, 4HRX =, 10X, 6HS/XS =, D14.7, 5X, 6HS/XS =, D14.7,
   1        5X, 6HS/XS =, D14.7, 5X, 6HS/XS =, D14.7 ///(2X, 0PF6.3, 10
   2        X, 1PD20.13, 5X, 1PD20.13, 5X, 1PD20.13, 5X, 1PD20.13))
    WRITE(6,800) (RLMDA(K), K=17, 20)
800 FORMAT (/3X, 10HRESOLUTION, 5X, 1PD20.13, 5X, 1PD20.13, 5X, 1PD20.
   1        13, 5X, 1PD20.13)
    WRITE (6,850)  SR(21), SR(22), SR(23), SR(24), (BRX(L), (XLMDA(L,
   1               K), K=21,24), L=1,LL)
850 FORMAT (///3X, 4HRX =, 10X, 6HS/XS =, D14.7, 5X, 6HS/XS =, D14.7,
   1        5X, 6HS/XS =, D14.7, 5X, 6HS/XS =, D14.7///(2X, 0PF6.3, 10
   2        X,  1PD20.13, 5X, 1PD20.13, 5X, 1PD20.13, 5X, 1PD20.13))
    WRITE (6,900) (RLMDA(K), K=21, 24)
900 FORMAT (/3X, 10HRESOLUTION, 5X, 1PD20.13, 5X, 1PD20.13, 5X, 1PD20.
   1         13, 5X, 1PD20.13)
    GO TO 14
950 WRITE (6,955) DATE1, DATE2, PHIN, PHI, WN, WP, DN, ORDR, DORDR,
   1      GEL, NEL, NSUB, THETA, HN, HP
955 FORMAT (1H1, 39X, 45HDISCONTINUOUS-ARRAY DESIGN PARAMETER ANALYSIS
   1        /56X, 14HPROGRAM TWELVE/51X, 15HD. T. ROETHIG  ,A6, A2////
   2         51X, 8HPHIN  = 1PD15.8/
   3         51X, 8HPHI   = 1PD15.8/
   4         51X, 8HWN    = 1PD15.8/
   5         51X, 8HWP    = 1PD15.8/
   6         51X, 8HDN    = 1PD15.8/
   7         51X, 8HORDER = 0PF3.0/
   8         51X, 8HDORDER= 0PF3.0/
   9         51X, 8HGEL   = 1PD15.8/
   1         51X, 9HNEL   =  I2/
   1         51X, 9HNSUB  =  I2//
   2         51X, 8HTHETA = 1PD15.8//
   3         51X, 8HHN    = 1PD15.8/
   3         51X, 8HHP    = 1PD15.8///,
   5         10X,  93HTHE INPUT PARAMETERS LISTED ABOVE DO NOT CORRESPO
   6ND TO A PHYSICALLY REALIZABLE CONFIGURATION. )
    GO TO 14
    END
```